AEDC-TR-76-5

TRANSIENT DEVELOPMENT OF EXCITED STATE DENSITIES IN ATOMIC HELIUM PLASMAS

ENGINE TEST FACILITY
ARNOLD ENGINEERING DEVELOPMENT CENTER
AIR FORCE SYSTEMS COMMAND
ARNOLD AIR FORCE STATION, TENNESSEE 37389

March 1976

Final Report for Period October 1969 — April 1975

Prepared for

DIRECTORATE OF TECHNOLOGY
ARNOLD ENGINEERING DEVELOPMENT CENTER
ARNOLD AIR FORCE STATION, TENNESSEE 37389

NOTICES

When U. S. Government drawings specifications, or other data are used for any purpose other than a definitely related Government procurement operation, the Government thereby incurs no responsibility nor any obligation whatsoever, and the fact that the Government may have formulated, furnished, or in any way supplied the said drawings, specifications, or other data, is not to be regarded by implication or otherwise, or in any manner licensing the holder or any other person or corporation, or conveying any rights or permission to manufacture, use, or sell any patented invention that may in any way be related thereto.

Qualified users may obtain copies of this report from the Defense Documentation Center.

References to named commercial products in this report are not to be considered in any sense as an endorsement of the product by the United States Air Force or the Government.

This report has been reviewed by the Information Office (OI) and is releasable to the National Technical Information Service (NTIS). At NTIS, it will be available to the general public, including foreign nations.

APPROVAL STATEMENT

This technical report has been reviewed and is approved for publication.

FOR THE COMMANDER

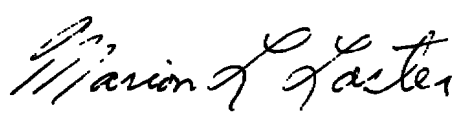

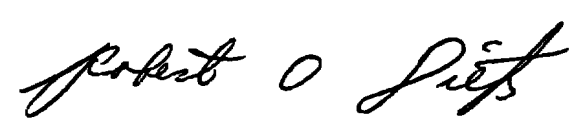

MARION L. LASTER
Research & Development
Division
Directorate of Technology

ROBERT O. DIETZ
Director of Technology

REPORT DOCUMENTATION PAGE		READ INSTRUCTIONS BEFORE COMPLETING FORM
1 REPORT NUMBER AEDC-TR-76-5	2. GOVT ACCESSION NO.	3 RECIPIENT'S CATALOG NUMBER
4 TITLE (and Subtitle) TRANSIENT DEVELOPMENT OF EXCITED STATE DENSITIES IN ATOMIC HELIUM PLASMAS		5 TYPE OF REPORT & PERIOD COVERED Final Report, October 1969 - April 1975 6 PERFORMING ORG. REPORT NUMBER
7 AUTHOR(s) C. C. Limbaugh, ARO, Inc.		8. CONTRACT OR GRANT NUMBER(s)
9 PERFORMING ORGANIZATION NAME AND ADDRESS Arnold Engineering Development Center (DY) Air Force Systems Command Arnold Air Force Station, TN 37389		10 PROGRAM ELEMENT, PROJECT, TASK AREA & WORK UNIT NUMBERS Program Element 65807F
11 CONTROLLING OFFICE NAME AND ADDRESS Arnold Engineering Development Center (DYFS), Air Force Systems Command, Arnold Air Force Station, TN 37389		12 REPORT DATE March 1976 13. NUMBER OF PAGES 118
14 MONITORING AGENCY NAME & ADDRESS(if different from Controlling Office)		15. SECURITY CLASS. (of this report) UNCLASSIFIED 15a DECLASSIFICATION DOWNGRADING SCHEDULE N/A

16 DISTRIBUTION STATEMENT (of this Report)

Approved for public release; distribution unlimited.

17 DISTRIBUTION STATEMENT (of the abstract entered in Block 20, if different from Report)

18 SUPPLEMENTARY NOTES

Available in DDC.

19 KEY WORDS (Continue on reverse side if necessary and identify by block number)

helium plasma
nonequilibrium flow
plasmas (physics)
models
radiation
coefficients
recombination reactions

20 ABSTRACT (Continue on reverse side if necessary and identify by block number)

The set of detailed rate equations describing the transient decay of singly ionized, constant temperature, constant pressure, monatomic helium plasmas is solved numerically for early times in the plasma decay. These equations, called the eigenstate rate equations (ERE), have been studied previously for late times in the decay through application of the quasi-steady-state (QSS) assumption and have resulted in the collisional-radiative recombination (CRR) model for description of the electron density decay rate in

DD FORM 1 JAN 73 1473 EDITION OF 1 NOV 65 IS OBSOLETE

20. ABSTRACT (Continued)

plasmas. The application of the QSS to the ERE makes it impossible to study the mechanisms and the transient coupling by which the final distributions are established. The QSS assumption is specifically removed in this study so that the ERE can be solved completely for the early transient characteristics of the plasma decay. In this way the validity of CRR theory can be assessed and the important mechanisms in the early plasma decay can be illustrated as well. In the range of conditions studied ($6{,}000^{o}K \leq T_e \leq 14{,}000^{o}K$, 2.69×10^{11} 1/cm^3 $\leq n_e \leq 1.63 \times 10^{15}$ 1/cm^3, 5.0×10^{13} 1/cm^3 $\leq n_o \leq 1.63 \times 10^{17}$ 1/cm^3), it is found that CRR can be applied to the electron density decay before the atomic eigenstates in the plasma reach the QSS. Times for the QSS to be established ranged from 3×10^{-9} sec for the high density plasmas to 7×10^{-4} sec for the low density plasmas. It is found that in a plasma decay the ground state rate and the free electron decay rate can overshoot the QSS condition before returning to it. This is due to the transient coupling between the 2^3S state and adjacent states and is a transient phenomenon which requires the ERE for elucidation. It is also found that when the plasma is subjected to a decaying electron temperature the plasma may never achieve the QSS. In this situation the QSS will continually lag behind the temperature decay.

PREFACE

The work reported herein was conducted by the Arnold Engineering Development Center (AEDC), Air Force Systems Command (AFSC), at the request of the Air Force Aerospace Research Laboratories (ARL), under Program Element 65807F. The results of the research were obtained by ARO, Inc. (a subsidiary of Sverdrup & Parcel and Associates, Inc.), contract operator of AEDC, AFSC, Arnold Air Force Station, Tennessee, under ARO Project Number R33A-00A and predecessors. The author of this report was C. C. Limbaugh, ARO, Inc. The manuscript (ARO Control No. ARO-ETF-TR-75-64) was submitted for publication as partial results of the research efforts on May 23, 1975.

The work discussed herein was first reported in a University of Tennessee Space Institute Ph. D. dissertation under the guidance of Dr. A. A. Mason. The author wishes especially to acknowledge Dr. W. K. McGregor, ARO, Inc., for the numerous discussions which both initially inspired this work and also contributed materially to its progress. Appreciation is also extended to Mr. E. W. Dorrell, Central Data Processing, ARO, Inc., who performed the initial programming for the computer code used here.

CONTENTS

ILLUSTRATIONS

Figure | Page

Figure | Page

TABLES

1.0 INTRODUCTION

The description of nonequilibrium phenomena in gases is of importance to the aerospace sciences because these phenomena are present in such diverse applications as hypersonic flow fields, rocket exhaust plumes, and low density, high enthalpy wind tunnels. Experimental and calculational techniques to study the physical mechanisms contributing to the nonequilibrium situation are at best difficult because of the complexity of the necessary mathematical system as well as a lack of knowledge of many of the fundamental constants. Although still present, these drawbacks are reduced in decaying low density plasmas and such plasmas can be used for studying the fundamental manifestations of the nonequilibrium phenomena. This study usually proceeds through interpretation of measured spectral line intensities, electron densities, etc. in terms of recombination rates and other useful properties of the plasma. Proper and complete interpretation of these data requires knowledge of the distribution of population densities among the different energy modes of the plasma, and in the nonequilibrium environment, this is generally not describable by a Boltzmann distribution.

The majority of the work in recent years has been concerned with electron-ion recombination and the distribution of the population densities of electronic states in atomic plasmas. In most of this work, the assumption that the population densities of excited states are quiescent was required in order to make the calculations tractable. This assumption, called the quasi-steady-state (QSS) assumption, although apparently reasonable, results in the masking of the transient physical mechanisms that contribute to establishing the final distribution. Implicit to the QSS is the assumption that the occurrence of atomic collisional processes is sufficiently rapid that macroscopic phenomena, such as gas dynamic effects, are negligible.

The intent of this study is to remove the QSS assumption so that the detailed processes establishing the transient behaviour of the population densities can be studied during the establishment of the final distribution. The present study is confined to helium plasmas because the helium atom has been extensively studied both experimentally and theoretically so that the fundamental quantum mechanical structure is well known. The study further ignores the possible effects introduced by gas dynamical and other macroscopic effects. Including these phenomena at this point would only complicate the problem without

materially adding to the fundamental description of the necessary microsopic processes.

1.1 BACKGROUND

The following review of the wealth of literature available on the subject of electron-ion recombination in atomic hydrogen and helium plasmas is not an exhaustive one, and the bibliography is not complete by any means. There have been a large number of investigations of recombination in helium, and enumeration of each would not illuminate the subject materially beyond those which are reviewed. Rather, the events and highlights leading to the present study are indicated.

Early experiments on recombination in ionized gases provided recombination rates which were about two orders of magnitude greater than theoretical values obtained by considering only two-body encounters (i.e., radiative recombination) (Ref. 1). Early in 1961, D'Angelo (Ref. 1) examined the recombination rates obtained by considering three-body encounters (two electrons and an ion), resulting in a neutral atom and a free electron for hydrogen plasmas. The captured electron was considered to be in a bound energy state, and the excited atom subsequently decayed radiatively to the ground state. The results of D'Angelo's calculations showed that considerations of three-body collisions yield recombination rates appreciably larger than for radiative recombination. Thus, it was believed that three-body collisions would explain the large recombination rates observed in plasmas. This appears to have been the first work in which the three-body collision theory was applied to recombination studies.

Byron, Stabler, and Bortz (Ref. 2) subsequently (1962) further refined the calculative procedure. They considered three-body recombination along with collisional de-excitation and radiative de-excitation and calculated recombination rates for hydrogen plasmas. Their work was based on the simplification that at equilibrium there is a minimum in the total rate of de-excitation of excited atoms with increasing quantum number. This minimum results because the collisional de-excitation rate increases with increasing quantum number, caused by the lower energy difference between states, while the radiative de-excitation rate decreases with increasing quantum number due to the smaller transition probabilities for states of larger quantum number. They then solved the problem for the total recombination rate by obtaining the quantum level at which the minimum occurs and finding its net rate of de-excitation.

During this time, Bates, Kingston, and McWhirter published several papers concerning recombination. Their work, based upon a statistical approach to the problem, culminated in two comprehensive papers in 1962 on collisional-radiative recombination (Refs. 3 and 4). They included all the salient processes which contribute to level populations of a hydrogenic plasma in a set of rate equations. The result of these studies was a model which could be generally applied to decaying plasmas; the model is usually termed the "collisional-radiative recombination" (CRR) model. In this model a Boltzmann distribution of population of upper excited states is maintained which is in equilibrium with the free electron density.

The aforementioned studies form the basis of the present day theories of electron-ion recombination in atomic plasmas. The primary emphasis in each has been to obtain recombination rates which were more consistent with experiment. In each it was necessary to invoke the QSS assumption, and thus information as to the mechanisms for the establishment of a final distribution of excited state population densities was lost.

Before the establishment of the CRR model, it was generally necessary to revert to two basic models for the analytic study of excited state population densities. One of these, the local thermodynamic equilibrium (LTE) model (Ref. 5) is useful when the densities are sufficiently high to maintain strong collision dominance and Boltzmann distributions of excited state densities are maintained. The other model, the corona model, applies to the low density situation (Ref. 5) where radiative rates are competitive with collisional rates and the distributions are non-Boltzmann. McWhirter and Hearn (Ref. 6) calculated the instantaneous population densities for the excited levels of hydrogenic plasmas based upon the CRR model for a variety of plasma conditions. Their results are in basic agreement with the LTE and corona models and provided validity for the QSS calculation at intermediate conditions when the simpler models were not valid. There was no way in using these models for excited state density determinations that the validity of the QSS assumption applied to a real plasma could be checked. Rather, all that was known was that the various theories, based upon the QSS assumption, agreed.

The feeling that apparently has prevailed since about 1964 is that the recombination rate problem has been solved for hydrogenic plasmas. There are occasional papers in which the CRR ionization and recombination coefficients are computed using later and more accurate cross-section calculations (Ref. 7) or introducing another class of collisions

(Ref. 7), or including estimated relaxation times to the steady state (Ref. 9). This work all depends on the QSS, however.

The difficulties encountered in studies of recombination in helium plasmas largely paralleled those for hydrogen plasmas. A wealth of experimental data from microwave and spectroscopic measurements in decaying afterglows was available which indicated significant differences in the calculated and measured recombination rates. Indeed it was just such discrepancies that prompted the analytic work in the hydrogenic plasmas. Shortly after D'Angelo (Ref. 1) published his work, Hinnov and Hirschberg (Ref. 10) applied the three-body theory to helium recombination experiments in the B-1 Stellerator at Princeton. By also including inelastic electron collisions for excitation and superelastic collisions between bound atomic states they obtained good correlation between theory and experiment. In later work Hinnov and Hirschberg (Ref. 11) extended the interpretation to locating a "critical level" which is defined as the lowest principal quantum level in equilibrium with the free electrons. This critical level serves as an upper bound on the quantum levels affecting the electron density decay. They refer to favorable comparisons of their work to the preliminary studies which led to the CRR model of Bates, Kingston, and McWhirter (Refs. 3 and 4).

Robben, Kunkel, and Talbot (Ref. 12) made a spectroscopic study of the freely expanding recombining plume of a helium arc jet in 1963. They determined population densities of upper excited states including substates for each principal quantum level greater than two. Their measurements showed that the sublevels within a principal quantum state exhibited Boltzmann distributions at the same excitation temperature. Recombination rates based upon the QSS were approximately determined and were in reasonable agreement with the CRR models of Bates, et al. (Refs. 3 and 4) and Hinnov and Hirschberg (Ref. 11). Their population density measurements were not compared to calculation.

One of the recurring problems of experimental studies of helium recombination was the role of the molecular helium ion He_2^+. In 1964 Collins and Robertson (Refs. 13, 14, and 15), with a series of selective excitation experiments on a flowing afterglow, and Niles and Robertson (Refs. 16 and 17), using a series of interference filters to study the spectral emission, found that He^+ recombination dominated the afterglow at low pressures (less than about 20 torr) and above this the molecular recombination quickly dominated the afterglow. Both species were found to follow CRR, although at different rates, even in the

presence of the other. At about the same time, Rogers and Biondi (Ref. 18) published the results of experiments on the helium afterglow in which the attempt was made to reconcile the observed large electron-ion recombination losses. Although the goal was not fully realized, they argue that dissociative recombination appeared to be the most likely candidate for the line shapes observed in the late afterglow.

Collins and Hurt (Ref. 19) report on helium afterglow spectral line measurements made in 1967 from which they determined population densities of eigenlevels through principal quantum number 25. They found that there were three separate groups of quantum levels characterized by decay times. A lower group and an upper group exist whose quantum levels within the group decay with the same lifetimes, although the lifetime is different between the two groups. The other group is an intermediate one in which the quantum levels within the group all decay with different lifetimes. They found excitation temperatures of 300°K for the upper group and 2,000°K for the lower group. The upper group was determined to be in equilibrium with the free electrons by comparing exponential decay constants of the levels, the free electron density, and a calculated decay constant for He^+. By a similar comparison it was determined that the decay rate of the lower group is proportional to the square of the electron density and the first power of the concentration of He^+. In a follow-up analysis, Collins (Ref. 20) computed the logarithmic derivative of excited state populations as functions of logarithmic electron density. These calculations, based upon the quasi-steady-state approximation, yielded recombination rates in semiquantitative agreement with experiment (Ref. 19).

Recent studies of helium recombination of some significance are those of Chen (Ref. 21) and Johnson and Hinnov (Ref. 22), both published in 1969. Chen appears to have made the first direct calculation of helium recombination rates, as well as those of other atoms, based on the QSS assumption. Chen's approach was the same as that of Byron, et al. (Ref. 2) and Bates, et al. (Ref. 23) for hydrogen, in which the minimum in the total rate of de-excitation of atoms as a function of the energy level of the excited states is found. Chen also made experimental measurements of recombination rates in a discharge tube and found more or less satisfactory agreement with calculation.

Johnson and Hinnov (Ref. 22) made spectroscopic measurements of excited state population densities in the C-Stellerator at Princeton and compared them to quasi-steady-state calculations of the densities using various assumed formulations for collisional cross sections and at

various excitation temperatures. These measurements were at quite low pressures so that the presence of molecular helium could be discounted. The comparison between their calculated and measured recombination rates was quite good for moderate times in the afterglow. At early times, however, the calculated rates were noticeably smaller than the measured rates.

The aforementioned studies of helium recombination have assumed the QSS a physical as well as a mathematical reality, just as in the analytic studies of hydrogenic recombination. Little of that previously cited work was concerned with comparison of measured and calculated excited state densities in the region of nonequilibrium. The work of Johnson and Hinnov (Ref. 22) is an exception to this but they also use the QSS and this leads to discrepancies. This is discussed further in Section 7.0.

The solution to the original system of rate equations from which Bates, et al. (Refs. 3 and 4) obtained the CRR model does not demand the QSS assumption, although the calculations are made much easier by its use. A solution of the complete set of Eigenstate Rate Equations (ERE) is possible using modern computational methods, and makes possible a more detailed examination of the approach to the QSS and permits estimates to be made of the time to reach the QSS solution to the ERE.

Since 1967, two groups of investigators (Refs. 24, 25, 26, and 27) have attacked the problem of removing the QSS assumption for hydrogen plasmas. Limbaugh, Carstens, McGregor, and Mason (Refs. 24, 26, and 27) were primarily concerned with the pure afterglow problem in which the electron temperature remains constant. The purpose of that investigation was to examine the fundamental consistency of the collisional-radiative recombination model to the full transient solution and to determine quantitatively the differences in the decay of plasmas in which a radiative metastability existed. Among the findings was that the metastable state definitely affected the decay and that under reasonable conditions, there could be a physically significant time before the QSS is established. Gordiets, Gudsenko, and Shelepin (Ref. 25) were primarily concerned with the effects of sudden changes in the plasma parameters, such as excitation temperature or free electron density upon the plasma decay. They show that in such cases the parametric changes could have an appreciable effect upon the plasma decay. Although detailed quantitative comparisons between the results of the two studies are difficult because of the different problems being solved, they do show qualitative agreement with each other.

1.2 APPROACH AND GOALS

The relative success of those earlier studies illustrated the potential of the ERE to provide a detailed accounting of the interaction between free electrons and the various energy states of the afterglow plasma. This success, along with the realization that only through use of the ERE rather than CRR theory could the acquisition of the QSS be studied, and a curiosity about the processes which bring a plasma to the QSS, provided the underlying motivation for the study reported here.

For these purposes, it was decided to extend the earlier work, summarized in Ref. 26, to the helium atom. Helium is next to hydrogen in simplicity and has been investigated extensively experimentally. In addition, its electronic structure seems to promise more interesting study since the low-lying energy levels are farther apart than those of hydrogen and contain both singlet and triplet states. The larger energy spacing causes the collisional effects to be less effective than for hydrogen. To the author's knowledge, this is the first application of the ERE to helium and the present computer program is the only one in existence which can obtain the transient solution to the ERE.

The purpose of this study is to investigate the basic mechanisms by which the QSS is established and to attempt to assess the validity of CRR theory as applied to physically realizable plasmas. To achieve this, the transient solution to the ERE with the restrictions and assumptions to be discussed below will be obtained for several plasma conditions. These studies break into two groups: (1) pure afterglows and (2) perturbations. The pure afterglows are studies in which the plasma is allowed to relax from an initial LTE distribution toward the QSS distribution. The perturbations are studies in which certain plasma parameters are perturbed from the acquired QSS and the relaxation of the plasma is observed.

In the realization of the final goal of this study there are several significant objectives:

1. To determine the mechanisms by which the QSS is established for helium plasmas.
2. To observe the decay characteristics of both the excited state distribution and the free electron density in He plasmas and to determine the applicability of the results of CRR theory to helium in the early portion of plasma decay.

3. To observe the variation in the time for QSS to be established in He plasmas for different values of electron temperature, electron density, and total number density, and to observe the systematic trends.
4. To gain insight into the total coupled processes by which plasmas decay.

In the following pages, Section 2.0 contains the theoretical model and indicates those physical processes which are ignored and the physical assumptions which are made in setting up the theoretical description of the plasma. Section 3.0 includes a brief examination of the various rate coefficients and transition probabilities used in the ERE and indicates the accuracy of the specific technique used to evaluate the collisional cross sections. In Section 4.0 the numerical techniques used to effect the solution to the ERE are described and the limitations of the present computer program are indicated. In Section 5.0 and 6.0 the results of the computations are reported, and in Section 7.0 the data are interpreted in terms of effects on measurements and application to decaying helium afterglow plasmas. The findings of this study and comments upon their impact on the interpretation of existing measurements and the design of future experiments are summarized in Section 8.0. Also included in Section 8.0 is a discussion of recommended future research using the ERE, and certain simplifications which should be incorporated in further work are pointed out.

2.0 TRANSIENT PLASMA BEHAVIOR

This section examines the development of the system of equations which will describe the transient properties of the population density of the various internal energy states available to a singly ionized monatomic plasma. In the following subsections a generalized description of the physical problem shows the role of the separate processes contributing to the excitation or de-excitation. Subsequent to this discussion each of the phenomena will be discussed separately leading to a detailed mathematical description of each process. Included in this discussion will be the simplifications and approximations which are necessary to make the mathematical system tenable to the physical problem at hand. Finally the detailed descriptions are combined to illustrate the full description of the physical problem and the development of the CRR model is described.

2.1 THE GENERALIZED PROBLEM

To provide a detailed description of a plasma which may not be in equilibrium it is necessary to include each energy state available to each plasma constituent. By considering some arbitrary control volume in space and examining each energy state within the control volume it is possible to arrive at a simple model for the plasma. The dimensions of the control volume will be assumed to be small with respect to the total extent of the plasma yet large enough that there are a sufficient number of particles contained within it for statistical properties to be meaningful. Any property measured or ascribed to the constituents of the plasma within the control volume is assumed constant throughout the control volume. If the plasma exists in field-free space, then the population density of a given energy state will be affected by local interactions between the constituents of the plasma contained within the control volume and by a net flow of the plasma constituents across the boundaries of the control volume.

The time rate of change of the population density of some specific energy level within the control volume can be written symbolically:

$$\frac{dn(p)}{dt} = \left(\frac{\partial n(p)}{\partial t}\right)_{micro} + \left(\frac{\partial n(p)}{\partial t}\right)_{space} \qquad (1)$$

where n is population density, p symbolically represents the set of quantum numbers necessary to describe the particular energy state, t is time, and the subscripts "micro" and "space" refer to the microscopic processes and spatial variation described above. An equation of this general type must be written for each of the energy states available to each plasma constituent and the solution of the resultant system of equations will yield a time-dependent function for the population density of each state.

Including that portion of Equation (1) which refers to the spatial variation of n (p) will generally necessitate including the statements of conservation of energy and momentum as well as the statement of conservation of mass. As discussed earlier, the effort here is an examination of the mechanisms by which the QSS is obtained and an assessment of the importance of including the transient coupling in analysis of helium plasmas. The present work is to be considered a first step leading to eventual modeling of plasma phenomena, and inclusion of the spatial

variations, although necessary for final realization of the goal, is inappropriate at this stage of development. Hence, subsequent discussion will consider all of space as being filled with the plasma, with no sources or sinks, and with no gradients present.

2.2 THE EIGENSTATE RATE EQUATION (ERE)

The physical phenomena comprising the contributions to the transient description of the population density on the microscopic level can be treated by examining the plasma within the control volume as if there were no convective variations. Within this control volume, the monatomic plasma consists of neutral atoms in each of the possible electronic energy states, ions, and free electrons. For this work which will be concerned with the helium atom single ionization will be assumed so that the concentration of ions and free electrons will be identical. Further, the electrons will be assumed to exhibit a Maxwell-Boltzmann velocity distribution independent of the kinetic temperature of the atoms or other heavy bodies.

Each of the mechanisms causing a change in the population density of a particular eigenstate can be characterized by a rate coefficient. The instantaneous rate by which the level is being populated or depopulated by a given mechanism is the product of the rate coefficient and the concentrations of the reaction partners. The microscopic processes, the instantaneous rates, and the rate coefficients included in this study can be listed as follows:

1. Inelastic and super-elastic electron-atom collisions. For inelastic excitation, the necessary energy to effect the transition is supplied by the kinetic energy of the free electron. For the super-elastic de-excitation, the excess energy increases the kinetic energy of the free electron. The rate coefficient for this reaction is K(p;q) where p and q represent initial and final energy states of the bound electron. The instantaneous rate for this process is given by

$$\frac{dn(p)}{dt} = -n_e \; n(p) \; K(p;q) \qquad (2)$$

for depopulating of state p to state q. In the above, n represents population densities and the subscript e refers to the free electron density. Obviously the same expression with a plus sign will describe populating of state q from state p. Units of K(p;q) are cm^3/sec.

2. Electron-ion encounters in which a single ion captures a free electron into some bound energy state with an attendant emission of radiation. This is more commonly called radiative recombination and is described by the radiative recombination coefficient, β (p). The instantaneous rate of filling of state p is given by

$$\frac{dn(p)}{dt} = n_e \, n^+ \, \beta(p) \tag{3}$$

where n^+ is the ion concentration. Units of β (p) are cm^3/sec.

3. Electron-electron-ion encounters resulting in a neutral atom with one electron in a bound energy state and the excess energy contributing to the kinetic energy of the free electron. This three-body recombination reaction is characterized by K (c;p) where c symbolizes the electron continuum as the initial state of the reaction partners. The instantaneous rate is given by

$$\frac{dn(p)}{dt} = n_e^{\,2} \, n^+ \, K(c;p) \tag{4}$$

Units of K (c;p) are cm^6/sec.

4. Ionization collisions in which a free electron impinges upon a neutral atom with sufficient energy to ionize the atom resulting in a singly charged ion and two free electrons. This reaction might be thought of as the equilibrium partner of the three-body recombination described above and is characterized by K (p;c). The instantaneous rate is

$$\frac{dn(p)}{dt} = -n_e \, n(p) \, K(p;c) \tag{5}$$

Units of K (p;c) are cm^3/sec.

5. Spontaneous radiative transitions in which a bound electron relaxes spontaneously to a lower bound state with an attendant emission of radiation. This mechanism can contribute to both populating and depopulating a level and is characterized by the Einstein transition probability

A (p;q). The instantaneous rate for depopulating state p to some lower state q is

$$\frac{dn(p)}{dt} = -n(p)\ A(p;q) \tag{6}$$

while the instantaneous rate for populating state p from some higher state m is

$$\frac{dn(p)}{dt} = n(m)\ A(m;p)$$

Units of A (p;q) are 1/sec.

In addition to the above processes other phenomena which must be considered for their effect upon the population densities are: atom-atom and atom-ion collisions, photon absorption, induced emission, and the molecular ion effects. This study will involve pressures sufficiently low that the molecular ion can be ignored (Ref. 14).

Heavy body collisions can be ignored for this application also because of the low densities and heavy body temperature examined in this study. For example, for a total particle density of 10^{15} $1/cm^3$ and a heavy body temperature of 3,000°K, an elevated state population density typical for an electron velocity distribution at 10,000°K is of order 10^6 $1/cm^3$. Considering collisions between excited state atoms and assuming an atomic radius of 1 Å, one finds the collision frequency to be of order 10^2 encounters/sec/cm^3 for these atom-atom collisions. The electron-atom collision frequency, assuming an electron temperature of 10,000°K and 1-percent ionization, is of order 10^{10} encounters/sec/cm^3. Obviously the atom-atom encounters are insignificant in this study compared to electron-atom collisions.

Absorption and stimulated emission can also be discounted for the purposes of this study. Since the stimulated emission and absorption coefficients differ only by the ratio of statistical weights, only absorption of resonance radiation can be significant. Accurate accounting of absorption requires including geometry considerations, and this is beyond the scope of this study. An estimate of absorption effects is obtained from Robben, Kunkel, and Talbot (Ref. 12) who found that for a heavy body temperature of 1,000°K and particle density of order 10^{17} $1/cm^3$ the mean free path of the helium $1^1S - 2^1P$ resonance radiation was about 0.2 mm. This distance, although small enough to make it

necessary to consider resonance radiation absorption in many physical experiments, is sufficiently large that there will not be appreciable absorption in the small control volume on which the present study is based. Further, as will be seen, the particle density used in the estimate (Ref. 12) is near the upper bound of the total densities of the plasmas studied here. Thus, absorption can be neglected for the purposes of this study and the plasmas are considered to be optically thin. For one set of plasma conditions, comparative calculations are made at different optical thicknesses to examine the effect upon the mechanisms by which QSS is acquired.

The total time rate of change of the population density of state p is just the algebraic sum of the five basic processes described above:

$$\frac{\partial n(p)}{\partial t} = -n_e n(p)\left[\sum_{q=1}^{\infty} K(p;q) + K(p;c)\right] - n(p) \sum_{q<p} A(p;q)$$

$$+ n_e \sum_{q=1}^{\infty} n(q)\, K(q;p) + \sum_{q>p}^{\infty} n(q)\, A(q;p)$$

$$+ n_e^2\, n^+\, K(c;p) + n_e\, n^+\, \beta(p) \qquad (7)$$

In the formulation of Equation (7) all K(p;p) are zero and any A(p;q) is zero if the dipole selection rules are violated.

In Eq. (7) the first three terms express the rate with which state p is depopulated due to collisional internal transitions (Eq. (2)), collisional ionization (Eq. (5)), and spontaneous radiative transitions (Eq. (6)), respectively. The remaining terms express populating rates due to collisional internal transitions (Eq. (2)), radiative transitions (Eq. (6)), three-body recombination (Eq. (4)), and radiative recombination (Eq. (3)).

There will be a similar equation for each eigenstate avilable to the atom. In addition, the continuum density n_e enters into each equation as a product with each of the other bound state densities. Hence, the resultant system of equations is a rectangular non-linear system of infinite extent. However, by requiring that there by no loss or gain of atoms by diffusion or convection, the total concentration will be constant. Thus, taking advantage of single ionization so that the electron and ion

densities are identical, the conservation of heavy particles is expressed by the equation

$$\sum_{p=1}^{\infty} n(p) + n_e = n_o \tag{8}$$

where n_o is the total heavy particle concentration. Equation (8) added to the system causes the system to become square and in principle determinate.

The system of equations has the capability of yielding a complete description of the instantaneous population density distribution for those monatomic plasmas in which there are electronic transitions only because of reactions between the microscopic constituent particles. Additional processes, such as those ignored in this study, can be accounted for by expressing them functionally the same way as processes 1 through 5.

Although the system is infinite in extent, thus making the solution impossible, it may be truncated at some finite energy level as a reasonable approximation. This is because for progressively higher energy levels the population densities decrease monotonically with energy for an equilibrium plasma. Hence, there will be an upper energy level above which all levels have population densities insignificant with respect to the lower energy levels and the continuum. Also, reactions between plasma constituents causing a transfer to bound electrons between the low-lying states and upper states will be insignificant compared to transfer rates between energy states lying close together. Finally, because of the close-lying energy levels of the upper states and their close proximity to the ionization potential, reactions with the free electrons will establish an equilibrium configuration among these upper states as well as with the continuum. Hence, because of the relative insignificance of the densities of the high-lying levels, the relative unimportance of reaction rates between the low-lying and high-lying energy levels, and because there will be some upper energy level which is assuredly in equilibrium with the continuum, the system of equations can be truncated at this upper level with minimal loss of accuracy.

The minimum energy level for which this is true, of course, depends upon the kinetic temperature exhibited by the free electrons. It should also be noted that this is in effect postulating the existence of the so-called critical level, which has been described as the lowest-lying energy level in equilibrium with the continuum. For the purposes of this study, the upper level considered was dictated more by available

computer size than by physical considerations and thus the critical level will be indicative of limits on plasma conditions which can be studied with the present program.

2.3 THE COLLISIONAL-RADIATIVE RECOMBINATION (CRR) MODEL

The system of Eqs. (7) and (8), with the truncation considerations discussed above, provides the starting point for the development of the CRR model (Refs. 3 and 4) which previous investigators have used to study plasma decays. This model for optically thin plasmas utilizes the QSS approximation which assumes that the time rate of change is zero for all bound states other than the ground state. The CRR model is applied to those plasmas in which the ground state density and free electron density are much larger than excited state densities and in which the electronic kinetic temperature is much less than the first excitation energy so that collisional transfers from the ground state are small. These conditions lead to the assumption that a quasi-equilibrium distribution is established "almost instantaneously" without appreciable effect on the continuum density and that collisional excitation and de-excitation rates will so largely dominate the decay rate for the plasma that the QSS configuration is maintained. Consequently, the derivatives for the time rate of change of these excited levels can be set to zero. In such a situation the time rate of change of the ground state is the algebraic negative of the time rate of change of the free electrons, $\dot{n}(1) = -\dot{n}_e$. The excited state densities are constant and the system, Eqs. (7) and (8), becomes a single differential equation and a system of algebraic equations. The only variables are the ground state density and the continuum density so that Eq. (7) for the ground state can be written

$$\frac{dn(1)}{dt} = \alpha n_e^2 - S\, n(1)\, n_e \tag{9}$$

where α and S are defined as the collisonal-radiative recombination and collisional-radiative ionization coefficients, respectively. The α and S can be expressed as functions of n_e, electron temperature, and atomic parameters by reduction of the algebraic portion of the system. The determination of α and S under these approximations was the problem to which Bates, Kingston, and McWhirter (Refs. 3 and 4) addressed themselves.

Although the values of α and S for various plasmas are periodically improved and updated as knowledge progresses, the basic model utilizing the QSS assumption and depicted by Eq. (9), or some variations of

Eq. (9), has become the standard model by which plasma decay and growth phenomena are analyzed. Even in applications where the physical problem supports transient density or electron temperature changes the QSS condition is assumed to establish itself in infinitesimal times compared to other characteristic times for the plasma.

In most applications, as in the case here, the collisional-radiative ionization coefficient, S, is an ignorable quantity. In this case the recombination of the free electrons depends only upon the CRR coefficient, α,

$$\dot{n}_e = - \alpha n_e^2$$

The very assumption of QSS is alien to a detailed study of the mechanisms by which a plasma decays. The only way to examine this is to actually solve the transient problem with all the non-linearities and coupling between states for several plasma conditions and this is the subject of this study.

2.4 THE CRITICAL LEVEL AND EQUILIBRIUM CONFIGURATION

The concept of the so-called critical level is very important to simplified methods of obtaining recombination rates (Refs. 11, 21, and 22). The concept is used here only to provide a bound on the plasma conditions for which the present computer program is valid.

Physically the critical level is that lowest energy level which is maintained in equilibrium with the free electron density. This equilibrium density is given by the modified Saha equation:

$$n(p) = n_i \, n_e \, \frac{g_p}{2g_i} \left(\frac{h^2}{2\pi m k T_e} \right)^{3/2} \exp \, (I_p/kT_e)$$

where n_i and n_e are the ground state ion and electron densities, respectively, and I_p is the ionization potential of quantum level p. All quantum states above the critical level will also be in equilibrium with the free electrons. Thus the net rate with which bound electrons above and including the critical level fall to energy levels below the critical level is immediately taken up by recombination of the free electrons into these upper levels and this is the recombination rate.

The critical state in other studies (Ref. 2) is found by formally minimizing the recombination coefficient with respect to energy state. Because of the form of the collisional rate coefficients Section 3.0, evaluation can become quite tedious.

Rather than attempt a formal analysis for the critical level in this study, the approach will be to observe the population densities of the various quantum levels in relation to the value which would be in theoretical equilibrium with the free electron density calculated from the modified Saha equation. In this manner the critical level can be empirically observed independently of problems attendant with evaluation of complicated expressions.

A term which is used in this study which merits explanation is "equilibrium configuration." This term applies to any two or more excited states whose densities satisfy the Boltzmann relationship

$$\frac{n(p)}{n(q)} = \frac{g_p}{g_q} \exp\left[-(E_p - E_q)/kT_e\right]$$

The densities of states which are in an equilibrium configuration satisfy the above equation regardless of their relationship to the rest of the distribution.

3.0 TRANSITION PROBABILITIES, RATE COEFFICIENTS, AND CROSS SECTIONS

Although the detailed rate coefficients and transition probabilities are not in themselves the object of this study, they are critical components of the full ERE and CRR models. The magnitude of each of the rate coefficients and transition probabilities indicates to what extent a particular type of transition will occur and the relative importance of the various mechanisms. This dependence of the results of either of the ERE or CRR models upon the various coefficients and probabilities makes it desirable to look at the detailed evaluation of these parameters.

3.1 EINSTEIN TRANSITION PROBABILITY

The Einstein spontaneous transition probability is the rate with which atoms radiatively decay from an excited electronic state to a lower electronic state. The value can be obtained from time-dependent

perturbation theory if one has at hand the wave functions of the various bound states. The transition probabilities presently available have been compiled in several publications (e.g., Refs. 28 and 29) but neither these nor any other reported results found in the literature include much detail concerning transitions involving high principal quantum numbers ($p > 5$). However, for these higher energy states the wave functions will be sufficiently similar to hydrogen wave functions that transition probabilities for hydrogen and helium will be approximately equal. Care must be exercised as this approximation will only be valid for interactions among upper states with some unspecified lower bound.

Niles (Ref. 28) has tabulated most of the radiative transition probabilities available at that time (1967). The compilation includes data for all transitions from levels with principal quantum number $p \leq 15$ to states with principal quantum number $p \leq 3$. In addition to these, the compilation includes transitions terminating on quantum level 4 except for the $4^{1,3}$ F - $p^{1,3}$ G transitions. The transitions listed include the interactions of those lower eigenstates where strong departure from the hydrogenic approximations should be observed. Hence, for these transitions to the lower energy states, the values reported by Niles (Ref. 28) were used.

Transition probabilities for the $4^{1,3}$ F - $p^{1,3}$ G and all higher transitions were computed using the hydrogenic approximation. These values for the transition from state (p, ℓ) to state $(p' \ell')$ are given by (Ref. 30)

$$A(p,\ell;p'\ell') = \frac{64\pi^4\nu^3}{3h\,c^3} \frac{\max\,(\ell,\ell')}{2\ell+1} e^2 a_o^2 \left| < p'\ell' \; r \; p\ell > \right|^2$$

where ν is the frequency of emitted radiation and a_o is the Bohr radius. The matrix elements,

$$<p'\ell' \mid r \mid p\ell> = \int_o^\infty R(p',\ell') \; r \; R(p,\ell) \; r \; dr$$

where $R(p, \ell)$ represents the hydrogen radial wave function, are listed by Green, Rush, and Chandler (Ref. 30) for angular momentum values through a principal quantum number of 20. Detailed results of these calculations will not be given because of the large bulk of the data and the relative availability of the values in the literature. The detailed transitions among the upper levels are relatively unimportant for this investigation because the conditions will be restricted to those

cases for which the plasma is strongly collision dominated among the upper levels. Under these conditions, the population density of the angular momentum states within a principal quantum level can be characterized by a Maxwell-Boltzmann distribution and the entire set of states is thus adequately described by a single state which has properties represented by an average of the detailed properties of the individual substates. In low density applications where radiative terms are important, the approximations made here would not necessarily be valid, and care must be exercised in applying the hydrogenic approximation.

3.2 RATE COEFFICIENTS

As mentioned earlier, the rate coefficients are related to the probability that a particular transition will occur upon collision. It is in fact the probability that a collisional transition will occur when an atom encounters an electron with kinetic energy between E and E+dE integrated over the kinetic energy distribution of the electrons.

If $f_e(E)$ is the fractional number of electrons with energy in the range E to E+dE, v_e is the kinetic velocity of these electrons, and n_e is the concentration of these electrons on a volume basis, then the product $n_e v_e f_e(E)$ is the number of encounters between the electrons and a hypothetical unit area per unit time along a velocity vector traveled by the electron. Now if $Q(E)$ is the effective area the atom presents to the electrons in this energy range for a particular transition, the number of encounters with this area per unit time is given simply by the product

$$Q(E)\ n_e v_e f_e(E)$$

Hence, if the concentration of atoms with cross section Q(E) is n, the total time rate of change of atoms due to collisions with electrons with all energies is

$$\frac{dn}{dt} = n\, n_e \int_0^\infty Q(E)\ f_e(E)\ v_e\ d\,E$$

Defining the rate coefficient as the integral

$$K = \int_0^\infty Q(E)\ f_e(E)\ v_e\ d\,E$$

noting that

$$E = \frac{1}{2} m_e v_e^2$$

and requiring the electron distribution to be Maxwell-Boltzmann,

$$f_e(E) = \frac{2}{\sqrt{\pi}} \left(\frac{1}{kT_e}\right)^{3/2} E^{1/2} \exp(-E/kT)$$

yields

$$K = \frac{8\pi}{\sqrt{m_e}} \left(\frac{1}{2\pi kT_e}\right)^{3/2} \int_0^\infty Q(E) \exp(-E/kT)\, E\, dE$$

for the rate coefficient.

The development to this point has been general, requiring only the assumption of Maxwell-Boltzmann statistics for the electron energy distribution and a delta function distribution in energy space for the atoms. Hence, if one has Q(E) for each of the various processes, the evaluation of each of the rate coefficients will proceed straightforwardly. It is this evaluation of Q(E) to which subsequent discussion is turned.

3.2.1 Two-Body Internal Transition Rate Coefficient, K(p;q)

The two-body internal transition rate coefficient is given by

$$K(p;q) = \frac{M8\pi}{\sqrt{m_e}} \left(\frac{1}{2\pi kT_e}\right)^{3/2} \int_{|E_p - E_q|}^\infty Q_{pq}(E) \exp(-E/kT)\, E\, dE \quad (9)$$

In the above equation, p and q symbolically represent sets of quantum numbers describing initial (p) and final (q) states, M is a parameter giving the number of electrons available for excitation (M = 2 for p = ground state, m = 1 for p > ground state), $Q_{pq}(E)$ is the energy-dependent cross section for collisional transitions from the p^{th} to the q^{th} bound states, E is the kinetic energy of the bombarding electron, and E_p and E_q are kinetic energies of the bound electron in the p and q states.

There are many techniques for the evaluation of Q_{pq} (E) for transitions between bound states utilizing various approximations. Moiseiwitsch and Smith (Ref. 31) give a comprehensive review of the various techniques and results from both theoretical calculations and experimental measurements available in 1968. The most extensive tabulation they give for helium excitation was first calculated by Ochkur and Bratsev (Ref. 32) and is based upon quantum mechanical considerations.

Rather than use the more satisfying quantum mechanical calculations, however, it was decided to use the simple classical Gryzinski method (Ref. 33) for these determinations. This choice is motivated primarily by the ease with which these cross sections may be evaluated, the observation that most previous investigators of CRR also used the Gryzinski method, and the fact that the method appears to be as accurate as other techniques.

Gryzinski's method is based on a classical analysis describing the collision as a two-body coulomb interaction between the orbital and incident electrons. In earlier work (Ref. 34) he assumed that the orbital electrons had a certain fixed energy. In later work (Refs. 33, 35, and 36) this was extended to the specific case of atomic collisions in which the bound electron has a velocity distribution

$$f_v = \left(\frac{v}{v_m}\right)^3 \exp\ (-v/v_m)$$

where v_m is the mean electronic velocity.

The choice for this distribution appears to be arbitrary, being based on phenomenological observation of results rather than developed from first principles. However, the relative success of the technique is sufficient to justify its use.

The cross sections obtained by the Gryzinski technique yield a result for a transfer of energy equal to or greater than some value U_{pq} from the incident electron to the bound electron. Expressed in terms of a parameter x, the Gryzinski cross section is written

$$Q_{pq}(x) = \frac{\pi e^4}{U_{pq}^2} \frac{A}{x} \left(\frac{x}{A+x}\right)^{3/2} \left(\frac{x-1}{x}\right)^{\frac{2A+1}{A+1}} \left[\frac{1}{A} + \frac{2}{3}\left(\frac{2x-1}{2x}\right) \ln\left(e+\sqrt{\frac{x-1}{A}}\right)\right] \tag{10}$$

where

$$x = E/U_{pq},$$

$$A = E_p/U_{pq}$$

In the above, E is the kinetic energy of incident electron, E_p is the kinetic energy of bound electron, e is the electronic charge, and e is the natural logarithm base.

Identifying U_{pq} with the threshold energy for excitation to the q^{th} state from the p^{th} state, the expression above gives the cross section for an energy transfer which not only is sufficient to excite the bound electron to the state E_q, but may be large enough to excite to the state E_{q+1}. Hence, in the determination of $Q_{pq}(x)$, it is necessary to form the difference:

$$Q_{pq}(x) = Q_{pq}\left(\frac{E}{U_{pq}}\right) - Q_{pq+1}\left(\frac{E}{U_{pq+1}}\right) \tag{11}$$

Note that $Q_{pq+1}(E/U_{pq+1})$ is vanishingly small for $E < U_{pq+1}$.

Using the parametric form of $Q_{pq}(x)$, the rate coefficient K(p;q) is

$$K(p;q) = \frac{M8\pi}{\sqrt{m_e}}\left(\frac{1}{2\pi kT_e}\right)^{3/2}\int_1^{\infty} Q_{pq}(x)\exp\left(-\frac{U_{pq}x}{kT_e}\right)U_{pq}^{2}\,x\,dx \tag{12}$$

Thus far there have been no applications of the results of quantum mechanics. The above discussion centered on a straightforward energy transfer from an incident classical electron impinging upon an orbital electron, the orbital electron receiving enough energy from the incident electron to raise it to some higher energy state. Now from quantum mechanics it is known that some transitions will be allowed and that other transitions are forbidden. Hence, the dipole selection rules $\Delta L = \pm 1$, $\Delta S = 0$ must be applied so that Eqs. (9) and (11) are used only for those transitions between energy states satisfying these rules.

Another process in these excitation collisions which can occur is that of an exchange collision in which the orbital electron is ejected and the impinging electron is captured by the nucleus in some higher energy

state. For these collisions, Gryzinski's development assumes that the orbital electron has zero velocity and results in the parametric form

$$Q_{pq}(x) = \frac{1}{2}\,\frac{\pi e^4}{U_{pq}^2}\begin{cases}\dfrac{x-1}{A(x+A)^2(x+A-1)}, & x \leq B\\[2ex] \dfrac{B-1}{(x+A)(x+A-1)(x+A-B)}, & x \geq B\end{cases} \tag{13}$$

where

$$x = E/U_{pq}$$

$$A = U_p/U_{pq}$$

$$B = U_{pq+1}/U_{pq}$$

$$U_{pq} = \left|E_p - E_q\right|$$

and

$$U_{pq+1} = \left|E_p - E_{q+1}\right|$$

The factor of 1/2 in the expression is the probability that an impinging electron has the proper spin orientation to effect the transition. The rate coefficient will have the same functional form as Eq. (12), the only real difference being the functional form of the cross section (Eq. (13) as opposed to Eq. (10)) and the restriction of its application to those transitions whose initial and final states violate the dipole selection rules $\Delta L = \pm 1$, $\Delta S = 0$.

There is some judgment required in determining precisely what state to use for U_{pq+1}. For those transitions which are dipole allowed, it is obvious that the state to use for U_{pq+1} is the next higher state which will also satisfy the selection rules. For dipole-forbidden transitions, however, the choice is not quite so obvious. The exchange cross section is applied to any transition which is dipole forbidden. This means any transition which has $\Delta L \neq \pm 1$ or $\Delta S \neq 0$. For a particular transition, there is a specific ΔL or ΔS. This implies specific conditions on the impinging electron. The next higher excitable state will be that one which is compatible with the ΔL or ΔS involved in the specific excitation of

interest. Hence, the q + 1st state will be the next higher state with the same ΔL or ΔS value as the q^{th} state. Dugan and Sovie (Ref. 37) examine the behavior of the Gryzinski cross sections with various choices of U_{pq+1} and this choice is in accord with their findings.

Because of the large bulk of the data involved in these calculations, a detailed accounting of the values for the rate coefficients will not be given here but rather the results of using the cross section expression applied to selected transitions will be discussed.

Figures 1 and 2 illustrate the results of the Gryzinski cross section calculations as well as calculations based on the Ochkur approximation compiled in Ref. 31 and experimental data (Refs. 38 and 39) for the 1^1S - 3^1P and the 1^1S - 3^3S transitions, respectively. Results of ground state excitation are assumed to be representative for the other excitations. A scarcity of data in the literature prevents comparisons of excitations among the higher states. As can be seen, the calculation based upon the Ochkur approximation gives more satisfying comparison with experimental data for both the direct excitation and the exchange excitation. However, use of the Ochkur approximation is in itself an adaptation of the Born-Oppenheimer method and is thus theoretically applicable only for the high-energy collisions. The electronic kinetic

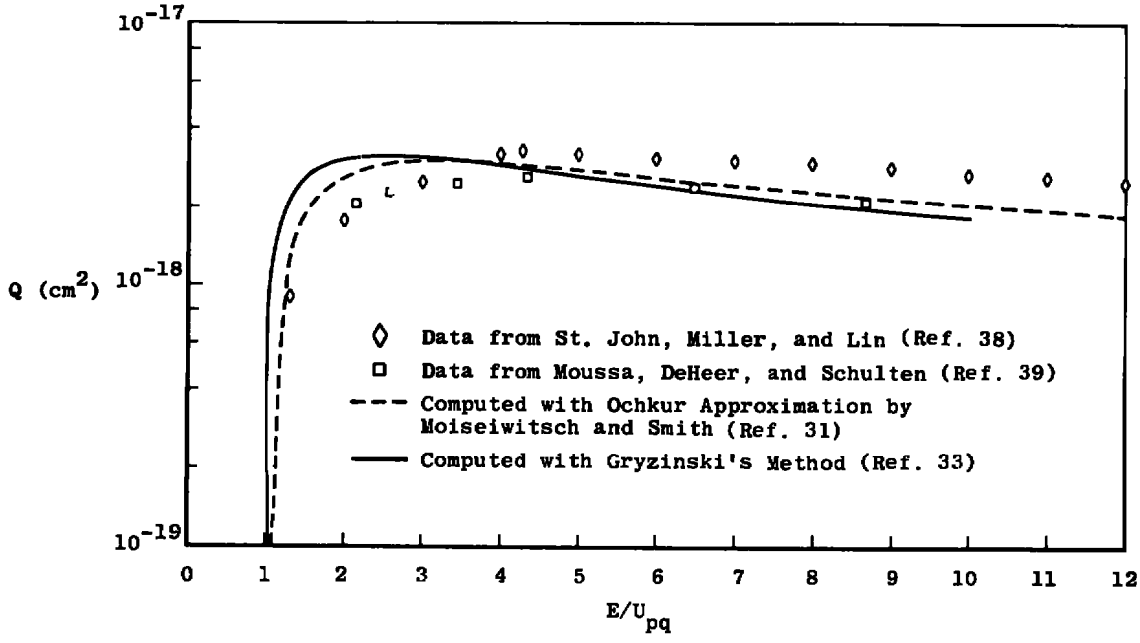

Figure 1. 1^1S - 3^1P excitation cross section.

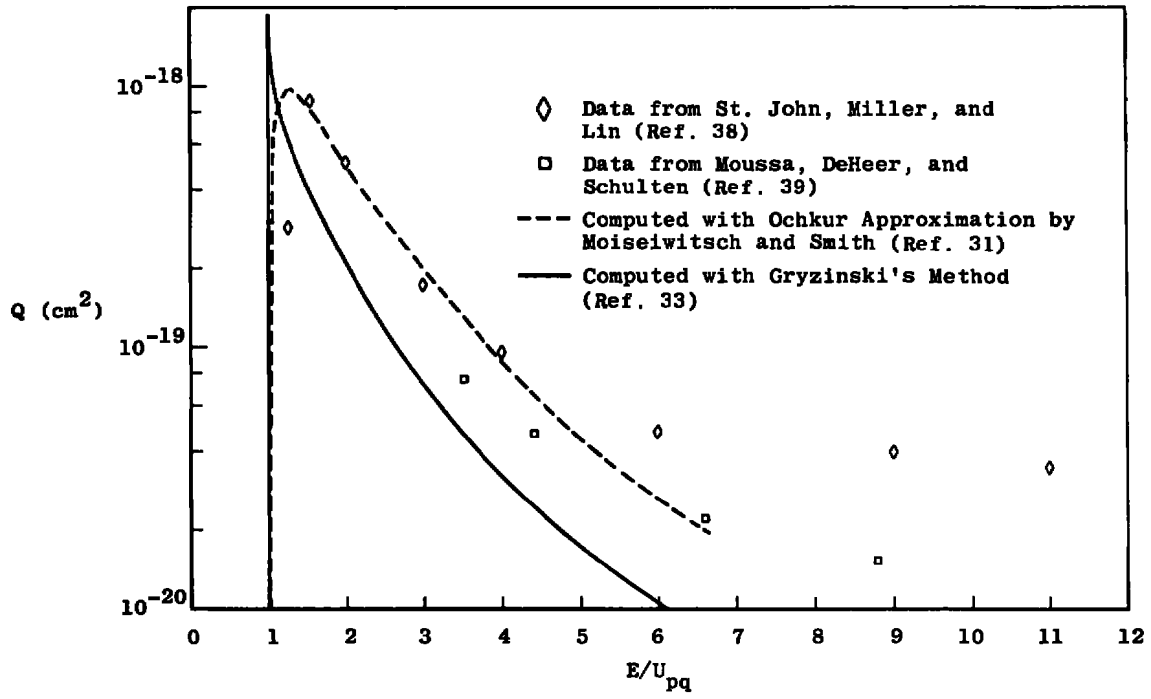

Figure 2. $1^1S - 3^3P$ excitation cross section.

energies with which this study is concerned will peak at about 1 ev or less so that the low energy region of the cross section is the most important.

In examining the lower energy region of Fig. 1 it can be seen that the Gryzinski cross section will overestimate the experimental work of St. John, et al. (Ref. 38) by at most about a factor of two in the energies close to threshold (x = 1). It is difficult to be more precise in these comparisons because of the scarcity of experimental work in these regions close to threshold. Calculations of the rate coefficient for the $2^3S - 3^3P$ transition using the Gryzinski technique and the Ochkur approximation for cross sections yield results which agree well within a factor of two. It is thus reasonable to expect the calculated rate coefficient to overestimate the true rate coefficient by no more than a factor of two and in fact probably to be better than this because of the underestimation of the cross section at higher energies by the Gryzinski method.

In examining the exchange cross section (Fig. 2) one can see that the comparison between calculation and experiment is not as good as that for direct excitation, although there does appear to be a convergence of sorts between the Ochkur approximation and the later experimental work of Moussa, et al. (Ref. 39). The Gryzinski cross section overestimates the other work by several orders of magnitude at the sharp peak and

underestimates the work of Moussa by typically a factor of two at the high energies. Hence, because of the sharp peak in the region of lowest energy, it is anticipated that the calculated rate coefficient will underestimate the true rate coefficient by somewhat less than the factor of two. At any rate the exchange cross sections will be somewhat less important than the cross sections for direct excitation because the rate coefficients for direct excitation are much larger than those for exchange excitation. For example, at an electronic kinetic temperature of 10,000°K, the rate coefficient for the $2^1S - 3^1P$ direct excitation is about 10^{-10} cm^3/sec, whereas for the exchange excitation to the adjacent 3^1D level ($2^1S - 3^1D$) the rate coefficient is about 10^{-13} cm^3/sec. This is not necessarily true for transitions among sublevels of the higher excited states where the energy levels are quite close together. However, these upper level rate coefficients will be large and the population densities will rapidly establish an equilibrium configuration among the sublevels. Requiring a detailed accounting of each sublevel is unnecessary for all but the earliest stages of the computation.

The preceding discussion has been concerned only with inelastic excitation between bound states of the atom. The inverse process, a superelastic collision resulting in de-excitation of the atom, is also included in this study. The rate coefficients for these processes come quite easily from equilibrium considerations.

At collisional equilibrium between two states, the rates of change of the two states will be equal. Further, detailed balance requires that rates due to individual processes be equal. Hence, one can set

$$n_e n_p K(p;q) - n_e n_q K(q;p) = 0$$

Thus,

$$K(q;p) = \frac{n_p}{n_q} K(p;q)$$

and, since this is an equilibrium condition,

$$\frac{n_p}{n_q} = \frac{g_p}{g_q} \exp\left[-\left(E_p - E_q\right)/kT_e\right]$$

Hence,

$$K(q;p) = \frac{g_p}{g_q} \exp\left[-\left(E_p - E_q\right)/kT_e\right] K(p;q)$$

3.2.2 Collisional Ionization and Three-Body Recombination Coefficients, K(p;c) and K(c;p)

The collisional ionization cross section is very readily obtained from the two-body internal transition cross section. This is accomplished by noting that the Gryzinski formulation for the cross section, Eq. (9), is inversely dependent upon the square of energy difference between the initial and final states, U_{pq}. For the final state being the continuum, this U_{pq} just becomes the ionization potential for state p. Hence, the parametric cross section for collisional ionization $Q_{pc}(x)$ is

$$Q_{pc}(x) = \frac{\pi e^4}{I_{p\infty}^2} \frac{1}{x} \left(\frac{x-1}{x+1}\right)^{\frac{3}{2}} \left[1 + \frac{2}{3}\left(\frac{2x-1}{2x}\right) \ln\left(e + \sqrt{x-1}\right)\right]$$

$$x = E/I_{p\infty}$$

and $I_{p\infty}$ is the ionization potential of the p^{th} quantum level. Hence the collisional ionization rate coefficient is written

$$K(p;c) = \frac{M8\pi}{\sqrt{m_e}} \left(\frac{1}{2\pi kT_e}\right)^{3/2} \int_1^\infty Q_{pc}(x) \exp(-I_{p\infty}x/kT_e) I_{p\infty}^2 \, x\,dx \tag{14}$$

In this case again, M = 2 for the ground state atoms since there are two electrons available for ionization from the ground state and M = 1 for atoms in higher energy states.

Figures 3 and 4 show results of the Gryzinski calculations for the ionization of the 1^1S and 2^3S levels, respectively, compared to experimental results reported in the literature (Refs. 40, 41, 42, and 43). The Gryzinski cross section overestimates the ionization cross section for the ground state atom by about 25 percent compared to the experimental data. Further, the peak of the calculated cross section occurs somewhat earlier than the experimental peak but for the purpose of this study the calculations can be considered to give satisfactory results.

The calculated cross section for the 2^3S ionization does not agree as satisfactorily with experiment as is shown in Fig. 4. For this the data of Long and Geballe (Ref. 42) are to be considered superior to those of Fite and Brackmann (Ref. 43) since the former data were taken from a source known to be the 2^3S atom, whereas Fite and Brackmann's source was an indeterminant mixture of the 2^3S and 2^1S atoms.

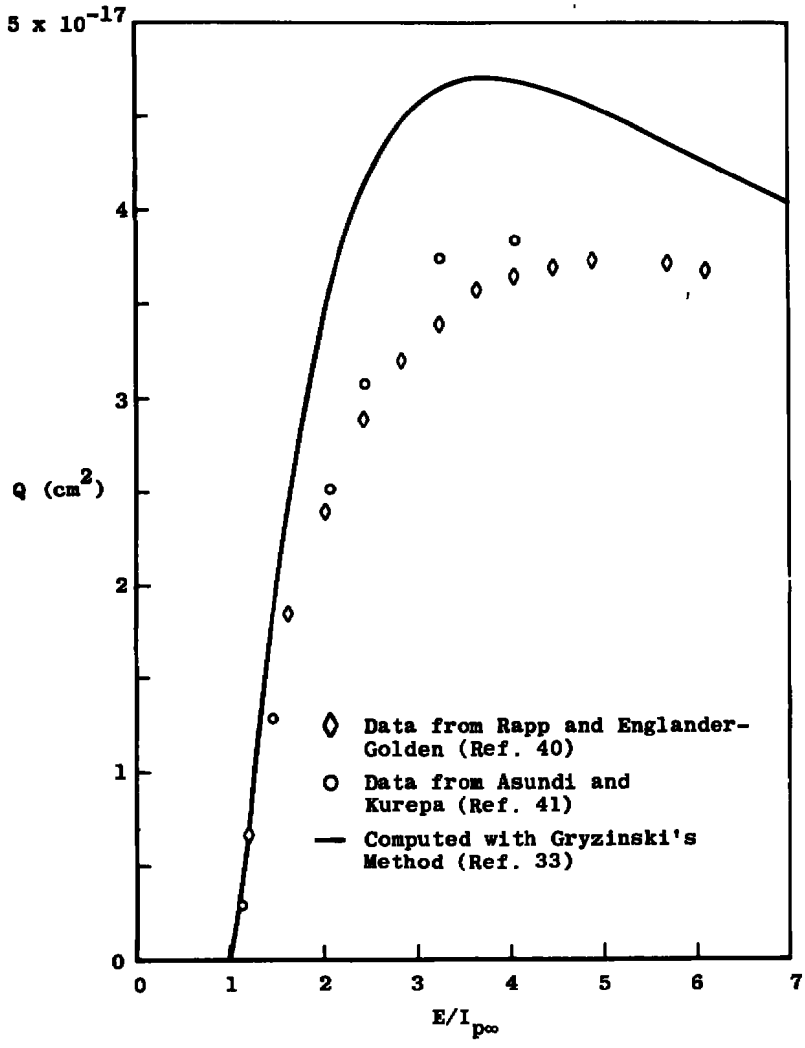

Figure 3. 1^1S ionization cross section.

For the purposes of this study, the agreement is considered satisfactory. It is expected that the characteristics of the ionization cross section calculations will follow the same pattern for the higher excited states.

The inverse of collisional ionization, three-body recombination, is described by the rate coefficient K(c;p). This coefficient is also obtained from equilibrium considerations. When equilibrium between state p and the continuum is established by these two processes, the rate of filling state p due to three-body recombination exactly balances the rate the state is depopulated via collisional ionization, or

$$n_e n_p K(p,c) = n_e^2 n_i K(c,p)$$

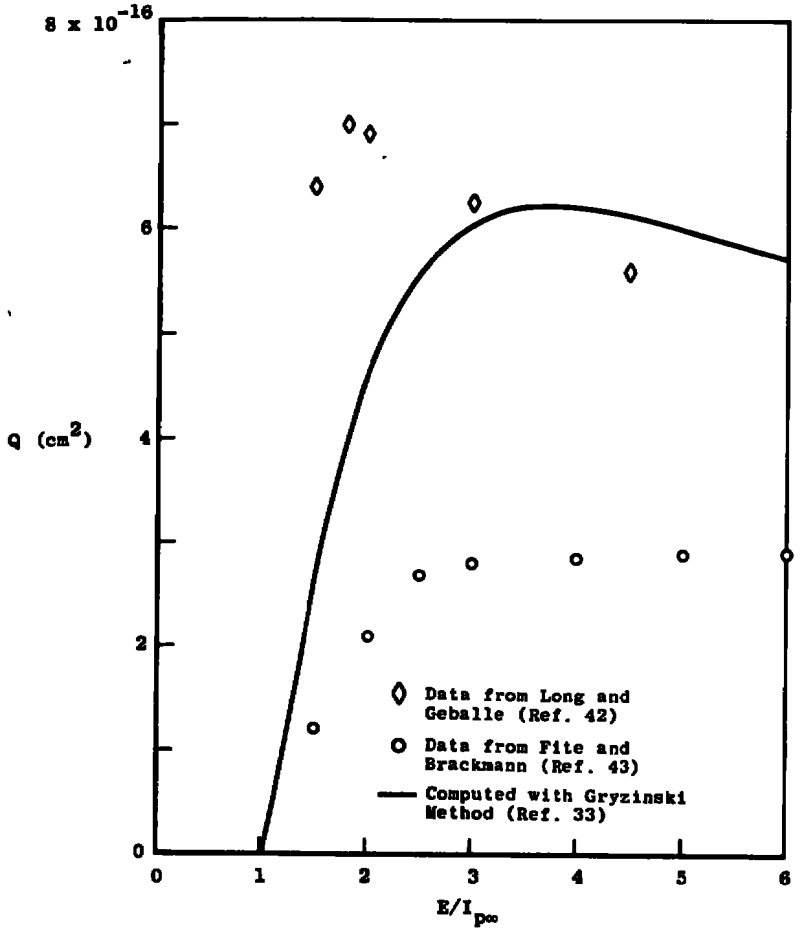

Figure 4. 2^3S ionization cross section.

where n_i is the population density of positive ions. Hence,

$$K(c;p) = \frac{n_p}{n_e n_i} K(p;c)$$

Since only single ionization is considered here, $n_e = n_i$. Further, this is an equilibrium relationship between state p and the continuum so that n_p and n_e are related by the modified Saha equilibrium relationship so that

$$K(c;p) = \frac{h^3}{(2\pi m_e kT_e)^{3/2}} \frac{g_p}{g_e g_i} \exp\left(I_{p\infty}/kT_e\right) K(p;c) \qquad (15)$$

3.2.3 Radiative Recombination Rate Coefficients, $\beta(p)$

The radiative recombination rate coefficient describes the filling of state p due to two-body encounters between electrons and ions in which the ion captures the electron into energy state p with the attendant emission of radiation. It is obtained in much the same way as the other rate coefficients although there is some difference in the physical analysis. The basic functional form for the rate coefficient is written as before,

$$\beta(p) = \frac{8\pi}{\sqrt{m_e}} \left(\frac{1}{2\pi kT_e}\right)^{3/2} \int_0^\infty Q_r(p) \exp(-E/kT_e)\, E\,dE \qquad (16)$$

where $\beta(p)$ is the radiative recombination rate coefficient for state p, and $Q_r(p)$ is the cross section for the capture.

The evaluation of $Q_r(p)$ does not proceed as straightforwardly here, however. To obtain this cross section it is necessary to use the principle of detailed balance for the relationship between the radiative recombination cross section and the photoionization cross section (or absorption coefficient) thus (Ref. 44),

$$Q_r(p) = \frac{g_p}{g_{ion}} \frac{1}{c^2} \frac{(h\nu)^2}{2m_e E} a_\nu(p) \qquad (17)$$

where g_p and g_{ion} are the statistical weights of the atom and ion, respectively, E is the kinetic energy of the electron, $h\nu$ is the photon energy emitted (or absorbed) in a photoelectric transition between the continuum and the state p, and $a_\nu(p)$ is the absorption coefficient for state p.

Noting that the energy of an emitted photon in the capture will include both the ionization potential of state p and the kinetic energy of the electron before capture,

$$h\nu = I_{p\infty} + E$$

Substituting, one obtains with this change in variable

$$\beta(p) = \frac{1}{c^2}\left(\frac{2}{\pi}\right)^{1/2}\left(\frac{1}{mkT_e}\right)^{3/2}\frac{g_p}{g_{ion}}\exp\left(I_{p\infty}/kT\right)\int_{I_p}^{\infty}(h\nu)^2 \exp\left(-h\nu/kT_e\right) a_\nu(p)\, d(h\nu) \tag{18}$$

The photoionization cross section is given for hydrogenic atoms by Seaton (Ref. 45):

$$a_\nu(p) = \frac{64\alpha\pi a_o^2}{3\sqrt{3}}\frac{p}{Z^2}\left(\frac{1}{1+u}\right)^3 g_{II}(p,u) \tag{19}$$

where α is the fine structure constant, a_o is the Bohr radius, Z is the nuclear charge, u is the ratio $E/I_{p\infty}$, p is the principal quantum number, and g_{II} is the Gaunt factor:

$$g_{II} = 1 + 0.1728\frac{u-1}{p^{2/3}(u+1)^{2/3}} - 0.0496\frac{u^2+4/3\ u+1}{p^{4/3}(u+1)^{4/3}} + \cdots \tag{20}$$

Noting that

$$h\nu = I_{p\infty}(1+u)$$

and substituting,

$$\beta(p) = B(p)\int_0^{\infty}\frac{\exp\left(-I_{p\infty}u/kT\right)}{1+u}\, g_{II}\, du \tag{21}$$

where

$$B(p) = \frac{64\sqrt{\pi}\alpha}{3\sqrt{3}\ c^2}\frac{a_o^2}{(m_e kT_e)^{3/2}}\frac{g_p}{g_{ion}}\frac{p}{Z^2}I_{p\infty}^3 \tag{22}$$

The expression is based upon a hydrogenic approximation in which p is the principal quantum number of the energy level. Because of this hydrogenic approximation, one would expect the calculations to give their worst results for the lower quantum levels and to converge to correct values for the upper levels. Figure 5 shows the results of the calculation of the absorption cross section for the ground state helium atom compared to the experimental results of Lowry, Tomboulian, and Ederer (Ref. 46). In this figure, in which the abcissa is wavelength, energy increases to the left, threshold energy (electronic velocity of 0) occurring at about 505 Å. In this case, a 1-ev electron would be ejected at an abcissa very near this threshold wavelength. Thus, for the rate coefficient calculation, the rightmost portion of the curve is most important, and as can be seen, the calculations reproduce the experiment in this region to within a factor of two or better. Thus, one would expect the radiative recombination rate coefficient to be correct to within a factor of two or better for the ground state and become progressively better for the higher quantum levels.

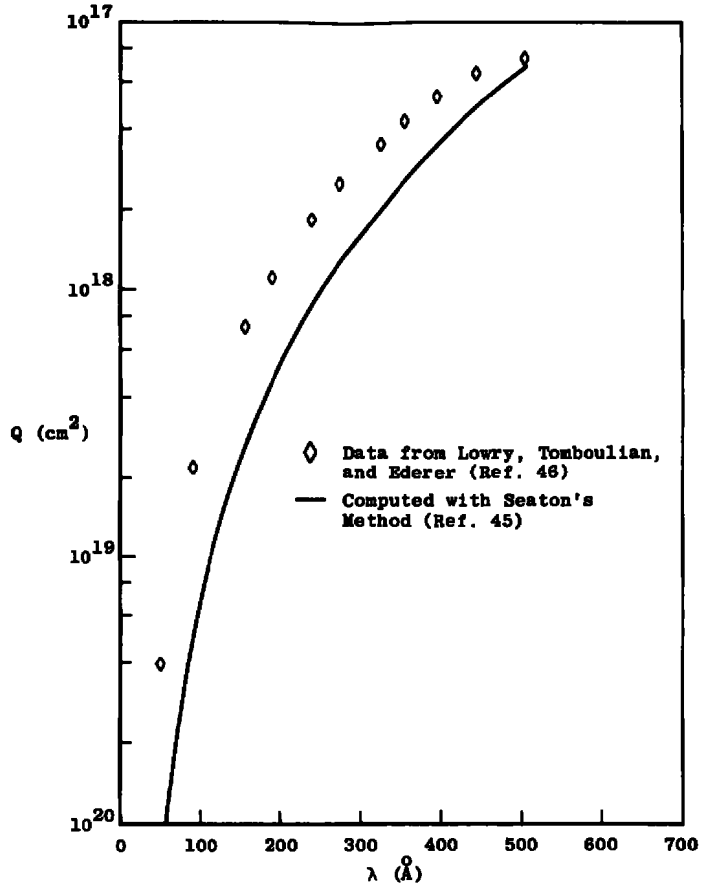

Figure 5. 1^1S absorption cross section.

4.0 TECHNIQUES

This chapter summarizes the various approximations and techniques which were utilized in obtaining the solution to the ERE. A detailed listing of the computer programs will not be included since the techniques are quite straightforward. Rather, a short discussion of programming considerations will be given; since the solution to the ERE is obtained numerically, certain approximations and compromises were necessary and these are discussed in detail.

4.1 ENERGY LEVELS

The helium energy levels used in this study were obtained from Moore (Ref. 47), who gives all the energy levels from which spectral lines have been observed. The precise energy values of all the detailed substates considered in the program are not known, or are so closely adjacent to other substates of the same quantum level that they have not been resolved. The energy differences between these states will be so small that they are negligible.

Evaluation of the rate coefficients required different substates to have different energies, however. This is because in the course of evaluation, differences in energies of the states are taken and a zero energy difference causes machine errors to occur. To prevent this condition simple linear interpolation was used to generate different numerical energies for the substates not given explicitly in Moore (Ref. 47). A listing of the energy levels used in this study is given in Table 1.

The size of the computer core dictated that not all energy states listed in Table 1 be used. For the higher principal quantum states the distribution of densities among the substates will be maintained in a Boltzmann configuration. The total density of the level immediately gives the density of any desired substate.

To meet the computer core requirement, the a priori assumption of the Boltzmann configuration among the substates of quantum levels 7 and 8 was made. These quantum levels were described by a single energy state chosen to be the lowest energy exhibited by any of the substates of that level. This assumption was used only for the final determination of states considered by the ERE. The rate coefficients were determined using detailed energies of the substates of these quantum levels, and average rate coefficients for the total quantum level were then determined from these values.

Table 1. Helium Energy Levels

State	g	E (1/cm)	State	g	E (1/cm)
1^1S	1	0.0	5^3G	27	193921.0
2^3S	3	159850.3	5^1P	3	193936.8
2^1S	1	166271.7	6^3S	3	194930.5
2^3P	9	169081.1	6^1S	1	195109.2
2^1P	3	171129.2	6^3P	9	195187.2
3^3S	3	183231.1	6^3D	15	195254.4
3^1S	1	184859.1	6^1D	5	195255.0
3^3P	9	185558.9	6^1F	7	195256.7
3^3D	15	186095.9	6^3F	21	195256.8
3^1D	5	186099.2	6^1G	9	195258.0
3^1P	3	186203.6	6^3G	27	195258.5
4^3S	3	190292.5	6^1H	11	195260.0
4^1S	1	190934.5	6^3H	33	195260.5
4^3P	9	191211.4	6^1P	3	195269.2
4^3D	15	191438.8	7^3S	3	195862.6
4^1D	5	191440.7	7^1S	1	195973.2
4^3F	21	191446.6	7^3P	9	196021.7
4^1F	7	191447.2	7^3D	15	196064.0
4^1P	3	191487.0	7^1D	5	196064.3
5^3S	3	193341.3	7^1F	7	196065.4
5^1S	1	193657.8	7^3F	21	196065.5
5^3P	9	193795.1	7^1G	9	196066.5
5^3D	15	193911.5	7^3G	27	196066.6
5^1D	5	193912.5	7^1H	11	196067.5
5^1F	7	193914.3	7^3H	33	196067.6
5^3F	21	193915.8	7^1I	13	196068.5
5^1G	9	193920.0	7^3I	39	196068.6
7^1P	3	196073.4	8^1H	11	196591.6
8^3S	3	196455.8	8^3H	33	196591.7
8^1S	1	196529.0	8^1I	13	196592.2
8^3P	9	196561.1	8^3I	39	196592.3
8^3D	15	196589.4	8^1J	15	196592.8
8^1D	5	196589.7	8^3J	45	196592.9
8^1F	7	196590.3	8^1P	3	196595.6
8^3F	21	196590.4	9	324	196856.4
8^1G	9	196591.0	10	400	197139.8
8^3G	27	196591.1	11-15	3420	197347.0

Quantum levels 9 through 15 have very small energy widths and a progressively larger number of substates with each principal quantum level. Consequently each was considered as a single energy level for all rate coefficient determinations.

The criterion for truncating the system of equations comprising the ERE is that some upper level will be in equilibrium with the free electron density. In order to maintain a correct description of the rate of this upper level, states above it must also be considered in order to have approximately correct values for collisional and radiative processes. Quantum level 10 was chosen to be the maximum quantum level for the critical level for this study. Since quantum levels 11 through 15 will therefore be in an equilibrium configuration, they were averaged together to form a reservoir for the various processes for quantum level 10.

An additional phenomenon which relates to the energy levels in partially ionized plasmas and must be taken into account is that of the lowering of the ionization potential. This arises because when a bound electron is in a sufficiently high energy state it can exceed the Debye shielding length for the plasma and thus becomes indistinguishable from the free electrons. However, at typical conditions encountered in this study, $n_e = 10^{15}$ 1/cm^3, $T_e = 10^4$ °K, the expression for the lowering of the ionization potential given by J. Richter (Ref. 48) gives a value of 74 1/cm, which is insignificant.

In summary, plasma conditions are restricted to such that at least quantum level 10 is in Saha equilibrium with the free electrons. A detailed accounting of all singlet and triplet states is maintained through quantum level 6. Principal quantum levels 7 through 10 are maintained separate from each other although a Maxwell-Boltzmann density distribution of the substates of each of these principal quantum levels is assumed.

4.2 PROGRAMMING CONSIDERATIONS

As indicated above, one important consideration in the development of the computer program is available computer core size. Arrays for each of the rate coefficients must be maintained as well as a work area. Utilizing a two-dimensional array for the K(p;q) and A(p;q) with the other parameters necessary in the solution, 47 separate energy states could be considered in approximately 116,000 bytes of core in the IBM S360/50 computer at the Arnold Engineering Development Center. Although more core was available at the time of this work, scheduling of

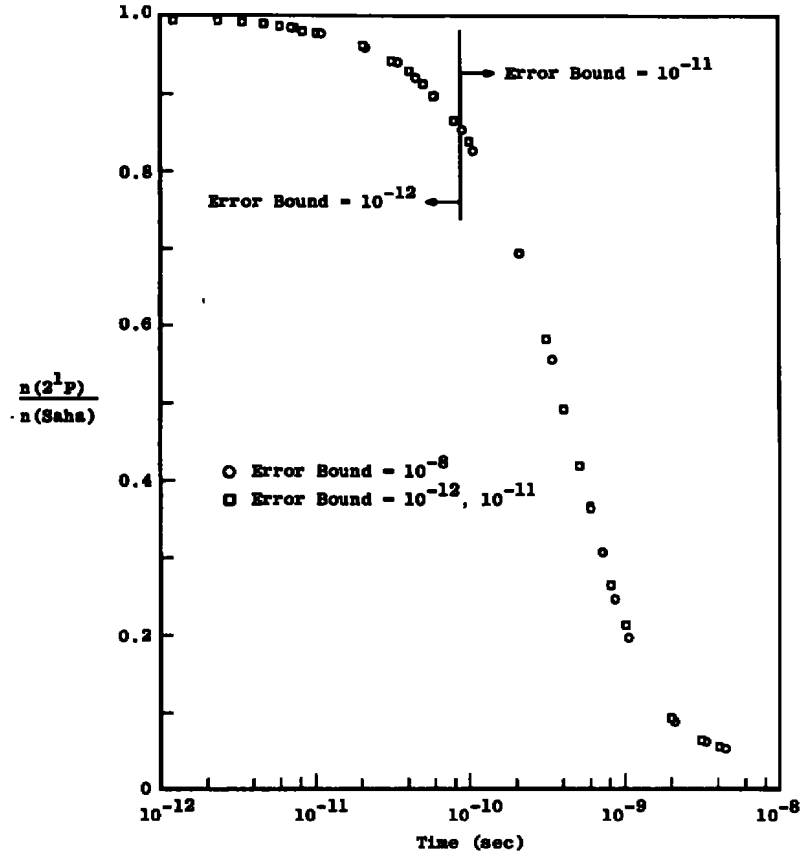

Figure 7. n(2¹P)/n(Saha) versus time for two error criteria.

error bounds. These calculations were performed for precisely the same plasma, Case C to be presented later, with the error bound the only difference. The first of these, 10^{-8}, is typical of the error bounds used in the other studies. The other error bound, 10^{-12} for $t < 10^{-10}$ sec and 10^{-11} for $t \geq 10^{-10}$ sec, is an extremely tight bound. Some experimentation was conducted at significantly lower error bounds and it was found that the solution would begin to oscillate if the bound was relaxed too much, although a subsequent tightening of the error bound would cause the solution to become stable again.

The repeatability of the solution under the two bounds indicated above illustrates the stability of the solution at the 10^{-8} bound which was used during the early part of the solution. It was found that after the early transients had died out the error bound could be relaxed substantially with no loss of stability. This stability along with numerical agreement with other independent calculations of the CRR coefficients, as will be indicated in Section 5.0, shows that the numerical technique used in these studies yields valid results.

Quantum levels 9 through 15 have very small energy widths and a progressively larger number of substates with each principal quantum level. Consequently each was considered as a single energy level for all rate coefficient determinations.

The criterion for truncating the system of equations comprising the ERE is that some upper level will be in equilibrium with the free electron density. In order to maintain a correct description of the rate of this upper level, states above it must also be considered in order to have approximately correct values for collisional and radiative processes. Quantum level 10 was chosen to be the maximum quantum level for the critical level for this study. Since quantum levels 11 through 15 will therefore be in an equilibrium configuration, they were averaged together to form a reservoir for the various processes for quantum level 10.

An additional phenomenon which relates to the energy levels in partially ionized plasmas and must be taken into account is that of the lowering of the ionization potential. This arises because when a bound electron is in a sufficiently high energy state it can exceed the Debye shielding length for the plasma and thus becomes indistinguishable from the free electrons. However, at typical conditions encountered in this study, $n_e = 10^{15}$ 1/cm^3, $T_e = 10^4$ °K, the expression for the lowering of the ionization potential given by J. Richter (Ref. 48) gives a value of 74 1/cm, which is insignificant.

In summary, plasma conditions are restricted to such that at least quantum level 10 is in Saha equilibrium with the free electrons. A detailed accounting of all singlet and triplet states is maintained through quantum level 6. Principal quantum levels 7 through 10 are maintained separate from each other although a Maxwell-Boltzmann density distribution of the substates of each of these principal quantum levels is assumed.

4.2 PROGRAMMING CONSIDERATIONS

As indicated above, one important consideration in the development of the computer program is available computer core size. Arrays for each of the rate coefficients must be maintained as well as a work area. Utilizing a two-dimensional array for the K(p;q) and A(p;q) with the other parameters necessary in the solution, 47 separate energy states could be considered in approximately 116,000 bytes of core in the IBM S360/50 computer at the Arnold Engineering Development Center. Although more core was available at the time of this work, scheduling of

core partitions dictated that the system requirements be kept within 133K bytes to expedite the work. Extension of the program to include significantly more detail would have caused the core requirements to exceed the optimum 133K bytes.

Also, because of available core, it was impractical to calculate the rate coefficients in the same program that obtained the solution to the ERE. Consequently, these calculations were accomplished in a separate program and rate coefficient data were preserved on magnetic tape in binary form to expedite I/O overhead.

The rate coefficients requiring integration are evaluated using 32-point Laguerre-Gauss quadrature and double precision arithmetic. This is a standard technique which is readily available; details of the integration are included in Appendix A.

The solution to the ERE was obtained by using the modified Euler's technique, which is an implicit method. Details of the application of this technique to the ERE are also included in Appendix A. A result of the technique is control of the increment of calculation based upon the desired relative error bound. The calculations presented here used various bounds, usually as high as 10^{-6} to 10^{-8} in the portion of the solution in which adjustments were taking place rapidly. After the rapid transients had died out, error bounds as low as 10^{-4} were used.

All calculations were performed with double precision arithmetic and with the program compiled with the IBM Fortran H-level compiler using full optimization so as to generate the most efficient machine code. In addition, variables and calculations were arranged in storage so as to take as full an advantage as possible of the optimization. To conserve compiler time, which is a minor consideration except for programs which are run many times, as this one was, the compiled program was preserved in machine language on disk pack for immediate recall at execution time. These efforts to reduce execution time realized an approximate reduction of 25 to 35 percent compared to an earlier version of the program. Even with the efforts to reduce program execution time, the run times can become quite long. Typical run times for each case studied here were 45 minutes to one hour. Subsequent computer system improvements have reduced these computer run times typically an order of magnitude.

Consequently, to conserve total machine time and insure that a solution that was invalid for some reason would not waste an inordinate amount of machine time, the program was set up to preserve important solution parameters. Thus one can restart the calculations at the point in time the parameters were preserved.

The preservation of these parameters occurred at selected clock time intervals and plasma time intervals so that an inadvertent machine or program failure would not cause the loss of a large amount of computer time. In addition the parameters were preserved at the last calculation each time the program was run so that if more calculations were necessary, the program could be restarted at the last calculation with a minimum of overhead. A desirable consequence of this is that external judgment control can be exercised over the execution of the program. Hence, the error bound can be changed as the solution indicates and the number of calculations judged necessary to effect the solution are under external control so that unnecessary calculations are minimized.

4.3 PROGRAM STABILITY

As indicated above and shown in Appendix A, the time step size in the solution is controlled by the desired error bound. Figures 6 and 7 show the results of obtaining a solution to the ERE under two desired

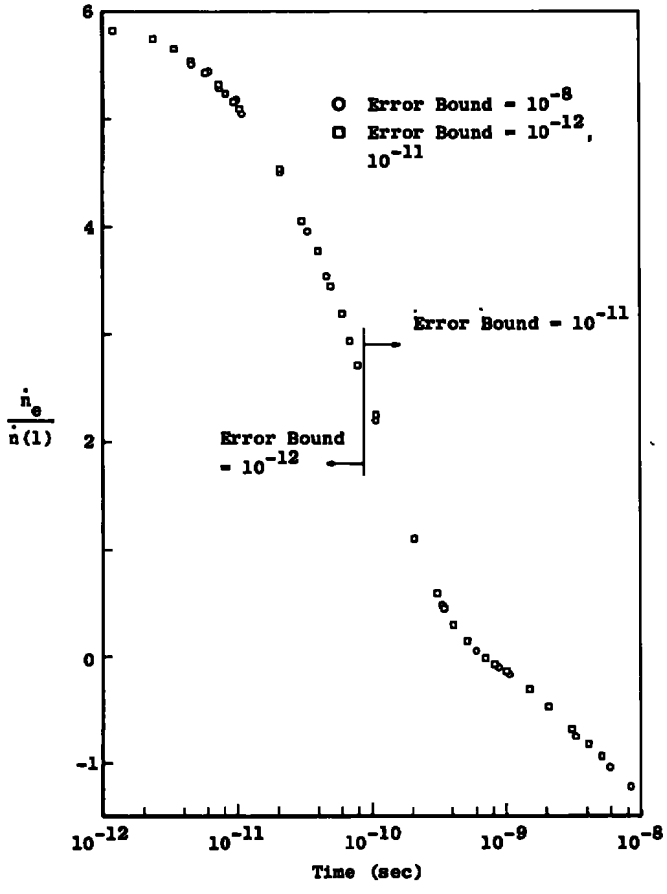

Figure 6. $\dot{n}_e/\dot{n}(1)$ versus time for two error criteria.

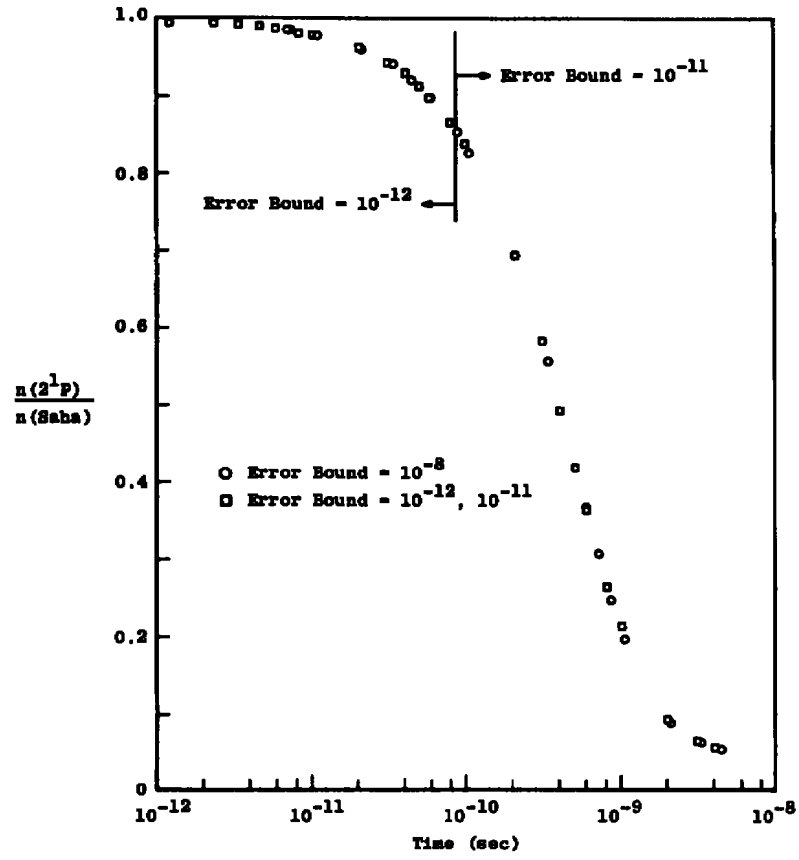

Figure 7. n(2¹P)/n(Saha) versus time for two error criteria.

error bounds. These calculations were performed for precisely the same plasma, Case C to be presented later, with the error bound the only difference. The first of these, 10^{-8}, is typical of the error bounds used in the other studies. The other error bound, 10^{-12} for $t < 10^{-10}$ sec and 10^{-11} for $t \geq 10^{-10}$ sec, is an extremely tight bound. Some experimentation was conducted at significantly lower error bounds and it was found that the solution would begin to oscillate if the bound was relaxed too much, although a subsequent tightening of the error bound would cause the solution to become stable again.

The repeatability of the solution under the two bounds indicated above illustrates the stability of the solution at the 10^{-8} bound which was used during the early part of the solution. It was found that after the early transients had died out the error bound could be relaxed substantially with no loss of stability. This stability along with numerical agreement with other independent calculations of the CRR coefficients, as will be indicated in Section 5.0, shows that the numerical technique used in these studies yields valid results.

5.0 PURE AFTERGLOWS

The transient solution to the ERE under the restrictions and assumptions discussed above was obtained for several plasma conditions. This chapter is devoted to the study of the pure afterglows in which the plasma was allowed to relax from an initial distribution.

5.1 REPORTING OF DATA

Because of the large bulk of the data from the calculations, the majority of the data will be presented in graphical form as continuous functions. Actual points from the calculations will not be shown since the lines are drawn to connect the points. Additionally, detailed plots from all calculations will not be presented but rather cases will be selected to illustrate trends of the plasma decay. The cases not shown in the detailed studies will be used for completeness in illustrating certain gross trends of the decay characteristics. Tabular information and precise numbers from the calculations will be used only as needed for detailed comparisons or when description of some phenomenon requires resolution beyond that of a graph.

5.2 PLASMA CONDITIONS

Transient solutions to the ERE under the restrictions and assumptions discussed above were obtained for several afterglow plasma conditions summarized in Table 2. The lower limits of electron temperature, degree of ionization, or total number density represent approximate lower bounds to the plasmas which could be solved with the present computer program because of the critical level limits described earlier. Although conditions above the upper limits of the parameters have not been investigated, it is believed that extension will not yield notably different data on the mechanism by which the QSS is established.

From Table 2 one can see that cases A through G compare plasmas at different total densities with the same degree of ionization and electron temperature and cases H through K compare plasmas at similar selected densities but at a higher electron temperature, 14,000°K. Cases L through O compare plasmas at constant density and electron temperature but different degrees of ionization. Cases C, I, P, and Q compare plasmas with the same total density and degree of ionization but different electron temperatures. By quantitative comparisons of the results for these conditions, insight into the trends of the processes by which QSS is established will be obtained.

Table 2. Summary of Plasma Conditions for Afterglows Studied with ERE

Case	n_o $1/cm^3$	n_e/n_o	T_e °K
A	1.63^{17}[a]	0.01	1.0^4
B	4.4^{16}	0.01	1.0^4
C	1.5^{16}	0.01	1.0^4
D	6.59^{15}	0.01	1.0^4
E	5.0^{14}	0.01	1.0^4
F	1.5^{14}	0.01	1.0^4
G	5.0^{13}	0.01	1.0^4
H	1.63^{17}	0.01	1.4^4
I	1.5^{16}	0.01	1.4^4
J	5.0^{14}	0.01	1.4^4
K	5.0^{13}	0.01	1.4^4
L	2.69^{15}	0.2	1.0^4
M	2.69^{15}	0.01	1.0^4
N	2.69^{15}	0.001	1.0^4
O	2.69^{15}	0.0001	1.0^4
P	1.5^{16}	0.01	8.0^3
Q	1.5^{16}	0.01	6.0^3

[a]Superscripts denote powers of 10 by which the numbers are to be multiplied.

The initial distribution for each of these cases was chosen such that all excited state densities were in Saha equilibrium with the free electron density. Consequently, the excited state densities exhibit a Boltzmann distribution. In most laboratory plasmas, the excited state distribution does not exhibit this Boltzmann distribution in its entirety. Rather, there can be significant deviations from this equilibrium distribution for the first few excited states. In this sense then, the initial conditions chosen for the afterglow studies are at variance with nature. However, the intent is to examine the mechanisms by which the QSS distribution is established and thus to determine the important phenomena required to maintain the QSS in an actual physical situation. In a physical plasma various of the plasma parameters will be changing and the QSS is not a static condition. By studying the pure afterglow phenomena with the perturbational studies the effect upon the QSS because of a change in the plasma parameters can be examined for valid application to physical plasmas.

5.2.1 Quasi-Steady-State Recombination Coefficients

As a final check of the numerical validity of the computer program the collisional-radiative recombination coeffieients α were obtained. These results were obtained by allowing the transient solution to develop until $\dot{n}_e$ and $\dot{n}(1)$ agreed to within five percent and then calculating α with the instantaneous values of $\dot{n}_e$ and $\dot{n}_e^2$, $\alpha = -\dot{n}_e/n_e^2$.

Table 3 shows the value of α obtained from the ERE and results reported by Chen (Ref. 21) using the QSS approximation. As is seen in Table 3, the present results compare favorably with those of Chen, being consistently slightly lower except for cases P and Q. No significance is placed upon the variance of case P, being less than ten per cent. Case Q will be discussed in more detail below. Chen also used Gryzinski's technique for obtaining collision cross sections but used a different source for the radiative transition probabilities. Chen did not include all collisional transitions, as this work does, and he used

Table 3. Quasi-Steady-State Collisional-Radiative Recombination Coefficients from the Eigenstate Rate Equations Solution

Case	T_e °K	n_e 1/cm^3	α(ERE) 1/cm^3/sec	α^a 1/cm^3/sec
A	1.0^{4}[b]	1.63^{15}	5.9^{-12}	7.0^{-12}
B	1.0^{4}	4.4^{14}	3.04^{-12}	3.4^{-12}
C	1.0^{4}	1.5^{14}	2.16^{-12}	2.25^{-12}
D	1.0^{4}	6.59^{13}	1.62^{-12}	1.8^{-12}
E	1.0^{4}	5.0^{12}	8.04^{-13}	9.5^{-13}
F	1.0^{4}	1.5^{12}	6.77^{-13}	8.1^{-13}
G	1.0^{4}	5.0^{11}	4.58^{-13}	6.5^{-13}
H	1.4^{4}	1.63^{15}	1.91^{-12}	2.1^{-12}
I	1.4^{4}	1.5^{14}	7.98^{-13}	1.05^{-12}
J	1.4^{4}	5.0^{12}	3.69^{-13}	5.6^{-13}
K	1.4^{4}	5.0^{11}	2.48^{-13}	3.7^{-13}
L	1.0^{4}	5.38^{14}	3.32^{-12}	3.7^{-12}
M	1.0^{4}	2.69^{13}	1.26^{-12}	1.35^{-12}
N	1.0^{4}	2.69^{12}	6.86^{-13}	8.5^{-13}
O	1.0^{4}	2.69^{11}	3.97^{-13}	6.0^{-13}
P	8.0^{3}	1.5^{14}	4.43^{-12}	4.1^{-12}
Q	6.0^{3}	1.5^{14}	1.25^{-11}	8.5^{-12}

[a] Chen (Ref. 21)

[b] Superscripts denote powers of 10 by which the numbers are to be multiplied.

the simplified technique of obtaining the minimum in the total rate of de-excitation as a function of the energy levels of excited states (Refs. 2 and 23). These differences can easily account for the slight differences in Table 3. It is believed that the inconsistent behavior of case Q is due to explicit inclusion of exchange excitations from the metastable 2^3S level to the adjacent metastable 2^1S level. This has the effect of maintaining a higher collisional rate to the adjacent 2^1P level (rapid direct excitation) so that a higher rate of radiation to the ground state is maintained. This rate at QSS is communicated back through the bound states to the free electrons, thus resulting in a high rate of recombination. Other workers (Ref. 49) have also calculated recombination coefficients but their conditions and resolution of their data make comparisons difficult.

It is notable that these recombination coefficients are typically a factor of two less than those reported for hydrogen by Bates, et al. (Ref. 3). This corresponds to a general trend in reported experimental values for helium recombination rates to be less than hydrogen recombination rates (Refs. 12, 22, 50, and 51). The true value will be somewhat in doubt because of the inability of the Gryzinski cross sections to predict accurately the true collision rates. However, the use of a consistent set of cross sections for both hydrogen and helium will indicate relative differences.

The favorable comparison of the results of the transient ERE solution and the QSS calculations shown in Table 3 indicates that the numerical technique used for the ERE will yield physically correct results. This observation coupled with the stability considerations described in Section 4.0 constitutes proof that the numerical results to be presented in the following pages do represent physical processes to the limit of the accuracy of the parameters used in the calculation.

5.2.2 Location of the Critical Level

The initial distribution for each of the plasmas was a Boltzmann distribution in equilibrium with the free electrons from the 2^3S level through the upper states considered. As the ERE solution develops in time, the levels below the critical level adjust to the final QSS distribution while those levels above and including the critical level remain in Saha equilibrium with the free electrons.

Although the concept of a critical level is not used in the present computations, the observation of the development of such a level in the

transient solution and the location of it is of interest as it pertains to the internal consistency of the calculations. The location of the critical level is useful for experimental determinations becuase it indicates that lowest level whereby spectral intensity measurements can be used to ascertain the kinetic temperature of the free electron distribution.

Table 4 lists the critical levels found for each of the plasmas. Two criteria were used for identification of the critical level: 3 percent and 10 percent, referring to the maximum deviation from Saha equilibrium with the free electrons for any of the substates in a principal quantum level for that principal quantum level to be considered as the critical level. The critical levels found for the high electron density, high temperature cases with the 10-percent criteria compare favorably with predictions by Hinnov and Hirschberg (Ref. 11) who indicate that at those conditions quantum number 4 will be the lowest level in Saha equilibrium with the free electrons. No comparisons were made at the low densities and temperature other than that they qualitatively show expected behavior.

Table 4. Total Number Density, Electron Density, Electron Temperature, and Location of Critical Level for Each of the Plasmas Studied

Case	n_o 1/cm^3	n_e 1/cm^3	T_e °K	Critical Level (Principal Quantum Number) 3%	10%
A	1.63^{17}[a]	1.63^{15}	1.0^4	4	4
B	4.4^{16}	4.4^{14}	1.0^4	5	4
C	1.5^{16}	1.5^{14}	1.0^4	5	4
D	6.59^{15}	6.59^{13}	1.0^4	6	5
E	5.0^{14}	5.0^{12}	1.0^4	8	6
F	1.5^{14}	1.5^{12}	1.0^4	9	7
G	5.0^{13}	5.0^{11}	1.0^4	10	7
H	1.63^{17}	1.63^{15}	1.4^4	4	3
I	1.5^{16}	1.5^{14}	1.4^4	5	4
J	5.0^{14}	5.0^{12}	1.4^4	8	6
K	5.0^{13}	5.0^{11}	1.4^4	9	7
L	2.69^{15}	5.38^{14}	1.0^4	5	4
M	2.69^{15}	2.69^{13}	1.0^4	6	5
N	2.69^{15}	2.69^{12}	1.0^4	8	6
O	2.69^{15}	2.69^{11}	1.0^4	10	8
P	1.5^{16}	1.5^{14}	8.0^3	5	4
Q	1.5^{16}	1.5^{14}	6.0^3	6	5

[a] Superscripts denote powers of 10 by which the numbers are to be multiplied.

5.3 TIME DEVELOPMENT OF THE ERE SOLUTION

The time development of selected quantum level densities for eight of the cases listed in Table 2 are presented on the following pages. The ordinate for each plot is the ratio of the instantaneous population density to the density required to be in Saha equilibrium with the free electron density. Thus, at t = 0.0 sec, each quantum level would have an ordinate of 1.0. The substates of only quantum levels 2 and 3 are shown. Those quantum levels between quantum level 3 and the critical level will show characteristics similar to the triplet and singlet states of quantum level 3, and any quantum level above and including the critical level will show a constant ratio of 1.0.

The two quantum levels are displayed together because substates of quantum level 3 are characteristic of the other upper levels while substates of quantum level 2 are in general quite different from each other and any of the other levels. The ground state density is not included since it shows nothing more than a slow, steady increase throughout time. The study of the rate of change of the ground state density is more pertinent and studies of certain of these will be presented later.

Figure 8 shows the time development for Case A, a high density plasma which is generally collision dominated. Figure 8 does not include any of the substates of quantum level 3 since their values fall into the same region as the 2^3S and 2^3P levels and would just clutter the plot.

This plasma is sufficiently collision dominated that the only significant change is due to the radiative depopulation of the 2^1P level. The metastable 2^1S and the 2^1P levels are coupled together strongly by two-body collisional processes so that as the 2^1P level decays radiatively, it is depressed below the equilibrium configuration. Consequently, the collisional excitation rate from the 2^1S level is greater than the super-elastic de-excitation from the 2^1P to the 2^1S level, and there is a net transfer of atoms from the lower to the upper state. The 2^1P level continues to decay radiatively and thus causes the 2^1S level to decay also. At about 1×10^{-8} sec, the 2^1P density has depressed sufficiently that the radiative depopulation rate has decreased to the point that the collisional population rate will balance the total rate of change towards zero, or the QSS. There are other collisional processes possible, namely exchange collisions, so that as the 2^1P density decreases, the other quantum levels in the vicinty of the 2^1P level are also depressed by

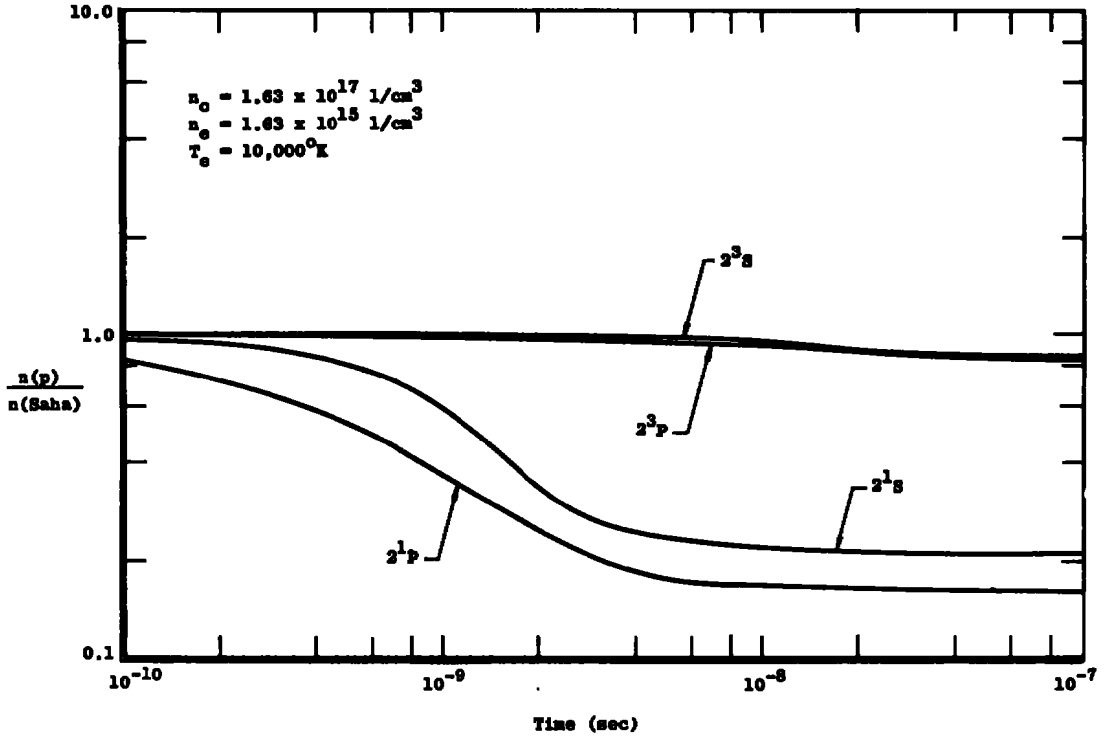

Figure 8. n(p)/n(Saha) versus time for quantum level two, case A.

collisional transfers to the 2^1P and 2^1S levels, and they all show a slight depression below the equilibrium value. All of the singlet states of quantum level 3 show a tendency to be populated slightly less than the triplet states, reflecting the more efficient collision processes to the 2^1P state from the other singlet states. However, the difference between the singlet and triplet states is only about 10 percent, and graphical distinction is not justified.

Figure 9 shows the time development of the substate of quantum levels 2 and 3 for case C. The 3^3P and 3^3D as well as the 3^1S, 3^1D, and 3^1P levels are close enough together energetically that at this density they are coupled together strongly and decay together. Thus, the two triplet states are plotted together as a single curve as are the three singlet states of quantum level 3. Case C is at a lower total density than case A and Fig. 9 illustrates this through the larger spread in the various densities. Again the 2^1P level tends to depopulate radiatively from t = 0.0 sec. The depression of the 2^1P density tends to depress the density of the other singlet states adjacent to it because of collisional transfer to the 2^1P state. The largest effect is on the 2^1S level because the 2^1S and 2^1P levels are closer together energetically than the 2^1P and 3^1S levels.

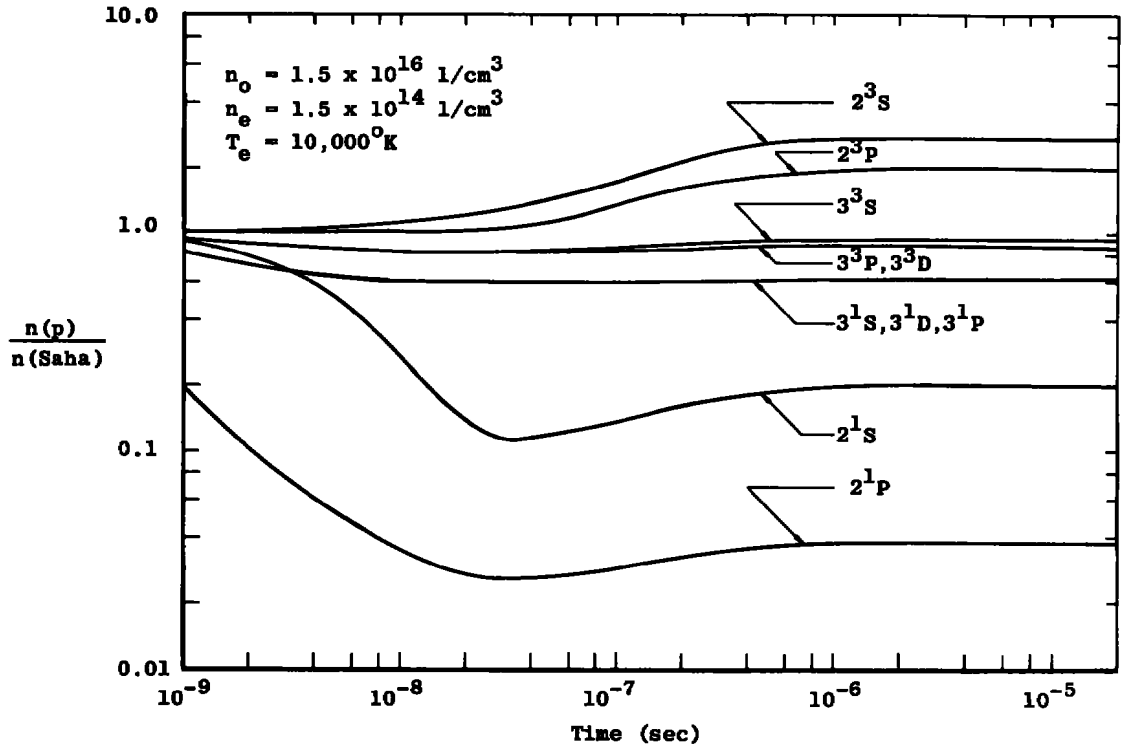

Figure 9. n(p)/n(Saha) versus time for quantum levels two and three, case C.

The metastable 2^3S level has a large radiative population rate so that from t = 0.0, it is increasing in density. Even though the 2^3S level is collision dominated, the radiative rate is of comparable magnitude at this density. Since the initial condition for this plasma was a Boltzmann distribution, the collisional population and depopulation rates balance each other so the net effect on the total rate for the 2^3S level is radiative. At about 3 x 10^{-8} sec, the 2^3S and 2^3P densities (the 2^3P increases because of strong collisional coupling to the 2^3S level) have increased in density enough that exchange transitions to the 2^1S and 2^1P levels balance the radiative rate from the 2^1P level and then, as the triplet states continue to increase in density, the collisional rate dominates and the densities of the singlet states increase until the plasma achieves QSS and computations are terminated.

Figure 10 shows the time development of the 2^1P radiative rate, two-body collisional rate, and total rate for case C. Each quantity is the algebraic sum of the populating and depopulating processes. As can be seen, the major contributor to the total rate for short times is radiative depopulation.

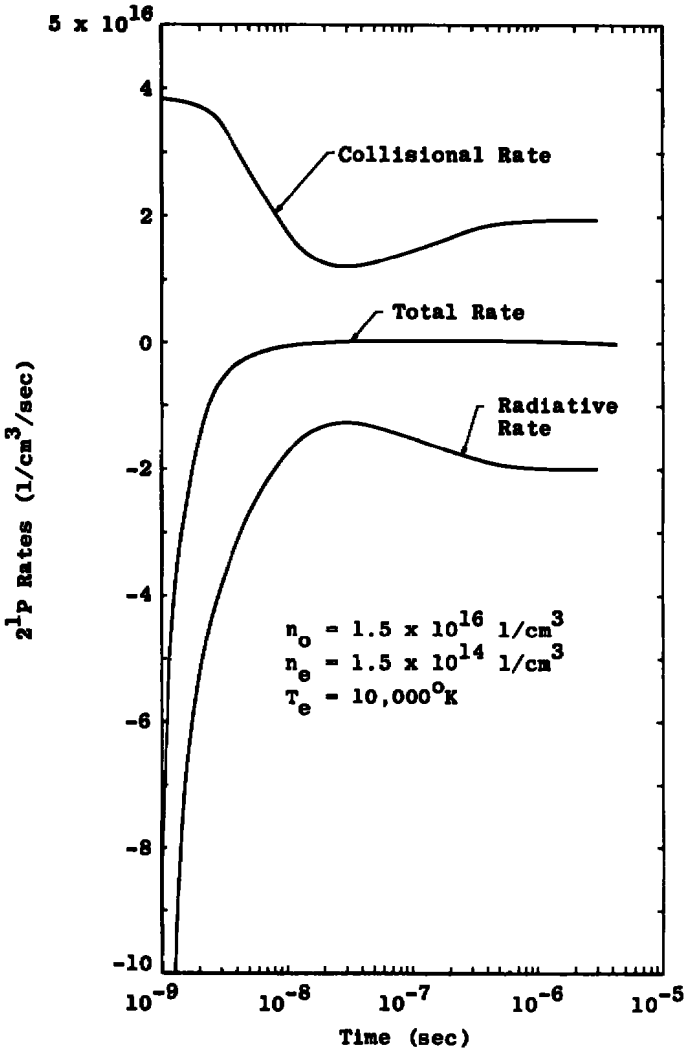

Figure 10. 2^1P collisional, radiative, and total rates versus time, case C.

Throughout this early time period, the radiative rate dominates sufficiently that the 2^1P density decreases. Thus, the radiative rate also decreases. This decrease in density causes a net depopulation of adjacent states so the collisional rate decreases. In the region 1×10^{-8} sec $\leq t \leq 3 \times 10^{-8}$ sec the 2^3S and 2^3P levels attain a high enough density that the collisional rate begins to increase. Although the scale of Fig. 10 is too large to provide visual resolution, at about 3×10^{-8} sec the total rate becomes slightly positive, reflecting the balance between the radiative and collisional rates. Subsequently, the collisional rate continues to increase because of the continuing increase in density of the adjacent levels. Reflecting the increase in the 2^1P density, the

radiative depopulation rate also tends to increase. Finally, at about 1×10^{-6} sec the collisional rate begins to flatten because QSS is being attained by the other levels and the collisional-radiative processes strike a final balance for the 2^1P level.

Figure 11 shows the two-body collisional depopulation rate, the two-body collisional population rate, and the radiative rate for the 2^1S level of case C. The radiative rate has been increased an order of magnitude for plotting purposes, and the collisional depopulation is plotted as a positive quantity.

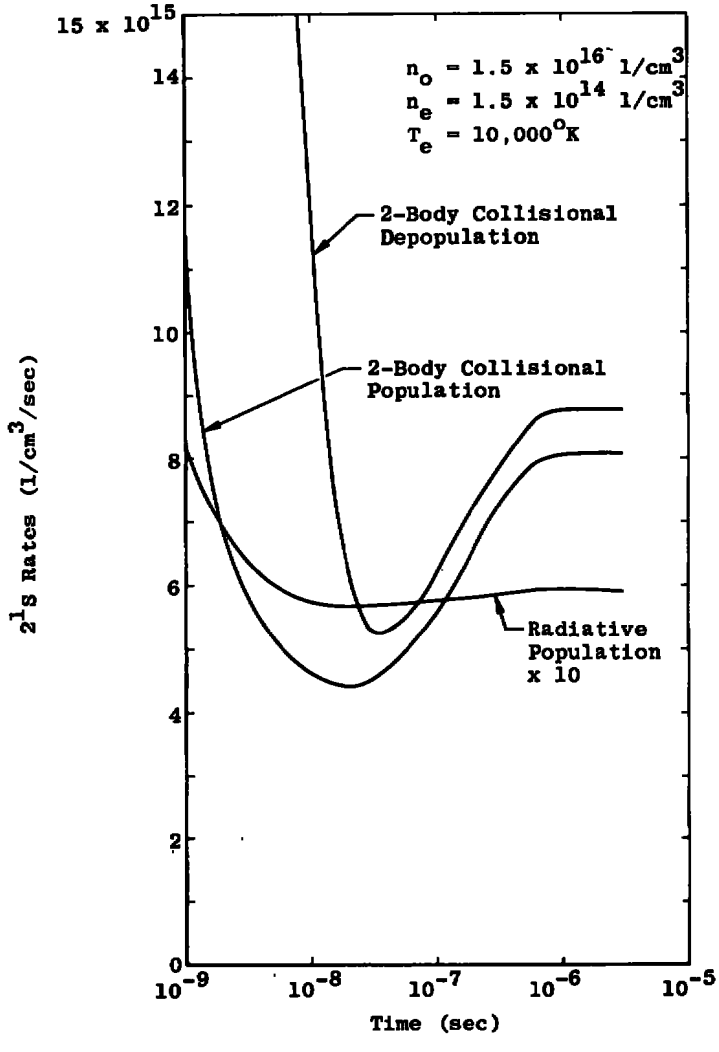

Figure 11. 2^1S radiative population, two-body collisional population and two-body collisional depopulation rates versus time, case C.

The decay of the 2^1S level is dominated strongly by the collisional depopulation rate until about about 3×10^{-8} sec. The collisional population rate shows a marked decrease through the early portion of the decay, primarily because of the decrease in the 2^1P density. By about 2×10^{-8} sec, however, the 2^1P density has decreased enough, and the 2^3S and 2^3P densities increased enough, that the exchange collisions from the 2^3S and 2^3P levels are an appreciable factor in the 2^1S collisional population rate. Subsequently, as these triplet states increase, so does the collisional population rate of the 2^1S level. The collisional depopulation rate shows a very steep decrease until about 3×10^{-8} sec reflecting the rapid decrease of the 2^1S level because of this process. At 3×10^{-8} sec, however, the radiative rate and the collisional population rate are sufficient to dominate the total rate, so the 2^1S density increases. With the increase in density, the collisional depopulation rate also increases. The noticeable difference between the collisional population and depopulation rates reflects the fact that the 2^1P density is below the equilibrium configuration with the 2^1S density, and collisional processes are attempting to bring the 2^1P density into this configuration. The flattening of the rates at about 10^{-6} sec shows that QSS for the entire distribution is being achieved. At 10^{-6} sec, the 2^1S total rate is 6×10^{11} atoms/cm^3/sec, significantly less than any of those rates plotted, and this shows the collisional radiative balance which is maintained at QSS.

Figure 12 shows the time development of the substates of quantum levels 2 and 3 for case E. This plasma is at the same electron temperature and degree of ionization as cases A and C but the total density is lower. Hence, the plasma is more radiation dominated and the spread of the various quantum levels is more dramatic. Because the plasma is less collision dominated, the 2^1S density tends not to decrease as far as in the previous cases. The triplet states of quantum level 3 show some separation at the early and the later times and the 2^1P level shows a very dramatic decrease in density.

The separation of the singlet and triplet states of quantum level 3 is much more evident here. The P and D states are quite close together energetically and thus are collisionally coupled together quite strongly. The 3^1P state is influenced by the large radiative rate to the ground state and hence the 3^1P and 3^1D levels show a noticeable reduction in density compared to the 3^1S state. In the early stages of decay the 3^3P rate is determined principally by the radiation to the 2^3S level so that the 3^3P and 3^3D levels decay rapidly. The 3^3S level rate is also largely determined by radiation to the 2^3P level but this proceeds at a slower rate than the 3^3P, 3^3D decay. At about 2×10^{-7} sec, the

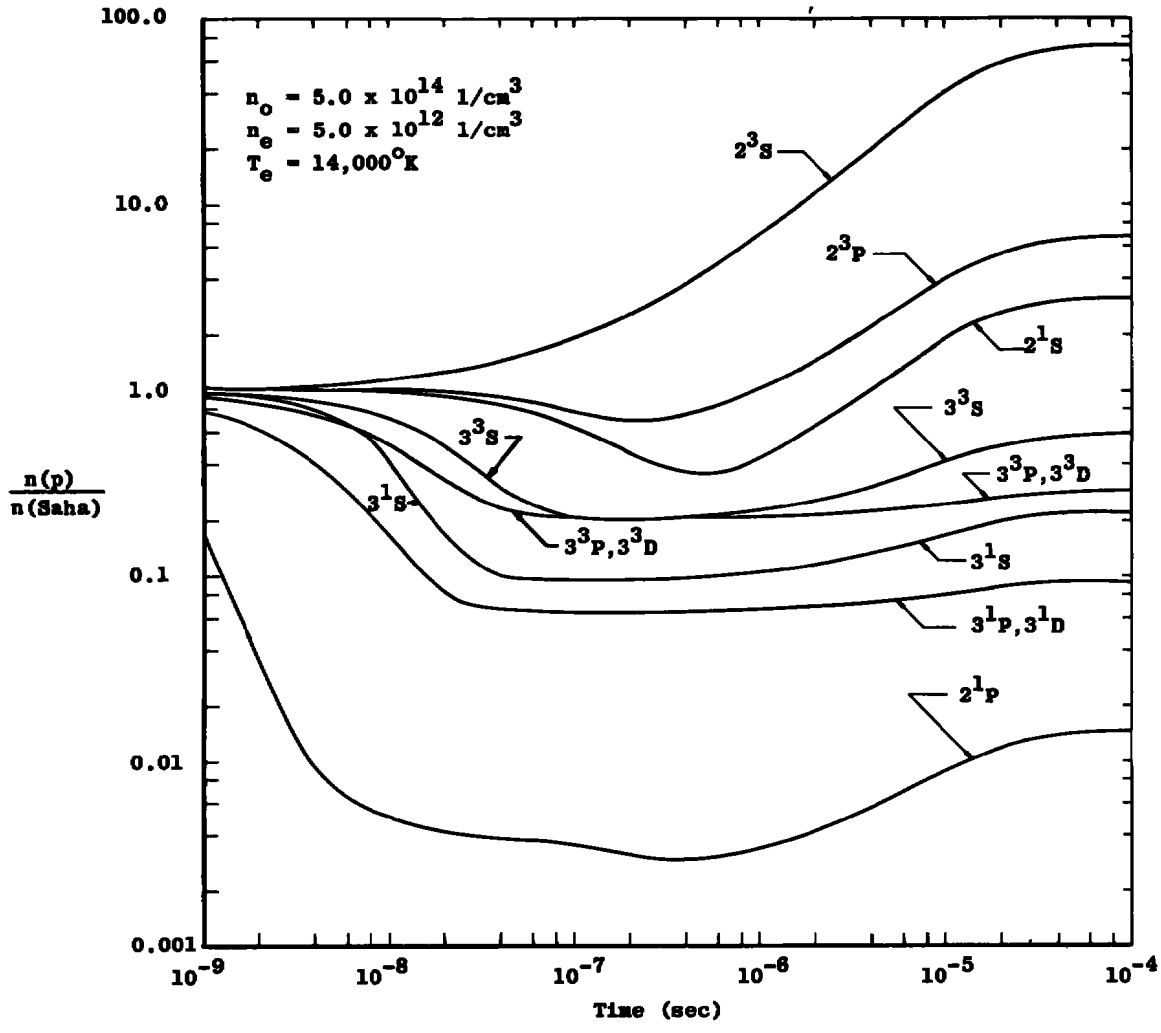

Figure 12. n(p)/n(Saha) versus time for quantum levels two and three, case E.

density of the 2^3S level has increased enough that collisional transfers to the 2^3P cause its density to begin to increase. During the period of balancing of collisional-radiative rates between the triplet states of quantum levels 2 and 3, 6×10^{-8} sec $\leq t \leq 3 \times 10^{-7}$ sec, collisional processes between the triplet states of quantum level 3 can bring these states into a Boltzmann configuration with each other. After about 3×10^{-7} sec, the 2^3S and 2^3P densities have increased to the point that the triplet states also start to increase in density. Because of the larger radiative rate from the 3^3P level, and the fact that as it adjusts it must also maintain the 3^3D state in a Boltzmann configuration, the 3^3P and 3^3D states do not show as marked an increase in density as the 3^3S state.

Figure 13 shows the same quantum levels for case J at the same conditions as case E except the electron temperature is 14,000°K. As a result the collisional processes for this plasma are stronger than case E and the curves do not show quite as much spread. The 3^3S density is separated somewhat more from the 3^3P and 3^3D densities because of the stronger coupling between the 2^3P and 3^3S state at the higher temperature. The 2^3S level tends to rise to a higher density for case J than for case E. This is because collisional processes are more efficient at the higher temperature so that the collisional population and depopulation rates remain closer together, tending to cancel each other. Thus, the 2^3S level must rise to a higher density in order for collisional depopulation to dominate collisional population sufficiently to also cancel the radiative population rate.

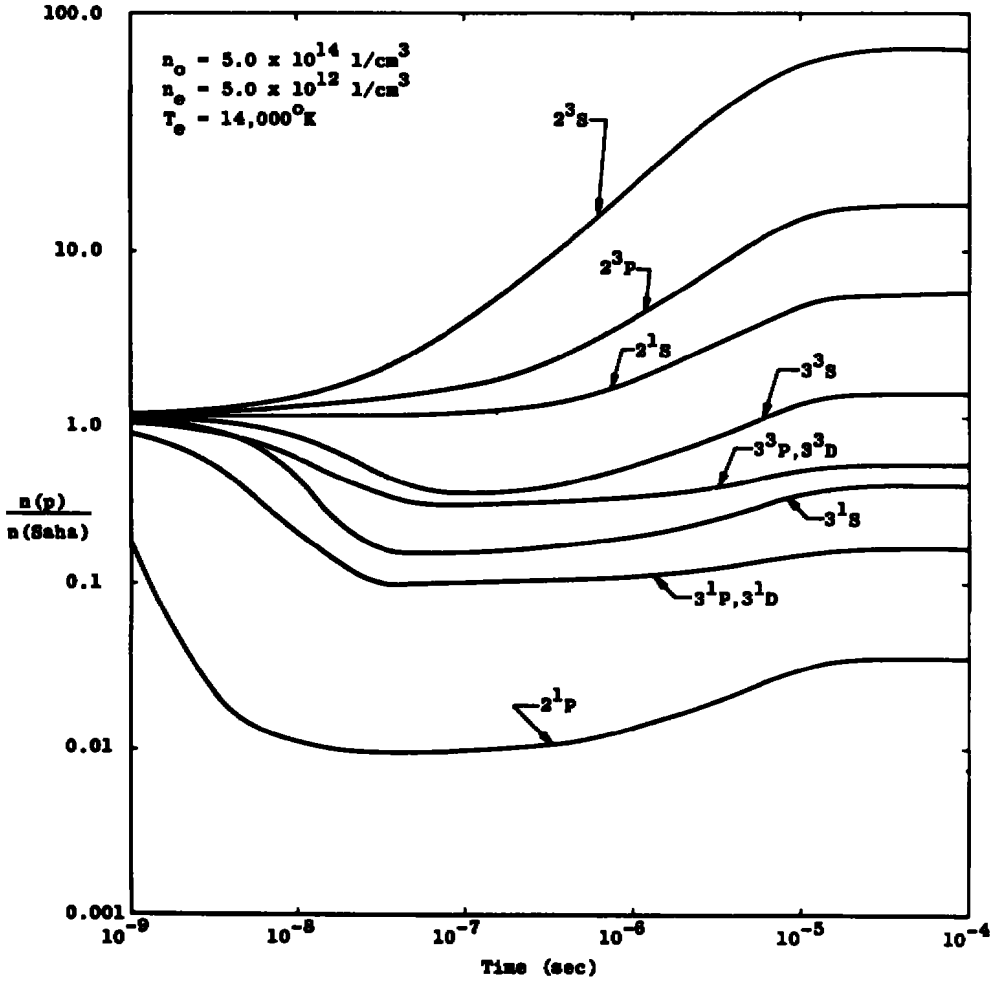

Figure 13. n(p)/n(Saha) versus time for quantum levels two and three, case J.

Figure 14 shows the time development of substates of quantum levels 2 and 3 for case N. This plasma is at a different total density than case E (5.0×10^{14} atoms/cm^3 for case E and 2.69×10^{15} atoms/cm^3 for

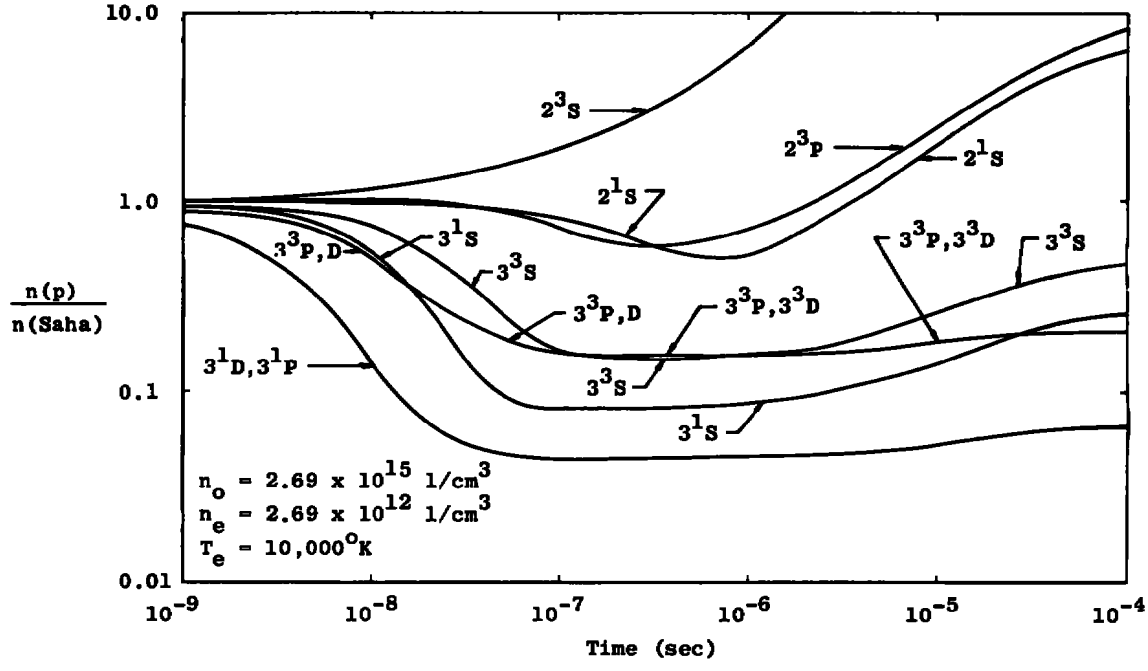

Figure 14. n(p)/n(Saha) versus time for quantum levels two and three, case N.

case N), but the electron densities are nearly the same (5×10^{12} for case E compared with 2.69×10^{12} for case N), and the electron temperatures are the same. The character of the curves is about the same in Figs. 14 and 12, with the slight differences reflecting the slight decrease in the magnitude of collisional processes due to the lower electron density. This is well illustrated by the fact that the 2^1S density tends to be slightly greater than the 2^3P level until about 3×10^{-7} sec. This is due to the small decrease in the collisional coupling of the 2^1S to the 2^1P level while the radiative transitions from the 2^3P to the 2^3S level play a proportionately greater role for the early portion of the decay. The 2^1P and 2^3S levels are not included in their entirety in Fig. 14 since their characteristics are now well documented by the previous figures. The 2^1P level reaches a minimum ordinate of 0.0023 at about 5×10^{-7} sec and returns to about 0.01 at QSS. The 2^3S level has a peak ordinate of 96.2 at QSS, $t \approx 4 \times 10^{-5}$ sec.

Figures 15, 16, and 17 show the time development of the substates of quantum levels 2 and 3 for cases I, Q, and P, respectively. These plasmas are all at the same densities and degrees of ionization but have electron temperatures of 14,000°K, 8,000°K, and 6,000°K, respectively.

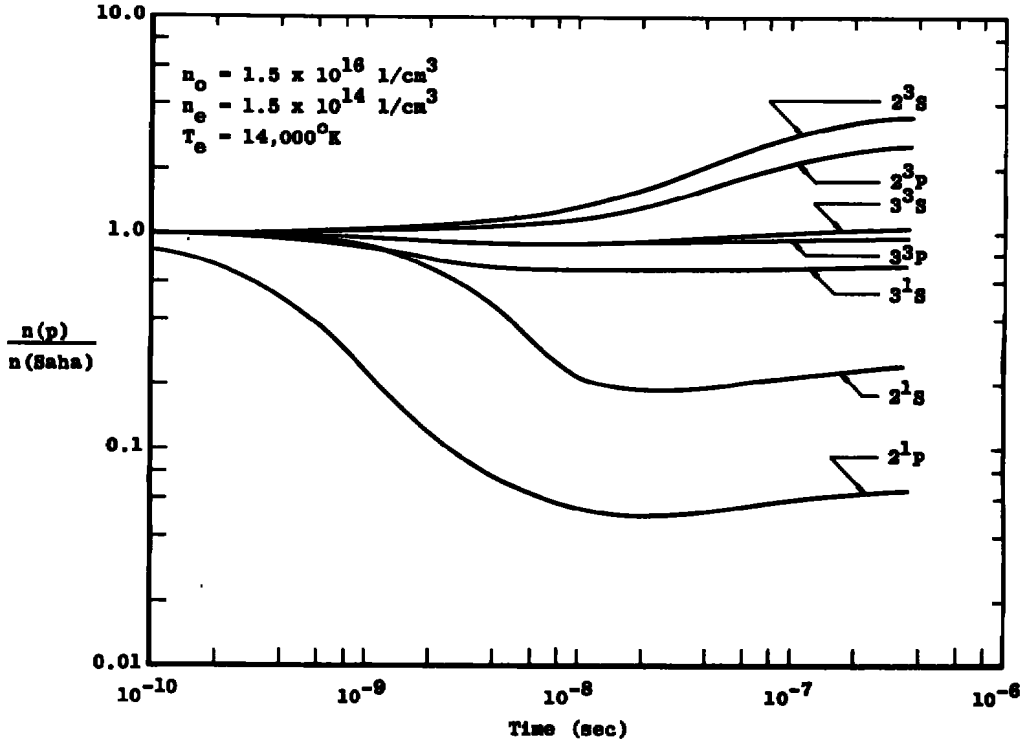

Figure 15. n(p)/n(Saha) versus time for quantum levels two and three, case I.

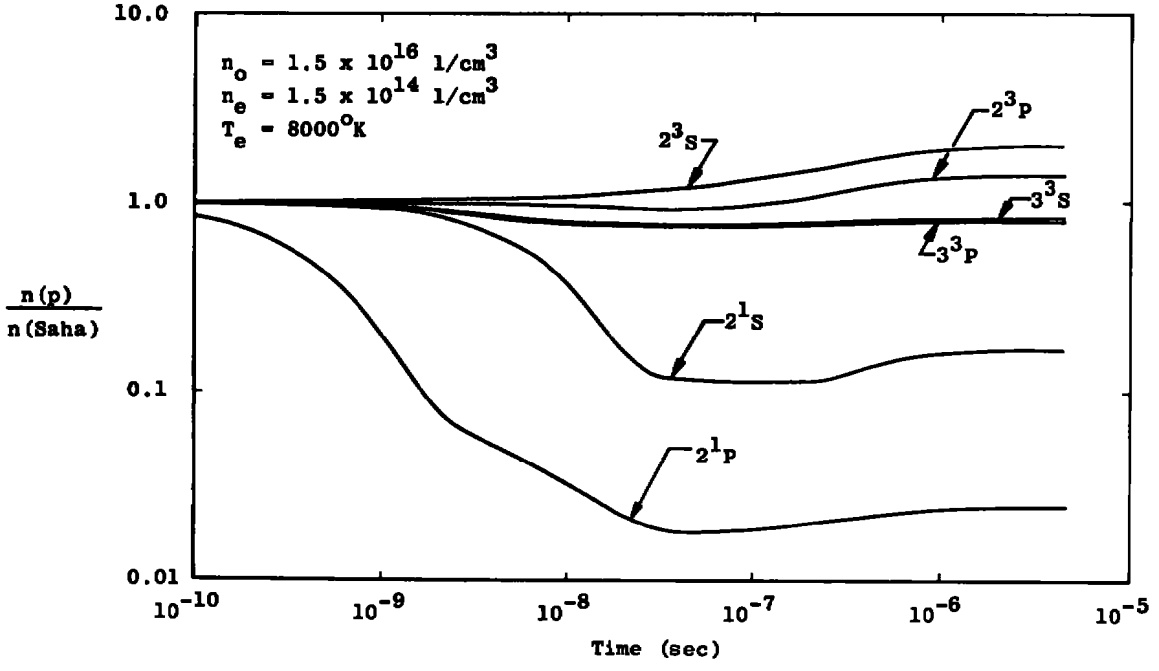

Figure 16. n(p)/n(Saha) versus time for quantum levels two and three, case P.

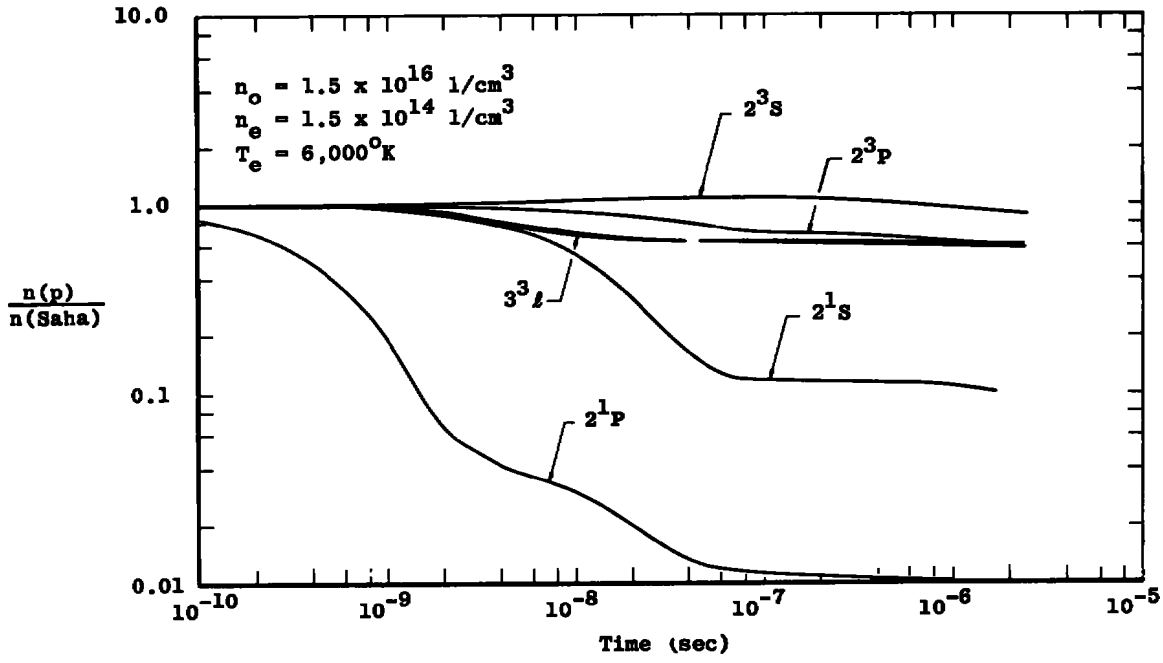

Figure 17. n(p)/n(Saha) versus time for quantum levels two and three, case Q.

Figure 9 (case C) showed the development of a plasma at the same density and degree of ionization with an electron temperature of 10,000°K. Comparison of Figs. 15, 9, 16, and 17 shows the steady decrease of importance of collisional processes and the steady increase of radiative processes as temperature is decreased.

The interplay of these collisional-radiative processes is quite complex and subtle. Detailed study of the change in the decay characteristics will be taken up later in this study. At this point, it will suffice to say that at the low temperature, Fig. 17, collisional processes are sufficiently inefficient that the radiative transitions of the 2^1P level depress it far enough that adjacent levels are also depressed in attempting to bring the 2^1P density back to the equilibrium configuration. This depression of adjacent levels in turn lowers particularly the radiative transition rate into the 2^3S level so that it does not show a marked increase in density. Without this increase in the 2^3S density, there is no subsequent increase in the other quantum levels because of collisional transfers from the 2^3S level. Thus, the entire distribution in the low-lying states is drawn below the equilibrium with the free electrons.

5.3.1 Acquisition of Quasi-Steady State

A consequence of the QSS for the optically thin plasma is the condition that the rate of change of the ground state density and the continuum density are equal in magnitude but opposite in sign (Section 2.0). Hence, observation of the time development of the ratio $\dot{n}_e/\dot{n}(1)$ will provide graphic illustration of the time development of the plasma as a whole to the QSS. At QSS, this ratio has a value of -1.

The initial conditions used for the calculations will certainly have a significant bearing upon the time development of $\dot{n}_e/\dot{n}(1)$. However, as described on the preceding pages, the initial conditions were such that the metastable 2^3S level density had to increase to reach the QSS and the other levels were both directly and indirectly affected by the metastable levels. Thus, if a physical plasma suffers a parametric change such that the densities of these levels are below their QSS value, the initial conditions chosen for this study do give realistic results.

Figure 18 shows the time development of $\dot{n}_e/\dot{n}(1)$ for cases A through G and case M. These plasmas all have an electron temperature of 10,000°K, one percent ionization, and progressively lower total densities. As one would expect, as conditions progress such that the plasma is less collision dominated, the time to acquire QSS becomes progressively

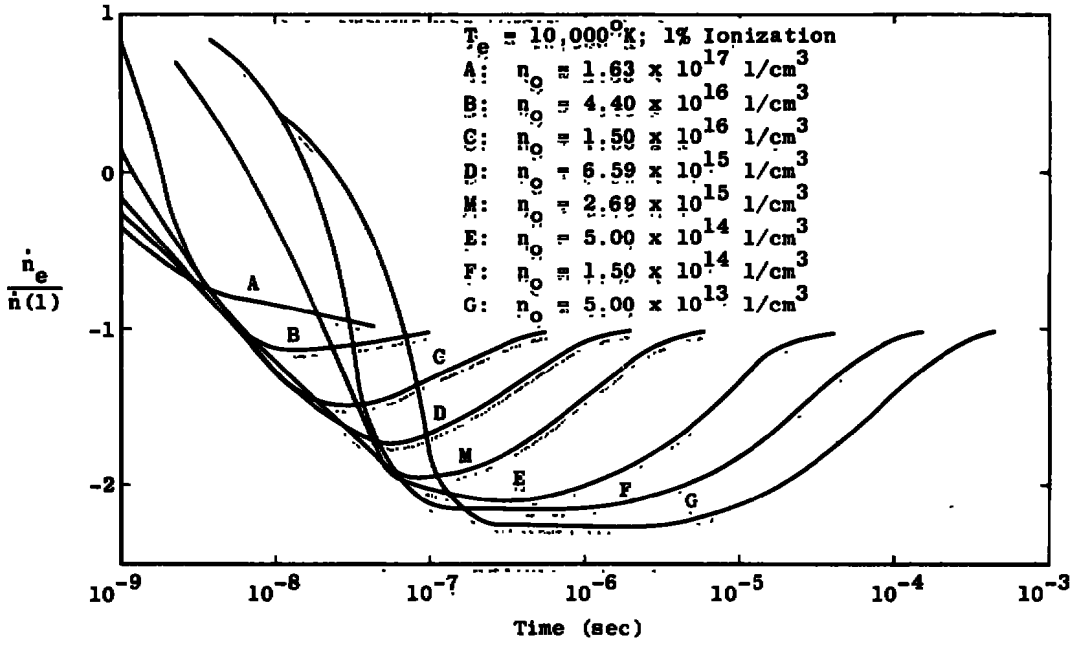

Figure 18. $\dot{n}_e/\dot{n}(1)$ versus time, cases A, B, C, D, E, F, G, and M.

longer. These times range from 3×10^{-8} sec for case A to 3.5×10^{-4} sec for case G. The criterion used for these and subsequent cases is that when $\dot{n}_e$ and $\dot{n}(1)$ agree within 5 percent ($-1.05 \leq \dot{n}_e/\dot{n}(1) \leq -0.95$) the plasma is considered to be at the QSS. A consistent (case A the only exception) characteristic is the overshoot of the QSS condition early in the decay of each plasma and then the subsequent slow recovery back to the QSS conditions. This phenomenon will be studied in detail below.

Figure 19 shows the time development of $\dot{n}_e/\dot{n}(1)$ for cases H through K. These plasmas are at similar densities and degrees of ionization as cases A, C, E, and G, respectively, except that the electron temperature is elevated to 14,000°K. The character of the curves in Fig. 19 compared to those in Fig. 18 is quite similar, except that the QSS is achieved slightly sooner (2.5×10^{-8} sec for case H compared to 2.5×10^{-8} sec for case A, 2.3×10^{-4} sec for case K compared to 3.5×10^{-4} sec for case G) and the magnitude of overshoot is slightly greater.

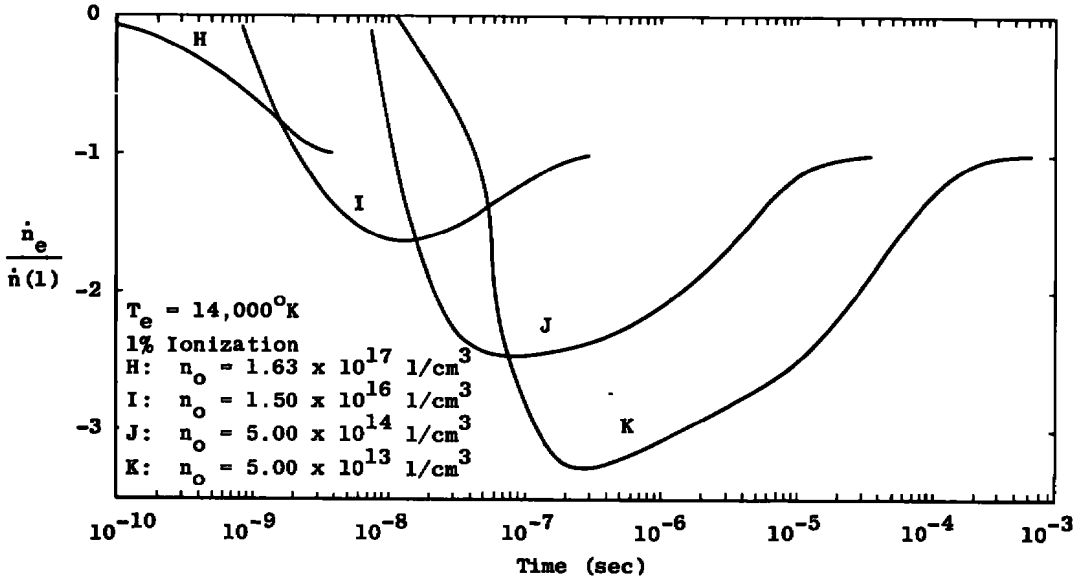

Figure 19. $\dot{n}_e/\dot{n}(1)$ versus time, cases H, I, J, and K.

Figure 20 shows the time development of $\dot{n}e/\dot{n}(1)$ for cases L through O. These cases are all at the same total density and electron temperature but at different degrees of ionization. The character of these curves is also consistent with those in Figs. 18 and 19.

Figure 21 shows the time development of $\dot{n}_e/\dot{n}(1)$ for cases C, I, P, and Q. These plasmas are all at the same density and ionization but

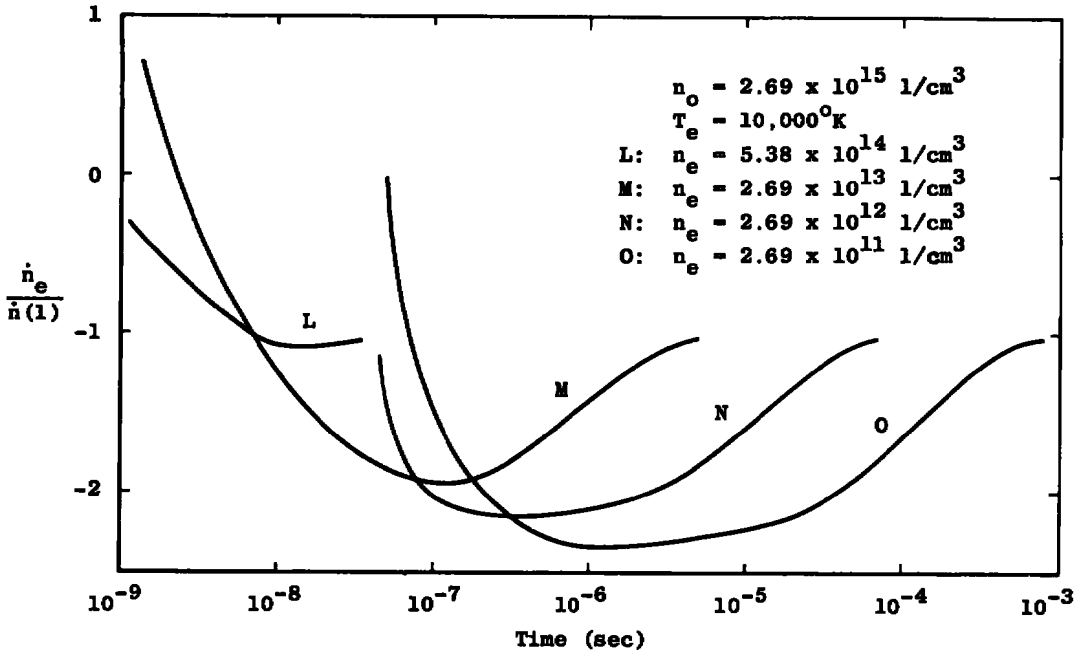

Figure 20. $\dot{n}_e/\dot{n}(1)$ versus time, cases L, M, N, and O.

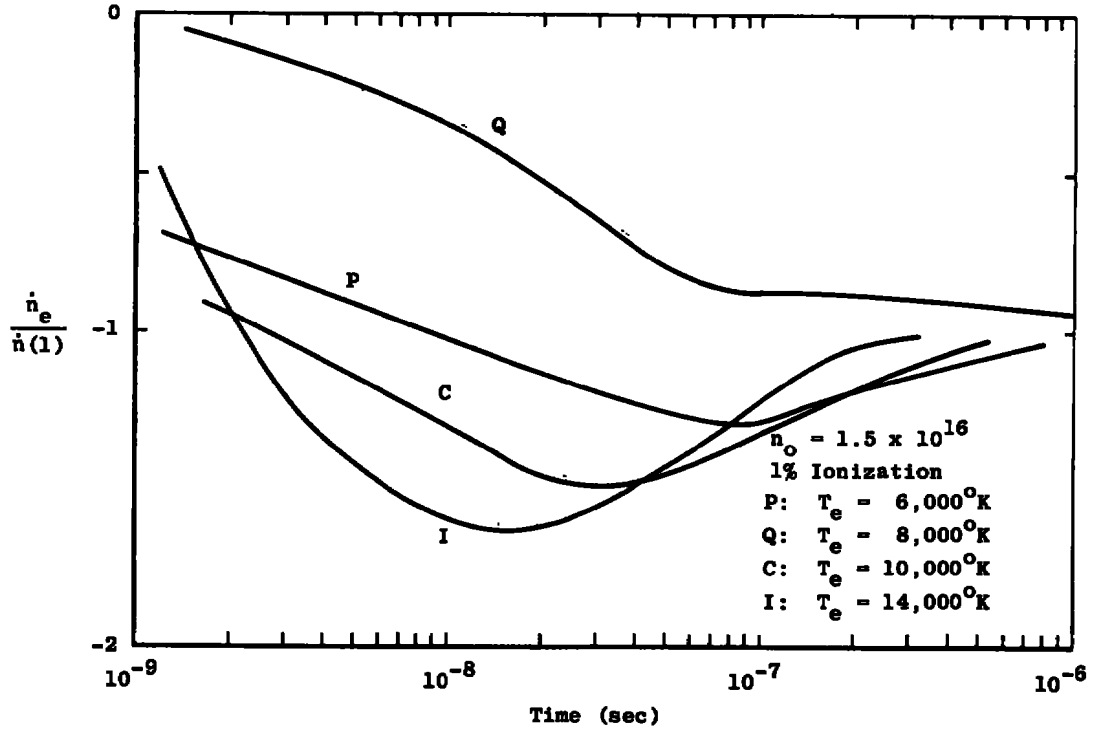

Figure 21. $\dot{n}_e/\dot{n}(1)$ versus time, cases C, I, P, and Q.

each is at a different electron temperature. This again shows the consistent behavior that as collisional rates get larger (increasing temperature) the time for the plasma to achieve QSS gets progressively smaller. One can also see the tendency for the overshoot to become progressively larger as the electron temperature becomes larger. Case Q, the lowest temperature case, does not show the overshoot and will be discussed in more detail below.

Regardless of the character of the decay, the time to achieve QSS was not extremely sensitive to the electron temperature, ranging from 2×10^{-7} sec for case I (T_e = 14,000°K) to 1.2×10^{-6} sec for case Q (T_e = 6,000°K).

5.3.2 Overshoot of Quasi-Steady State

A consistent character of the $\dot{n}_e/\dot{n}(1)$ curves is the overshoot of the QSS early in the decay of most of the plasmas (cases A, H, and Q the only exceptions) and then the slow recovery back to the QSS. This could be due to an overshoot of QSS conditions of either $\dot{n}_e$ or $\dot{n}(1)$ but in fact both quantities show the character to a greater or lesser degree. It is also tempting to ascribe the overshoot to numerical inaccuracies in the program but it is in fact a physical phenomenon depending upon the initial conditions.

The precise balancing between the various processes included in the ERE induces large time gradients in the excited state densities during the early stages of computation. However, these numerical requirements are satisfied very early ($t < 10^{-10}$ sec) in the decay with no appreciable changes in the excited-state densities. The subsequent plasma decay is attributable to the physical imbalance of the terms in the ERE because of the initial distribution. Thus physical plasmas which suffer parametric changes which require a significant 2^3S density increase to achieve QSS will also be subject to the overshoot phenomenon.

Case C was chosen to examine the overshoot phenomenon in more detail. This case shows the phenomenon quite well yet does not require such large times to re-establish QSS that study can become unwieldy.

Figure 22 shows the detailed time development of the rates of change of the continuum as well as the 1^1S, 2^3S, and 2^3P bound states for case C. This shows that both the ground state and free electron rates overshoot their QSS values and converge back toward their QSS value slowly. Of specific interest in this context is the 2^3P level. By

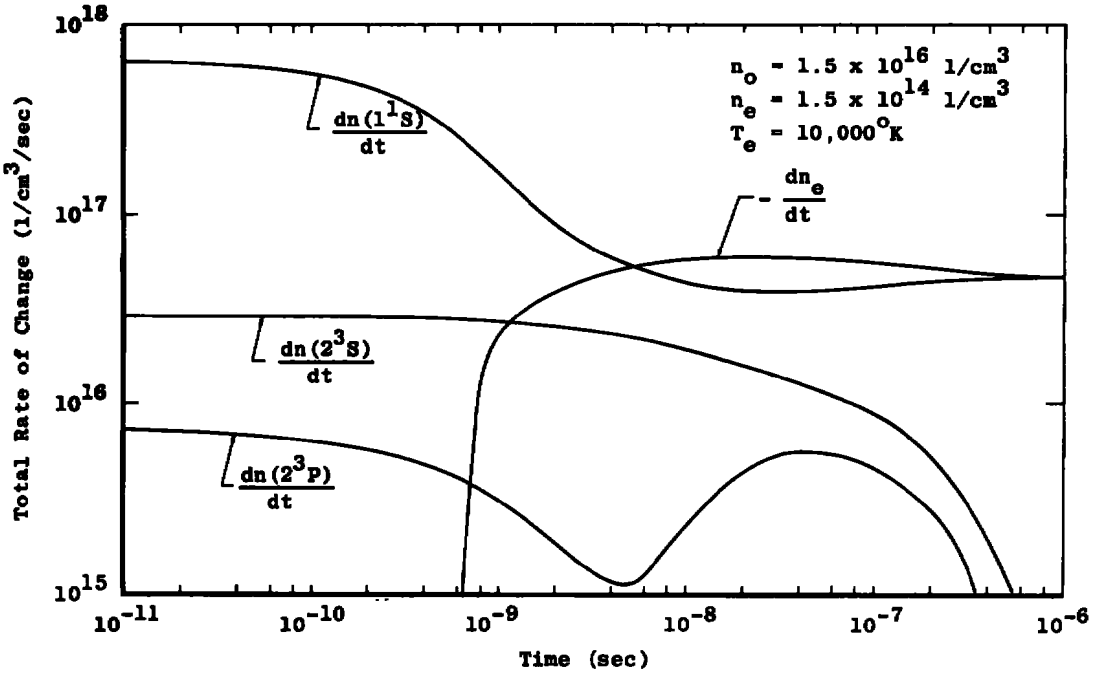

Figure 22. Total rate of change of 1^1S, 2^3S, 2^3P quantum levels and free electron density versus time, case C.

comparing the shape of the curves for the time development of the 2^3P and continuum rates, it is seen that the continuum overshoot follows the sudden growth of the 2^3P rate from about 5 x 10^{-9} sec through about 3 x 10^{-7} sec and then slowly falls to the QSS value with the fall of the 2^3S and 2^3P rates to the QSS. In this region of time some of the other quantum levels will also show a similar variation in their rates for the reasons described below. The early part of the continuum rate curve, $t \leq 10^{-9}$ sec, follows the adjustment of the other quantum levels toward their QSS value.

Figure 23 examines the time development of the 2^3P rate in more detail illustrating both the collisional and radiative contributions to the net rate. Initial conditions for this plasma were such that the 2^3P density is less than its QSS value so there is a tendency for the 2^3P level to populate radiatively in the early portion of the decay. As the level continues to populate radiatively, the density increases so that radiative population consequently increases and collisional depopulation decreases.

Hence, as time progresses, the radiative rate becomes progressively smaller and the collisional depopulation rate becomes larger for $t \leq 5 \times 10^{-9}$ sec. At this point, however, the collisional rate reverses

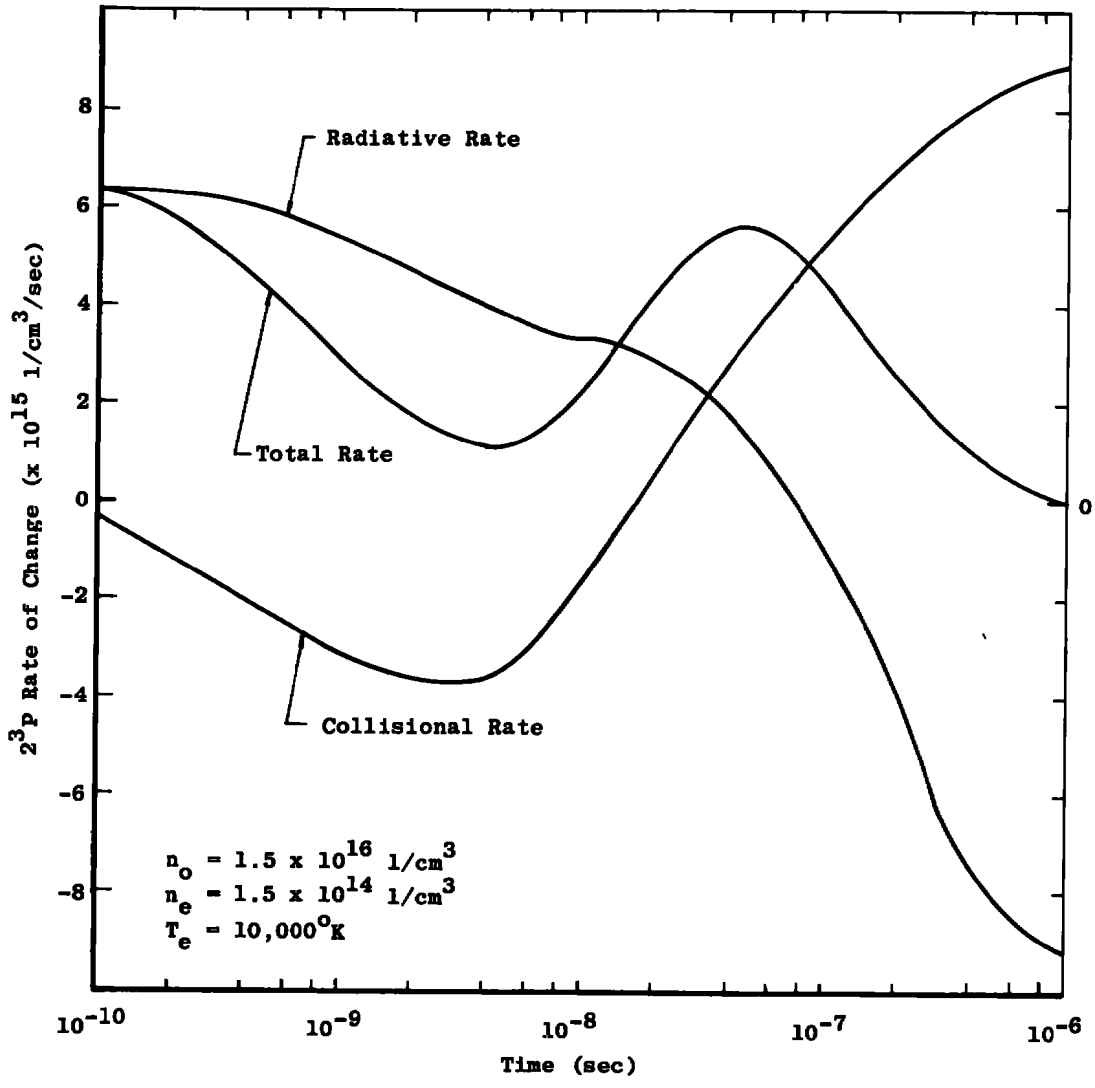

Figure 23. 2^3P collisional rate, radiative rate, and total rate versus time, case C.

directions from a depopulating effect to a populating effect. With the subsequent increase in the population density, the radiative rate serves to increasingly depopulate the state until about 10^{-6} sec when the collisional and radiative rates balance each other and the state approaches QSS. By referring to Fig. 22 one sees that throughout this oscillation of the 2^3P rate the metastable 2^3S level has been populating radiatively at a high rate. At about 5 x 10^{-9} sec the 2^3S level has become sufficiently populous that direct excitation 2^3S - 2^3P collisions with the continuum can begin to have a discernible effect upon the 2^3P rate. Collisional transfers out of the 2^3S level to all levels, however, are not sufficient to balance the radiative rate into it so that the 2^3S level continues to

populate, and thus the transfer rate to the 2^3P level becomes larger until QSS is reached. As the collisional rate from the 2^3S to the 2^3P rate becomes large enough to begin to balance the radiative rate, the 2^3S level rate decreases to its QSS value. As its total rate decreases toward zero, the collisional rate to the other quantum level flattens out so that the other collisional radiative processes can balance the total rate for each individual quantum level to the QSS value. The slow equilibration of the collisional and radiative rates for the 2^3S and 2^3P levels is communicated by collisional processes back through the bound states to the electron continuum. Thus as these rates fall to their QSS value, they have a decreasingly important contribution to the continuum rate, and the continuum rate can also slowly subside to the QSS value.

Figure 24 illustrates the time development of the population densities of the 2^3S, 2^3P, 2^1S, and 2^1P levels for case C. This shows the slow increase of the triplet states to their QSS value while examination of the singlet states reveals the cause of the ground state rate overshoot shown in Fig. 22. The 2^1P level has a large radiative transition probability to the ground state. Hence, its population density shows a very rapid decrease through the early part of the decay. As its density falls below the equilibrium configuration, collisions have a tendency to fill it and especially collisional transfers from the 2^1S state. Hence, the 2^1S state also shows a reduction in density but lags slightly behind the 2^1P level. At about 1×10^{-8} sec, the 2^1P level has lowered in density

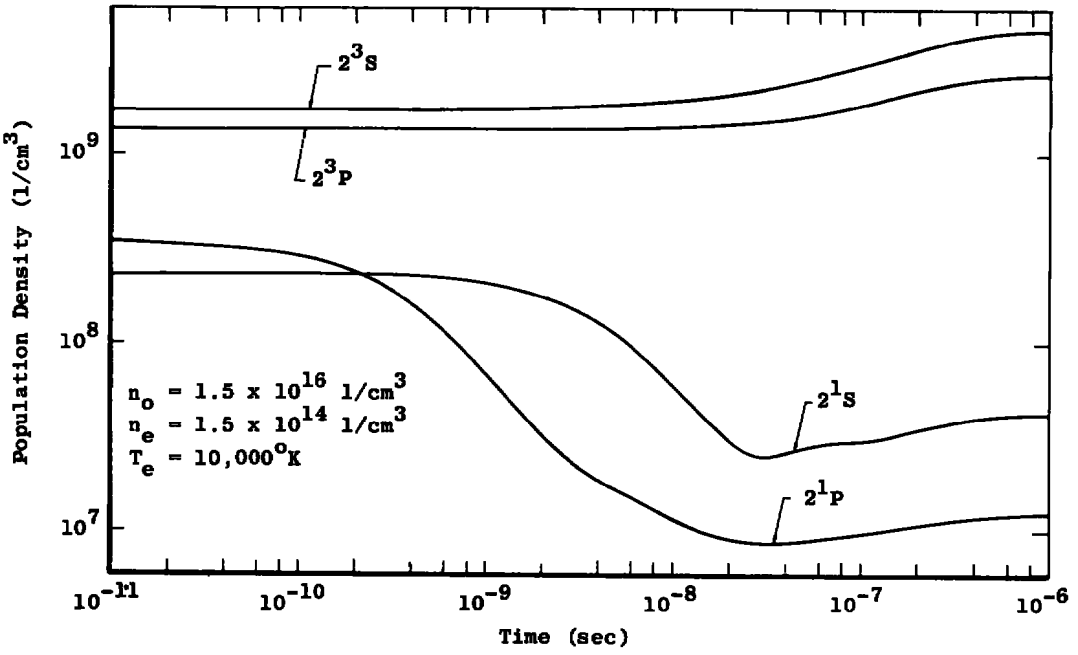

Figure 24. 2^3S, 2^3P, 2^1S, and 2^1P population densities versus time, case C.

sufficiently that collisional rates can begin to balance radiative rates, so the density curve begins to flatten. However, the triplet states are continuing to increase in density so that exchange transfers between the triplet and singlet states become more numerous and serve to elevate the population densities of the singlet states. The largest single contributor to the ground state rate is radiative transitions from the 2^1P state. By comparing the ground state rate in Fig. 22 to the 2^1P population density in Fig. 24, one sees that as the 2^1P density decreases, goes through a minimum, and slightly increases, so does the ground state rate. This effect of the 2^1P level upon the ground state rate is prevalent for all cases which show overshoot.

In summary, those cases that show an overshoot of $\dot{n}_e/\dot{n}(1)$ do so basically because of the need of the 2^3S density to increase to its QSS value. This increase in density causes the continuum rate overshoot because the collisional transfers between the 2^3S level and adjacent quantum levels induce time rates of changes in these levels which are significant with respect to the continuum and ground state rates. The ground state rate overshoot is caused specifically because the increase in the 2^3S density induces an increase in the 2^1P density with an attendant increase in the 1^1S-2^1P radiation.

5.3.3 No Quasi-Steady-State Overshoot

As indicated previously, three of the plasmas studied showed no overshoot of the QSS condition but rather decayed directly to QSS. Two of these cases, A and H, are high density cases which are strongly collision dominated. Little needs to be said for these two as to why they do not show the overshoot characteristics. Since they are strongly collision dominated, slight changes in any quantum level's density is quickly communicated to the other levels so that the QSS distribution is quickly reached. No single process, e.g., 2^1P radiation, can cause one quantum level to over-depopulate but rather all levels approach QSS together.

The other case which shows no overshoot, case Q, is somewhat different in nature, however. In this low temperature situation (T_e = 6,000°K) the collisional processes are sufficiently inefficient that the radiative decay of the 2^1P density acts as a sink for the rest of the distribution.

Table 5 shows the radiative population rate for the 2^3S level for each of the cases C, I, P, and Q at initial conditions and at QSS. Inspection of this table shows that of these cases, case Q is the only one which

Table 5. Comparison of 2^3S Radiative Rates at Initial Conditions and Quasi-Steady State for Cases, C. I, P, and Q

Case	T_e °K	2^3S Radiative Rate atoms/cm^3/sec	
		Initial	QSS
I	1.4^4[a]	7.98^{15}	1.19^{16}
C	1.0^4	2.91^{16}	4.11^{16}
P	8.0^3	8.97^{16}	1.04^{17}
Q	6.0^3	6.14^{17}	3.77^{17}

[a]Superscripts denote powers of 10 by which the numbers are to be multiplied.

shows a decrease in the rate with which the 2^3S level increases because of radiative transitions. This implies that particularly the 2^3P level has suffered a significant decrease in density (at QSS for case I, the 2^3P contributes 55 percent of the 2^3S radiative rate). To understand how this comes about, it is informative to examine the rate coefficients for collisional transitions between the substates of quantum level 2. These are shown in Table 6 for electron temperatures of 6,000°K and 10,000°K for comparison. Included in the table for discussion purposes is the minimum temperature the projectile electron must exhibit to effect the transition.

Table 6. Comparison of Collisional Rate Coefficients for Quantum Level Two Transitions at 10,000°K and 6,000°K

Transition	Rate Coefficients cm^3/sec		Minimum Temperature °K
	$T_e = 1.0^4$°K	$T_e = 6.0^3$°K	
$2^3S - 2^1S$	7.03^{-9}[a]	3.10^{-9}	9.2^3
$2^3S - 2^3P$	1.58^{-7}	3.98^{-8}	1.3^4
$2^3S - 2^1P$	3.76^{-9}	1.17^{-9}	1.6^4
$2^1S - 2^3P$	1.42^{-8}	8.98^{-9}	4.0^3
$2^1S - 2^1P$	1.21^{-6}	4.79^{-7}	6.9^3
$2^3P - 2^1P$	1.77^{-8}	1.24^{-8}	3.0^3

[a]Superscripts denote powers of 10 by which the numbers are to be multiplied.

Examination of the rate coefficients at 10,000°K shows that, as would be expected, the direct transitions, $2^3S - 2^3P$ and $2^1S - 2^1P$, are the most important by at least an order of magnitude. However, at 6,000°K the $2^3P - 2^1P$ transition is competitive with the $2^3S - 2^3P$ transition. This is because at 6,000°K most of the electron distribution is still available to effect the transition (a 3,000°K electron has sufficient energy) and even though it is an exchange transition, the magnitude of the rate coefficient is not significantly altered. For the direct $2^3S - 2^3P$ transition, a 13,000°K electron is required and at 6,000°K an appreciable portion of the electron distribution has insufficient energy to effect the transition. Hence, the rate coefficient is markedly reduced. Similar arguments hold for the $2^1S - 2^3P$ transition, which requires a 4,000°K electron for the transition.

Thus at 6,000°K, as the 2^1P level depresses radiatively, the other levels attempt to bring it back to the equilibrium configuration and are also depressed. The details of this depend upon the following coupling processes.

The 2^1S level and the 2^3P level are the major contributors to repopulating the 2^1P level. The 2^1P radiation dominates this repopulation so that these two contributors are also depressed. At the high temperatures, the $2^3S - 2^3P$ rate coefficient dominates the $2^3P - 2^1P$ rate coefficient by an order of magnitude. Thus, the 2^3P level is prevented from being depopulated by $2^3P - 2^1P$ transitions. At the low temperature, the $2^3S - 2^3P$ rate coefficient is of the same order of magnitude as the $2^3P - 2^1P$ rate coefficient and as a result, the $2^3P - 2^1P$ transition forces the 2^3P density significantly below the equilibrium configuration. The 2^3S level is consequently depleted in attempting to fill the 2^3P level. This depletion of the 2^3S density in turn affects all the other level densities and thus, at 6,000°K, the entire distribution decays below equilibrium.

The foregoing discussion of overshoot has shown the specific mechanisms by which overshoot is established for the various plasmas. It has been shown that the overshoot characteristics are determined principally by the 2^3S state and the 2^1P state. The overshoot of the quantity $\dot{n}_e/\dot{n}(1)$ is caused by the overshoot of both the continuum rate and the ground state rate with the overshoot of the ground state rate showing a somewhat more consistent trend with varying plasma conditions. This is illustrated in Table 7, which has reordered the various plasmas studied in order of increasing overshoot of $\dot{n}_e/\dot{n}(1)$. Included in the table are the $\dot{n}_e(\max)/\dot{n}_e(QSS)$, $\dot{n}(1)(\min)/\dot{n}(1)(QSS)$, the ratio of the 2^3S collisional depopulation rate to the radiative population rate at

Table 7. Maximum Value of $\dot{n}_e/\dot{n}(1)$, $\dot{n}_e/\dot{n}$ (QSS), Minimum Value of n(1)/n(1) (QSS), and Ratio of Collisional Rate to Radiative Rate at Initial Conditions for the 2^3S and 2^1P Quantum Levels for Each of the Afterglow Plasmas Studied

Case	n_o $1/cm^3$	n_e $1/cm^3$	T_e °K	$\dot{n}_e/\dot{n}(1)$ maximum overshoot	$\frac{\dot{n}_e(max)}{\dot{n}_e(QSS)}$	$\frac{\dot{n}(1)(min)}{\dot{n}(1)(QSS)}$	Initial Conditions Collisional Rate / Radiative Rate 2^3S	2^1P
A	1.63^{17}	1.63^{15}	1.0^4	1.0	1.0	1.0	17.12	0.9
H	1.63^{17}	1.63^{15}	1.4^4	1.0	1.0	1.0	15.04	1.21
L	2.69^{15}	5.38^{14}	1.0^4	1.10	1.06	0.98	5.67	0.29
B	4.4^{16}	4.4^{14}	1.0^4	1.15	1.08	0.95	4.64	0.24
P	1.5^{16}	1.5^{14}	8.0^3	1.30	1.11	0.84	1.67	0.06
C	1.5^{16}	1.5^{14}	1.0^4	1.50	1.23	0.82	1.57	0.08
I	1.5^{16}	1.5^{14}	1.4^4	1.65	1.43	0.87	1.44	0.10
D	6.59^{15}	6.59^{13}	1.0^4	1.75	1.26	0.73	0.69	0.036
M	2.69^{15}	2.69^{13}	1.0^4	1.95	1.22	0.63	0.28	0.015
E	5.0^{14}	5.0^{12}	1.0^4	2.10	1.09	0.52	0.05	0.002
F	1.5^{14}	1.5^{12}	1.0^4	2.15	1.06	0.48	0.016	0.0008
N	2.69^{15}	2.69^{12}	1.0^4	2.15	1.07	0.50	0.028	0.0015
G	5.0^{13}	5.0^{11}	1.0^4	2.25	1.04	0.46	0.005	0.0002
O	2.69^{15}	2.69^{11}	1.0^4	2.35	1.04	0.44	0.003	0.0002
J	5.0^{14}	5.0^{12}	1.4^4	2.45	1.27	0.52	0.046	0.0046
K	5.0^{13}	5.0^{11}	1.4^4	3.26	1.15	0.35	0.0046	0.0013
Q	1.5^{16}	1.5^{14}	6.0^3	1.0	1.0	1.0	1.64	0.05

[a]Superscripts denote powers of 10 by which the numbers are to be multiplied.

the initial conditions, and the 2^1P collisional population rate to the radiative depopulation rate at the initial conditions. Case Q has been included at the bottom of the table for completeness. Table 7 shows that for those cases (A and H) which have strong collision dominance in the 2^3S level and competition between collisions and radiation in the 2^1P level there is no overshoot for any of the parameters. In general, as radiation becomes more important, the overshoot of $\dot{n}_e/\dot{n}(1)$ becomes greater. The ground state overshoot tends to follow a more or less consistent trend with changing plasma conditions whereas the continuum rate overshoot appears to go through a maximum in the region of conditions in which there is no clearcut domination of the 2^3S collisional or radiative rates. Cases J and K appear to be the principal inconsistent cases in the table but the better communication between the lower level rates and the continuum rates have already been discussed for these higher temperature cases. It should also be noted that cases J and K are consistent with cases H and I, which are also at an electron temperature of 14,000°K. The reason for no overshoot for case Q has also been discussed previously.

5.4 VALIDITY OF CRR

The preceding discussion of the mechanisms by which QSS is established showed that, except for a limited range of plasma conditions, the continuum rate does not deviate drastically from its QSS values. Thus one would expect the results of CRR theory to be applicable to the free electron density even though the QSS is not a physical reality. This in turn implies that CRR can occur physically independent of the QSS and indeed, the QSS may be unnecessary except as a mathematical convenience or in studying the quantum levels below the critical level.

This is exactly the situation as is shown in Figs. 25, 26, 27, and 28. Each of these figures displays the time-dependent CRR coefficient, $\alpha(t)$, based upon the electron density decay, $\alpha(t) = -\dot{n}_e/n_e^2$, referred to its value at QSS. Each of the Figs. 25 through 28 shows results for the same plasmas shown in Figs. 18 through 21. As expected, only those cases which showed significant continuum overshoot (Table 7, cases C, D, I, J, and M) show significant overshoot of the QSS. Even so the departure from the QSS is less severe than one would expect from examination of $\dot{n}_e/\dot{n}(1)$ shown in Figs. 18 through 21.

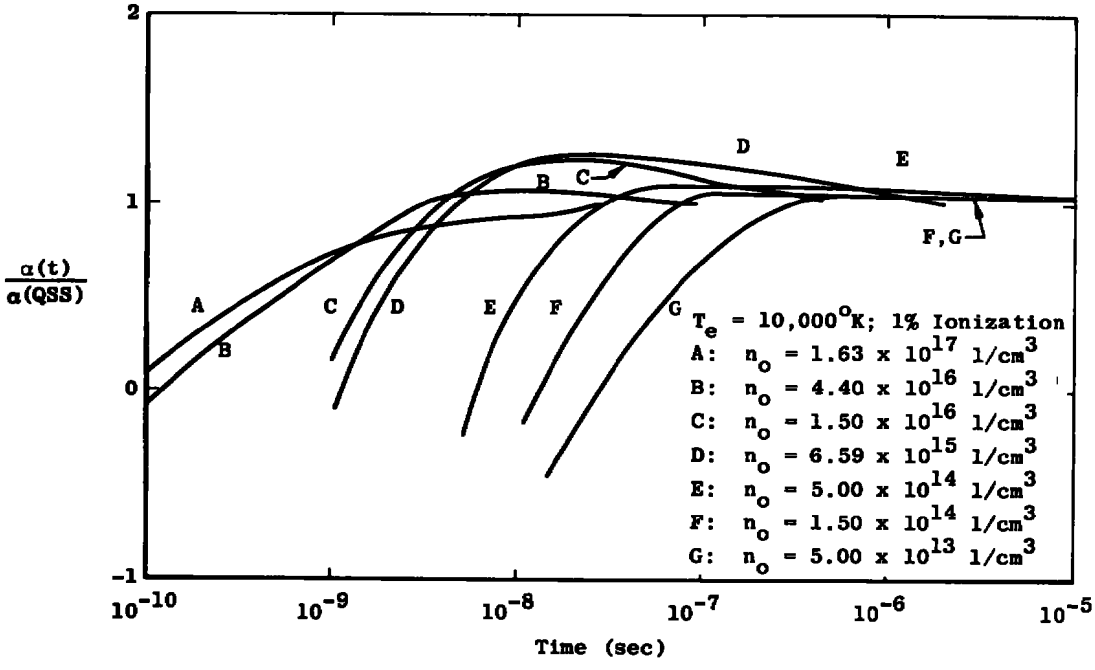

Figure 25. $\alpha(t)/\alpha(QSS)$ versus time, cases A, B, C, D, E, F, and G.

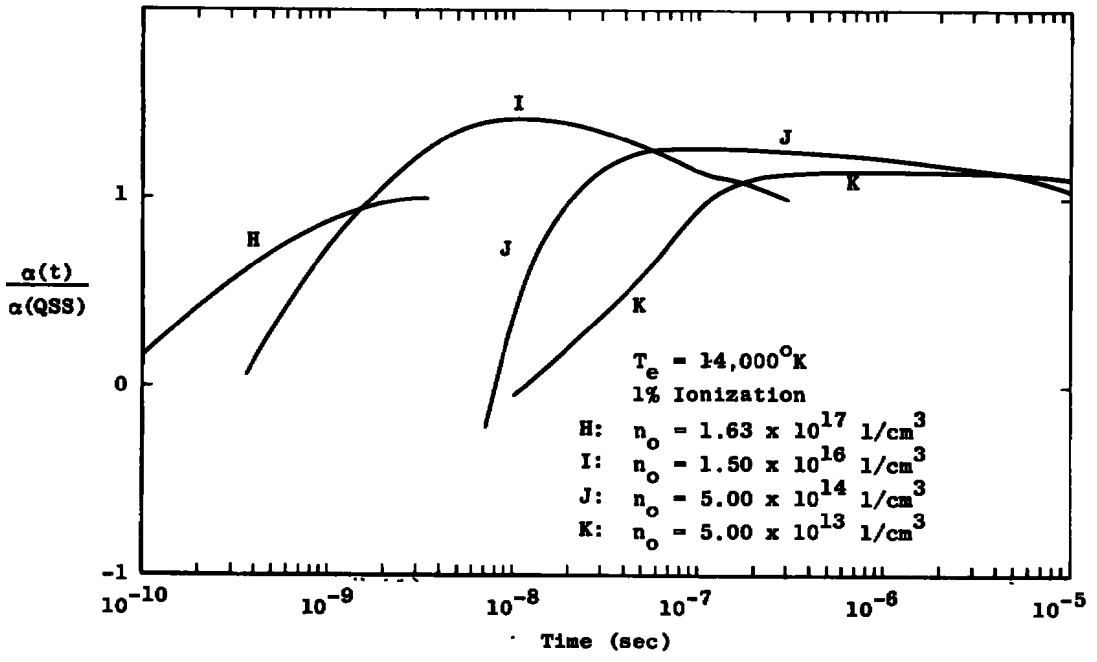

Figure 26. $\alpha(t)/\alpha(QSS)$ versus time, cases H, I, J, and K.

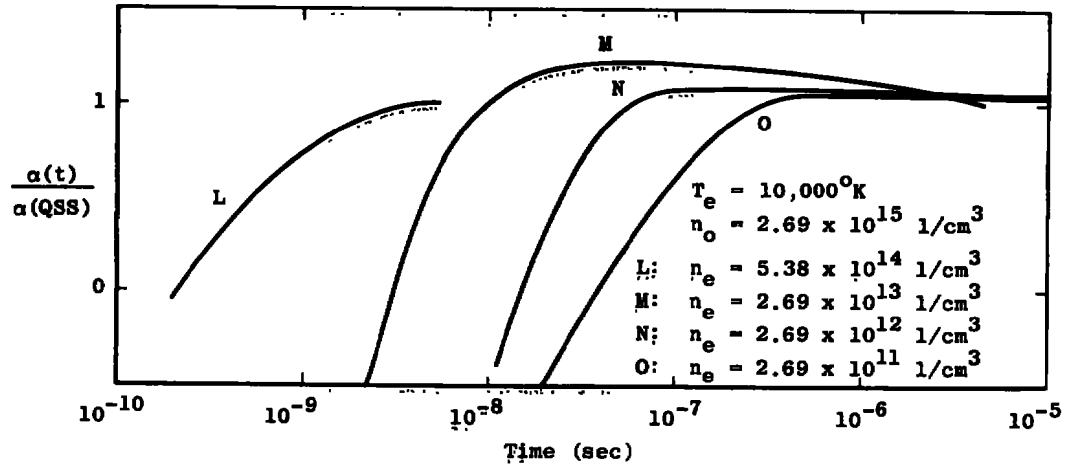

Figure 27. $\alpha(t)/\alpha(QSS)$ versus time, cases L, M, N, and O.

The conclusion from this, that CRR can be applied to the continuum rate for low density ($n_o \leq 10^{15}$ 1/cm^3), low excitation temperature ($T_e \leq 10,000$°K) plasmas before QSS is acquired is inescapable. The reason for this applicability of CRR to the continuum decay is fairly straightforward. If one writes the ERE equation for the rate of change of the ground state and factors out n_e^2 to put it into the proper form for identifying the CRR coefficient, one sees that the dominant contributors

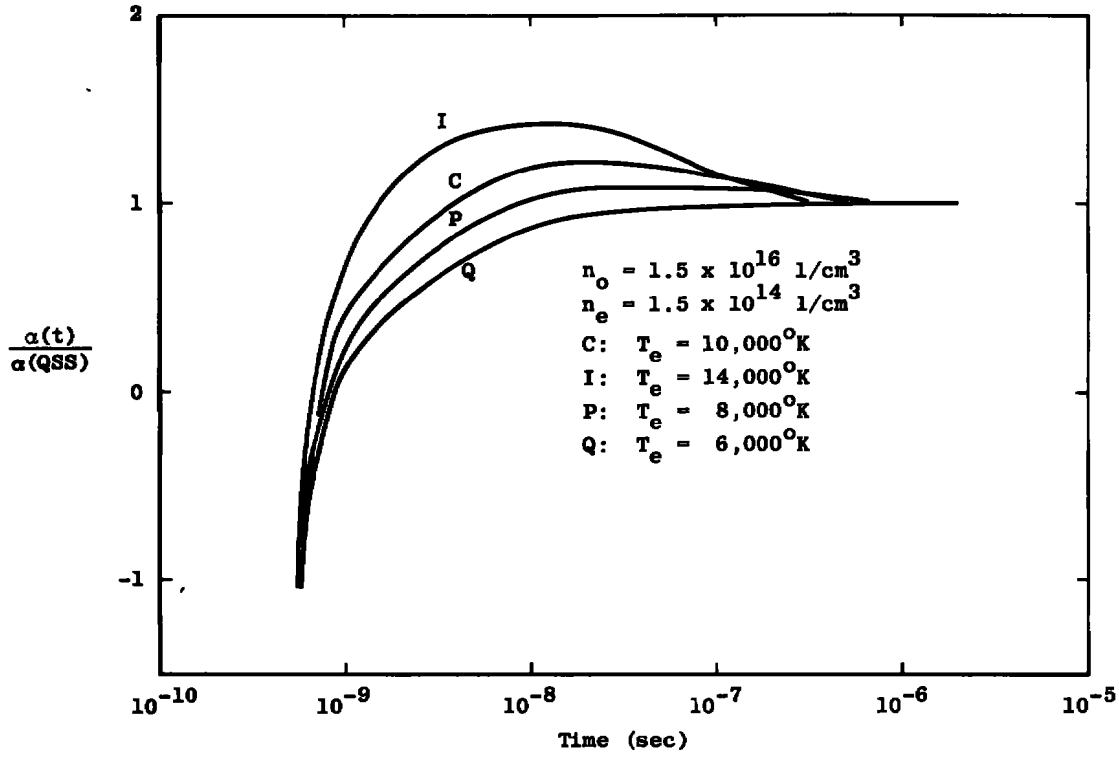

Figure 28. $a(t)/a(QSS)$ versus time, cases C, I, P, and Q.

to the ground state rate are those terms involving the low-lying energy levels, particularly radiation from the 2^1P level. Because of the energetically close proximity of the 2^1P level to the 2^3S, 2^3P, and 2^1S levels and the significant times required for them to reach their QSS value, it will require significant times for the QSS to be reached, so far as the ground state is concerned. However, for the "less collision dominated" plasmas, the upper quantum levels are the most important so far as the transfer of electrons between the continuum and the bound states are concerned. The lower levels populate by radiation from the upper levels. Hence, the continuum develops equilibrium with the upper states very rapidly and decays with them according to CRR as they radiatively fill the low levels until QSS for the entire plasma is obtained.

A dominant feature of the analysis of these plasmas has been the effect of the metastable levels upon the time required to reach QSS. The other levels adjust to some value near or below their QSS value early in the decay, typically at times of order 10^{-8} sec which is characteristic of radiative decay times. Then, as the metastable levels continue to populate radiatively, collisional processes from the metastable levels to the adjacent levels and subsequent excitation to higher

levels serve to raise the densities of these levels to their final QSS values. The amount of adjustment is dictated by the energy proximity to the metastable levels and whether the collisional excitations were governed by direct or exchange calculations. The importance of these metastable levels upon the time for a plasma to achieve QSS should not be neglected.

6.0 PERTUBATIONS

The study of the QSS development for the pure afterglow cases has provided a great deal of insight into the important mechanisms in a decaying helium plasma. Actual physical phenomena will more realistically involve the plasma changing from the QSS at one set of plasma conditions to the QSS at another set of plasma conditions. The study of the reacquisition of the QSS after a perturbation of existing QSS conditions will enhance the insight gained in the study of the pure afterglow plasmas for extension to the physical situation. For this, the QSS distribution was subjected to various perturbations, and these are summarized in Table 8.

Table 8: Summary of Perturbations of Case C

Case	Initial Conditions
CA	All excited-state densities doubled
CB	All excited-state densities halved
CC	Principal quantum level 3 density increased one order of magnitude
CD	Principal quantum level 3 density doubled
CE	Principal quantum level 6 density increased one order of magnitude
CF	3^3P density increased one order of magnitude
CG	6^3P density increased one order of magnitude
CH	T_e from 10,000°K to 9,500°K in one step
CI	T_e from 10;000°K to 9,500°K in 100°K increments
CJ	T_e from 10,000°K to 9,900°K in 10°K increments
CK	All K(p;q) halved

6.1 PERTURBATIONS OF ENTIRE DISTRIBUTION, CASES CA AND CB

Cases CA and CB, in which the entire excited-state QSS density distribution from case C was doubled and halved, respectively, is the largest perturbation since it affects the entire distribution. The quantities $\dot{n}_e/\dot{n}(1)$ and $\alpha(t)/\alpha(QSS)$ for these plasmas are illustrated in Fig. 29 along with the same parameters from case C for comparison. Figures 30 and 31 show the time development of quantum levels 2 and 3 population densities normalized to their Saha values for cases CA and CB, respectively. Included in Figures 30 and 31 is the time development of quantum level 6, which lies above the critical level.

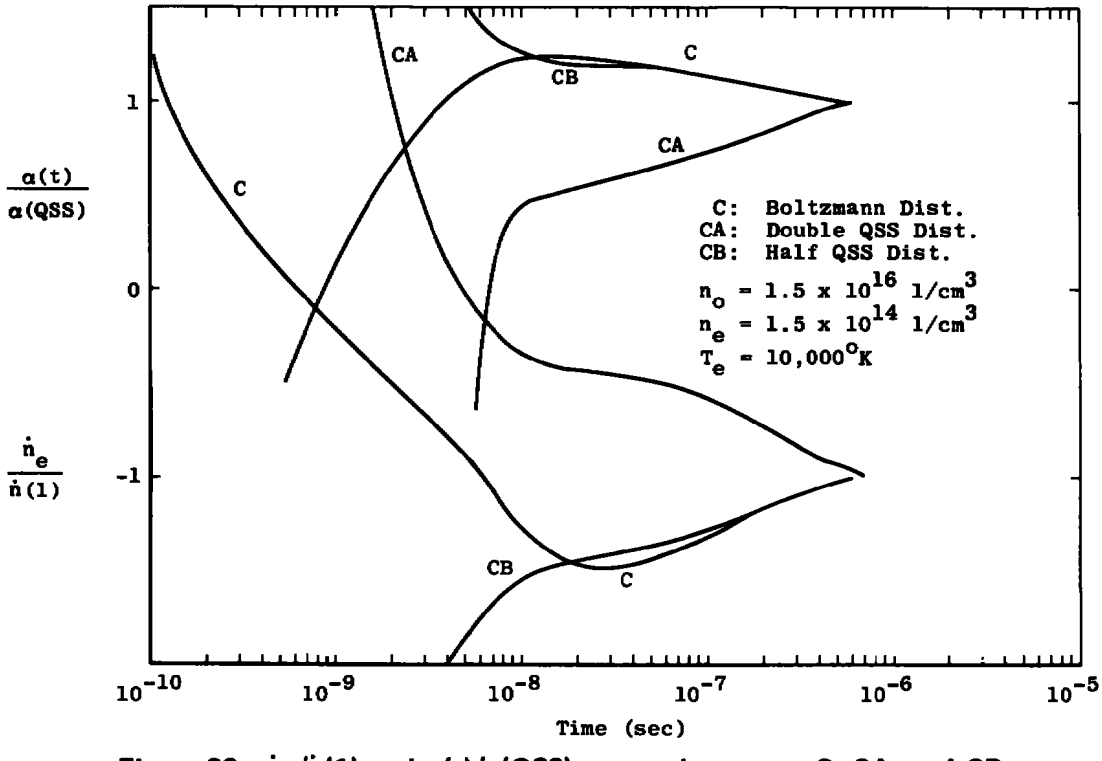

Figure 29. $\dot{n}_e/\dot{n}(1)$ and $\alpha(t)/\alpha(QSS)$ versus time, cases C, CA, and CB.

The comparison shows that the time to acquire QSS is quite similar for both conditions in spite of the fact that the initial conditions are quite diverse. Case C started with all excited states in equilibrium with the continuum, and the approach to QSS is primarily determined by the lower states. Cases CA and CB have as their initial conditions the densities of all excited states either double or half their QSS value, respectively, and again QSS is determined by the lower levels.

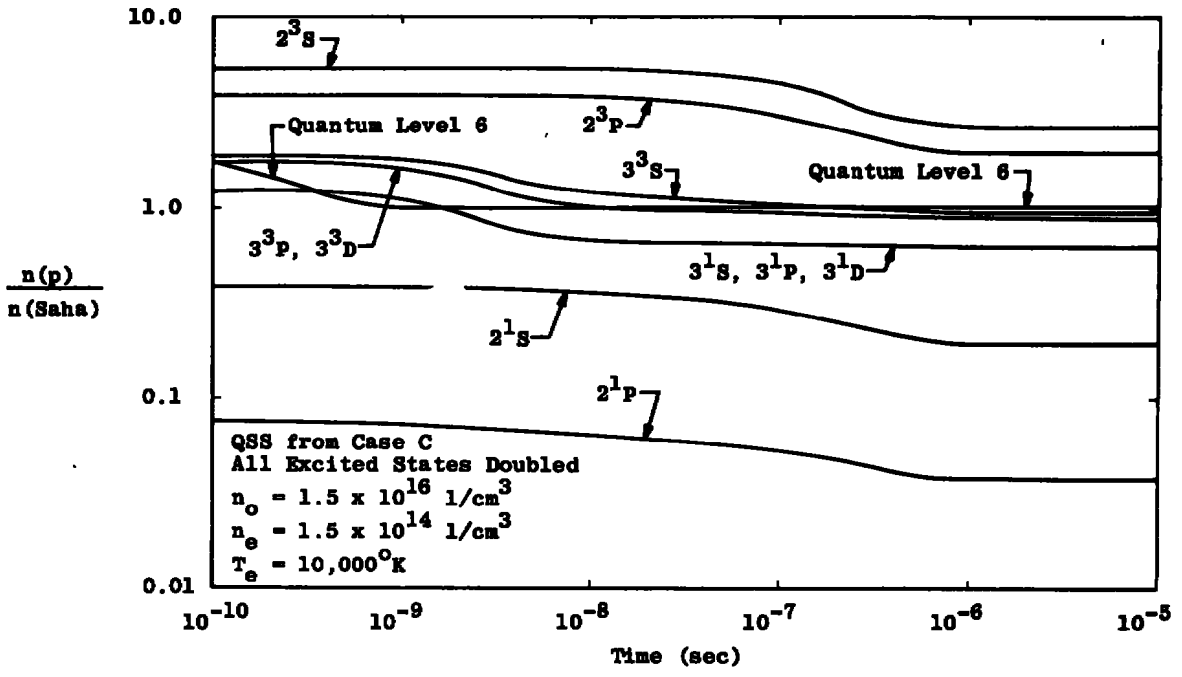

Figure 30. n(p)/n(Saha) versus time for quantum levels two, three, and six, case CA.

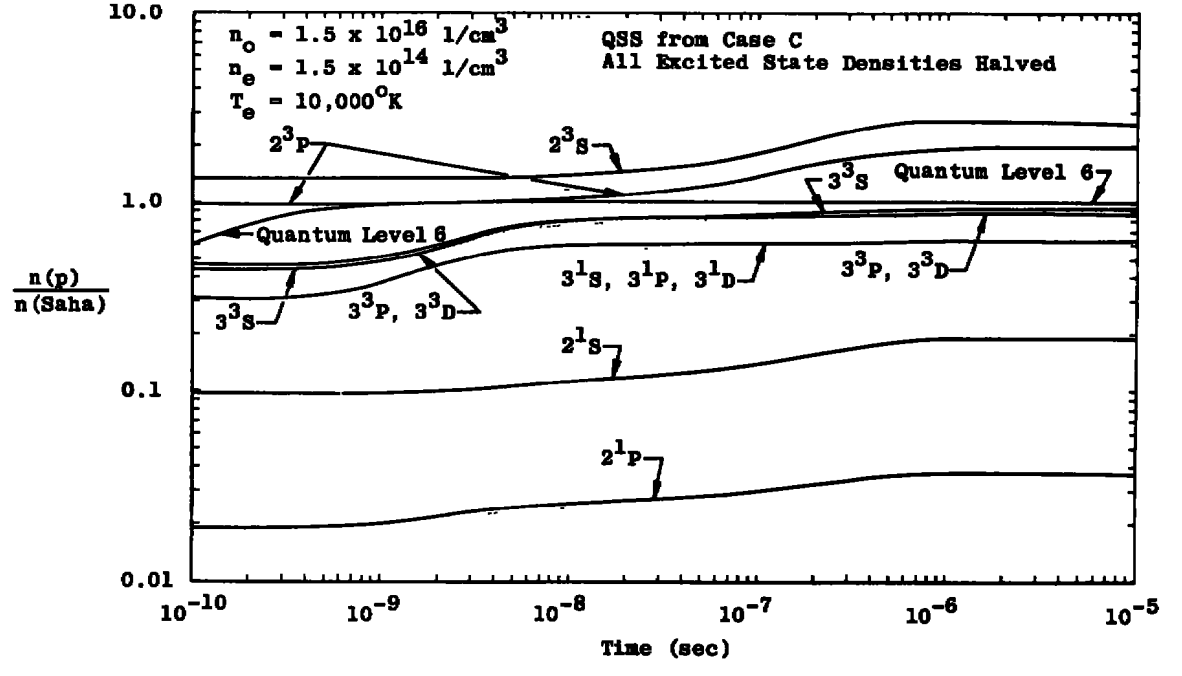

Figure 31. n(p)/n(Saha) versus time for quantum levels two, three, and six, case CB.

For case C the continuum rate and thus α are determined by recombination into the upper levels which then depopulate by radiation to the lower levels. For case CA these levels are overpopulated by a factor of two and because of ionization collisions the upper levels reach equilibrium with the free electrons early ($t \leq 10^{-9}$ sec) in the return to QSS. The lower levels are overpopulated and depopulate principally through collisional excitation to a higher level and then subsequent ionization. Thus, in this case the continuum rate is held towards a more positive value until QSS is obtained and there is no overshoot.

For case CB the levels are all underpopulated by a factor of two. Again the upper levels establish equilibrium with the free electron density earlier ($t \leq 10^{-9}$ sec) than the time required for the lower levels but the actual QSS is not obtained until considerably later ($t \approx 5 \times 10^{-7}$ sec). The similarity in the decay characteristics of cases C and CB for 1×10^{-8} sec $\leq t \leq 5 \times 10^{-7}$ sec is worth noting. For case C the energy states above the critical level were in equilibrium with the free electron density from t = 0.0 sec. For case CB the initial conditions were just half the initial conditions of case C for the states above the critical level and near the same for the quantum states below the critical level. Consequently, the decay characteristics of the two cases are quite different during the early part of the decay when the upper states can appreciably affect the characteristics. However, by $t = 1 \times 10^{-8}$ sec, all levels with the exception of the metastable levels have established a collisional-radiative balance among themselves and subsequent developments are a result of the coupling with the metastable levels. Thus, because of the similarity of the initial density of the 2^3S level, the decay characteristics for $t > 1 \times 10^{-8}$ sec are quite similar.

6.2 PERTURBATIONS OF PRINCIPAL QUANTUM LEVEL DENSITY, CASES CC, CD, AND CE

Cases CC, CD, and CE each suffered somewhat smaller perturbations, having but one principal quantum level affected. Cases CC and CD have the QSS density of quantum level 3 (below the critical level) increased a factor of 10 and 2, respectively. Case CE has the QSS density of principal quantum level 6 (above the critical level) increased by a factor of 10. Figure 32 summarizes the results for these cases with the ordinate the values of the ratios $\dot{n}_e/\dot{n}$ (1) and α (t) / α (QSS) as before. The plots show the not unexpected trends that case CE, in which quantum level 6 was increased an order of magnitude, comes to QSS very rapidly in both derivatives and CRR coefficients. Cases CC

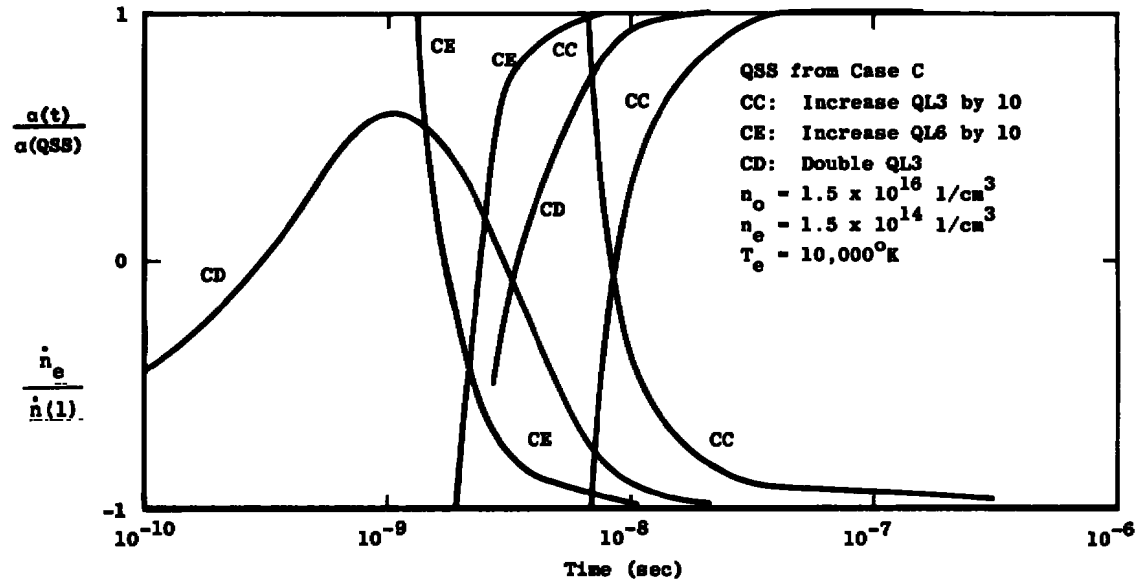

Figure 32. $\dot{n}_e/\dot{n}(1)$ and $a(t)/a(QSS)$ versus time, cases CC, CD, and CE.

and CD, which had quantum level 3 increased factors of 10 and 2, respectively, take longer - only slightly for case CD but an order of magnitude for case CC. The $\dot{n}_e/\dot{n}(1)$ curve for case CD shows an interesting character illustrating the role of bound states above the critical level as a communicator between the lower level and the continuum. Early in the decay ($t < 10^{-10}$ sec) few collisions have occurred which transfer electrons from quantum level 3 to some quantum level adjacent to the continuum. Thus, there is not sufficient ionization from the upper levels to appreciably affect the continuum rate. However, for $10^{-10} \leq t \leq 3 \times 10^{-9}$ sec there are sufficient numbers transferred to these upper levels that ionization overbalances recombination and the continuum rate actually goes positive for a short period of time before driving rapidly to the QSS by $t \approx 10^{-8}$ sec. Case CC exhibited this same character but because of the higher initial overpopulation of quantum level 3, the ratios could not be included on the scale of the plot. Case CE differed in this respect in that the continuum rate showed a very large positive derivative from $t = 0$.

Figures 33 and 34 explore cases CC and CE a little farther, showing the time development of the normalized population densities of the perturbed and two adjacent levels. In each the ordinate is the ratio of the time-dependent population density to the density in equilibrium with the free electrons. Figure 33 shows that the singlet and triplet states have slightly different decay characteristics for quantum level 3. This is primarily because of an initial difference in population densities. The

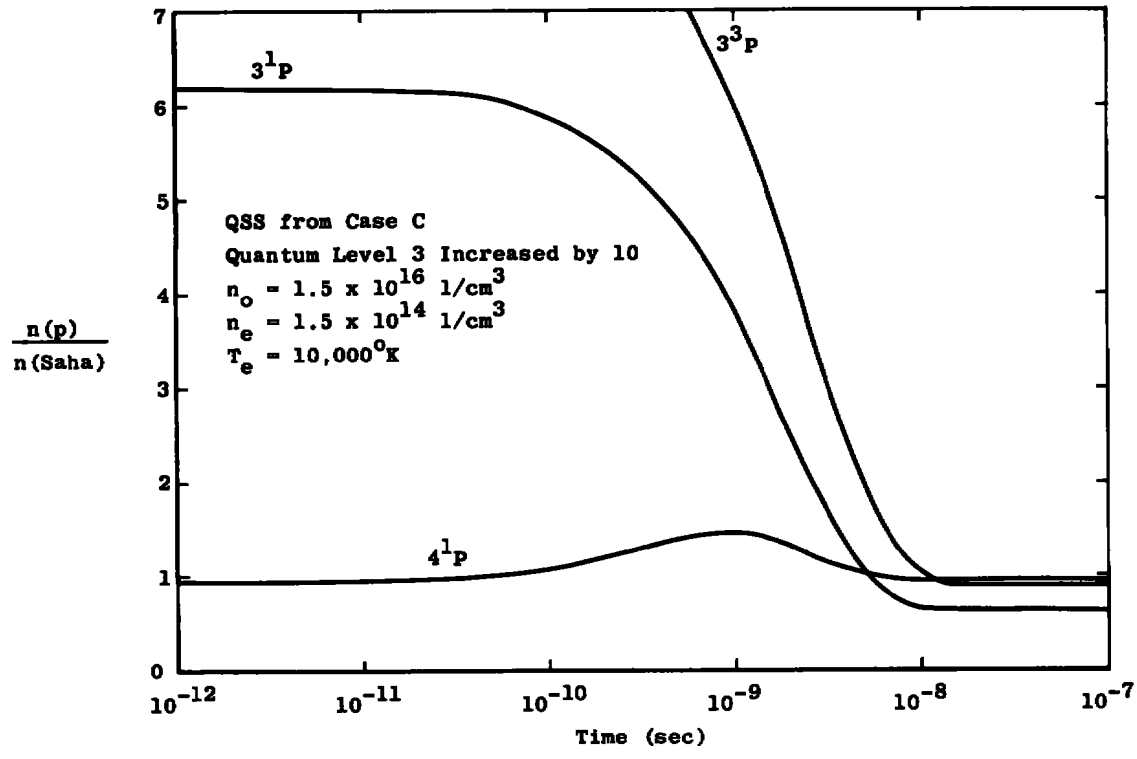

Figure 33. n(p)/n(Saha) versus time for 3^3P, 3^1P, and 4^1P quantum levels, case CC.

transient coupling to other states is illustrated by the development of the 4^1P density which shows an increase in density peaking at t $\approx 10^{-9}$ sec before falling back to the QSS value. All higher levels in fact show the same general nature as the 4^1P level, and the QSS values are not reached until times of order 10^{-7} sec.

Figure 34 illustrates the transient coupling between quantum level 6 and the adjacent levels. Because quantum level 7 is closer to 6 energetically than quantum level 5, it shows a rise in population density before quantum level 5 and then, because ionization is more efficient from quantum level 7, it has a tendency to return to QSS before the others. This is also why quantum level 5 tends to lag behind both quantum levels 6 and 7 in returning to QSS.

6.3 PERTURBATIONS OF DENSITY OF ONE EXCITED STATE, CASES CF AND CG

Figure 35 illustrates the character of the decay of cases CF and CG in which the densities of the 3^3P and 6^3P states, respectively, were

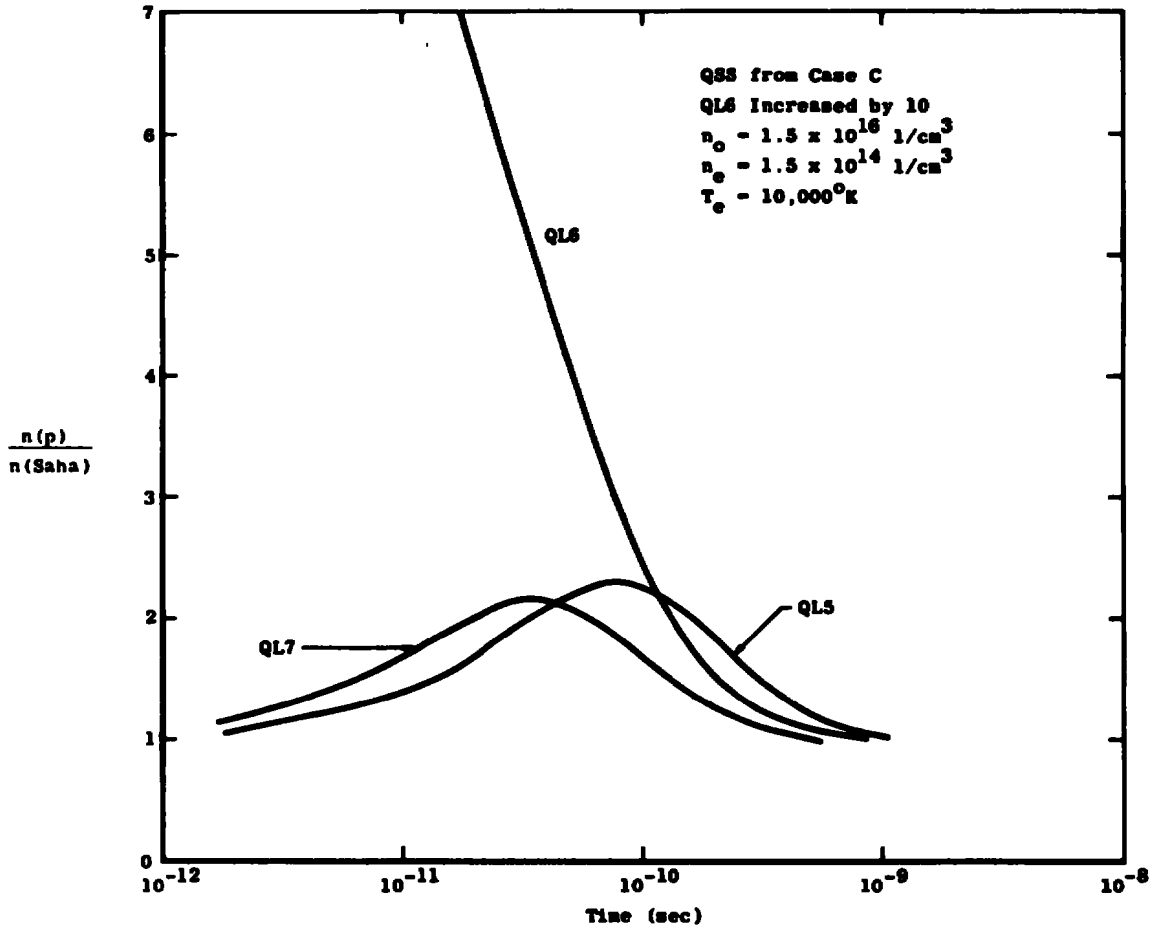

Figure 34. n(p)/n(Saha) versus time for quantum levels five, six, and seven, case CE.

perturbed upwards by a factor of 10. The ordinate again gives the values of the ratios $n_e/\dot{n}(1)$ and $\alpha(t)/\alpha(QSS)$.

These plasmas show characteristics similar to cases CC and CE by coming to QSS quite rapidly with the CRR showing the QSS value slightly before the rate ratio. Comparison with Fig. 32 shows that these plasmas achieve the QSS typically an order of magnitude before cases CC and CE which had the entire quantum level elevated by a factor of 10. Figures 36 and 37 illustrate the time development of selected population densities in the same manner as Figs. 33 and 34. Again the transient coupling is evident between the affected states and adjacent states with those lying energetically below the ^3P states lagging slightly. Although exchange collisions are included in the calculations, these rate coefficients are

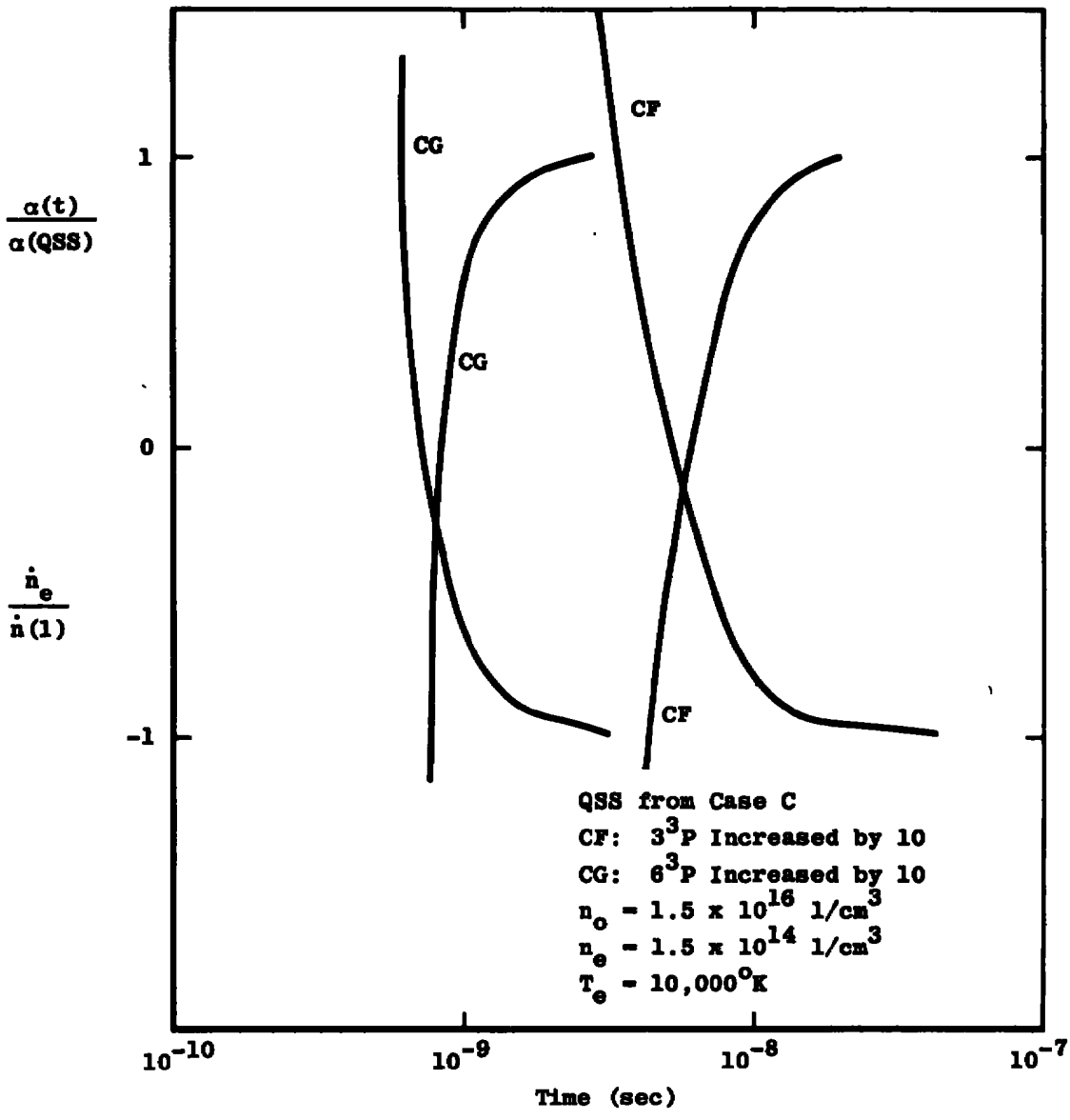

Figure 35. $\dot{n}_e/\dot{n}(1)$ and $\alpha(t)/\alpha(QSS)$ versus time, cases CF and CG.

very small and the effect of these perturbations upon singlet states, though resolvable in the calculations, is insignificant compared to the effect on the triplet states. Figure 37 does not show the effects upon a higher level because, although a slight increase is observable in these higher levels, it is fractional and would only tend to clutter the figure. This figure illustrates the strong coupling between the sublevels of the high quantum levels in that the 6^3P level and the other triplet states of quantum level 6 converge to the same relationship with the continuum at about 3×10^{-12} sec and then decay to QSS together.

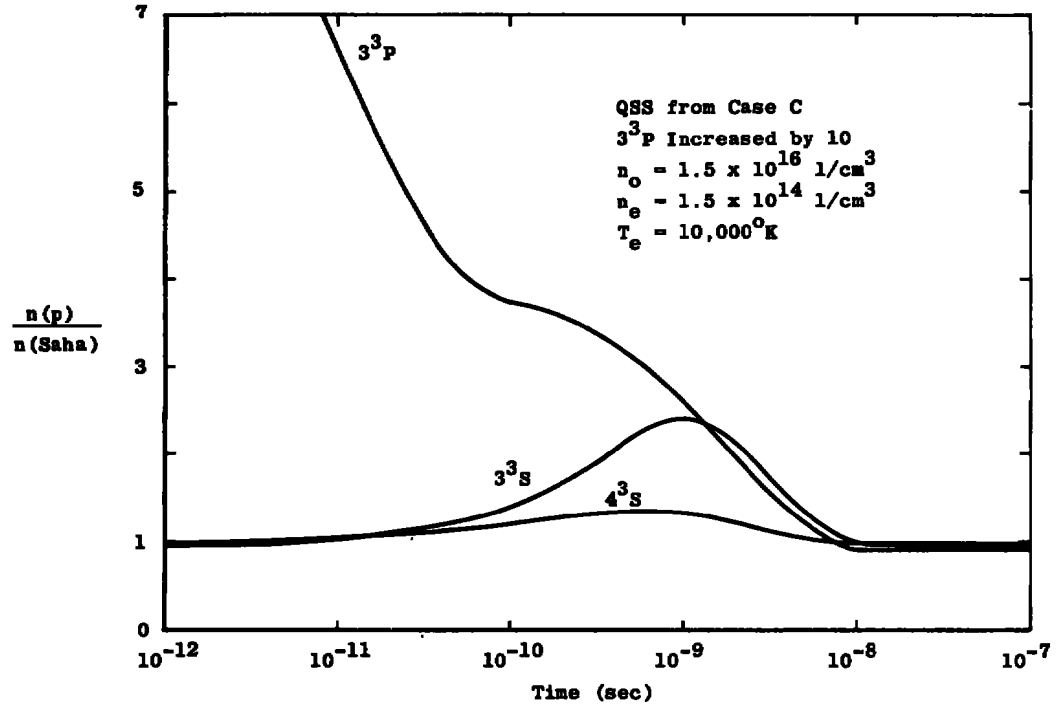

Figure 36. n(p)/n(Saha) versus time for 3^3P, 3^3S, and 4^3S quantum levels, case CF.

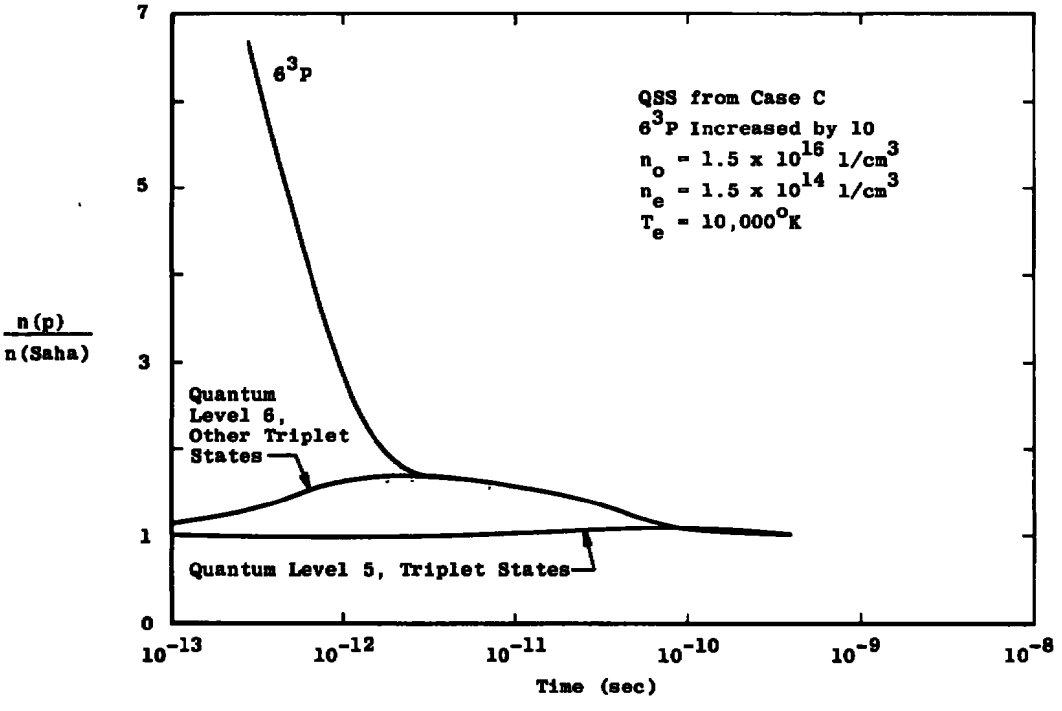

Figure 37. n(p)/n(Saha) versus time for 6^3P quantum level and triplet states of quantum levels five and six, case CG.

6.4 ELECTRON TEMPERATURE DECAY, CASES CH, CI, AND CJ

Most experimental studies of plasmas are subject to a decaying electron temperature. If the acquisition of the QSS under these conditions requires times in excess of the observed gradient times, then application of CRR theory may be inappropriate. The effects of a relaxing electron temperature were initially studied with the ERE with two cases, CH and CI. Each case used the QSS distribution from case C for the initial distribution but a different lower electron temperature. Although the present computer program will not support a variable electron temperature, the effect of an electron temperature change can be approximated by replacing the rate coefficients at the QSS temperature by rate coefficients calculated at some other temperature. Case CI investigated the approach to QSS by stepping the electron temperature from the 10,000°K of case C to 9,500°K in 100°K steps. The calculation was continued at each temperature until $\dot{n}_e/\dot{n}(1)$ indicated the plasma was within five percent of QSS. Case CH repeated the same conditions except the 500°K drop was made in one step.

Comparison of the two cases is made in Table 9. The first four columns refer to case CI with the first column indicating the electron temperature of each succeeding calculation. The second column is the time at which the ratio $\dot{n}_e/\dot{n}(1)$ came within the five percent criterion indicated above. Since provisions were not made to halt computations

Table 9. Times for QSS to be Established for Cases CH and CI

T_e °K	$t(-\dot{n}_e/\dot{n}(1) \leq 1.05)$ sec	t (computations stopped) sec	$\dot{n}_e/\dot{n}(1)$ t stop	$t(-\dot{n}_e/\dot{n}(1) \leq 1.05)$
9.9^{3}[a]	4.2^{-9}	8.1^{-9}	-1.03	
9.8^{3}	8.8^{-8}	8.8^{-8}	-1.05	
9.7^{3}	1.4^{-7}	1.8^{-7}	-1.04	
9.6^{3}	1.0^{-7}	3.3^{-7}	-1.02	
9.5^{3}	6.0^{-8}	3.0^{-7}	-1.02	
Sum	$= 3.92^{-7}$			3.1^{-7}

[a]Superscripts indicate powers of 10 by which the numbers are to be multiplied.

as soon as the five percent criterion was met, the third column indicates the time at which computations were stopped at each temperature with the fourth column showing the ratio $\dot{n}_e/n(1)$ at the time computations were stopped.

The QSS distribution at each of these temperatures was used for the initial distribution at the next lower temperature. The last entry in the second column is the sum of times to reach QSS at the five percent criterion and is to be compared to the single entry in column five, which is the time required for case CH, the single 500°K drop, to reach QSS at the five percent criterion. Comparison of the second and fifth columns of Table 9 shows that approximating the T_e change by a series of small changes will result in the plasma requiring longer to achieve QSS at the final T_e than if the change is made in one large jump.

An interesting feature of the decay, comparing columns four and two of Table 9, is that the farther away from QSS the initial conditions are, the longer the time required for the plasma to reachieve the QSS. Thus, for T_e = 9,900°K, it only required 4.2×10^{-9} sec for $\dot{n}_e/\dot{n}(1)$ to come within five percent of QSS (with $\dot{n}_e/\dot{n}(1) = -1.000$ at T_e = 10,000°K) but it required 1.4×10^{-7} for T_e = 9,700°K ($\dot{n}_e/\dot{n}(1) = -1.05$ at T_e = 9,800°K). This suggests that the instantaneous rates are quite sensitive to the value of the rate coefficients even though final QSS rates may not be appreciably different. This is supported by noting that a QSS, the instantaneous total rate of change of a quantum level will be several orders of magnitude below the instantaneous rate of change of either collisional population or collisional depopulation. Hence, a very slight change in the rate coefficient will cause appreciable changes in the $\dot{n}_e/\dot{n}(1)$ characteristic. Because of this, small changes in T_e will contribute significantly to the ratio $\dot{n}_e/\dot{n}(1)$.

With the electron temperature decaying continuously, as in a physical plasma, in the time following a T_e change and with the plasma approaching the QSS, there will be another T_e change, albeit slight, with the attendant deleterious effect upon the rates and the QSS. These observations lead to the hypothesis that in an environment in which the electron temperature decays continuously, the QSS will continually "chase" the T_e change and the plasma will never satisfactorily achieve QSS until the T_e time gradient becomes "sufficiently" flat.

These observations prompted the last temperature perturbational study, case CJ. The initial conditions were again the same as for cases CH and CI. This time, however, the plasma was subjected to a

constant temperature gradient, -9×10^9°K/sec, and the temperature increments were 10°K drops from 10,000°K to 9,900°K. The rate coefficients were assumed linear over the 100°K temperature range. Note that this gradient is only about one third that indicated in Table 9 for the first 100° K drop.

Figure 38 displays the ratio $\dot{n}_e/\dot{n}(1)$ at the point the computations were terminated at each temperature. The points at 9,990°K and 9,980°K are plotted at their respective plasma times of 1.1×10^{-9} sec each since those decays were inadvertently allowed to continue to a plasma time of 1×10^{-8} sec. The terminal distribution at each temperature provided the initial conditions for the next lower temperature.

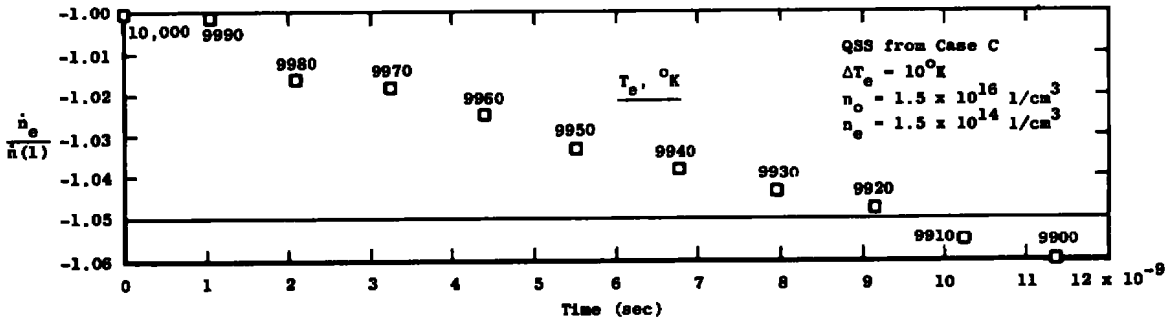

Figure 38. $n_e/\dot{n}(1)$ at times computations terminated, case CJ.

The figure shows that if the QSS plasma of case C is subjected to the constant temperature gradient of -9×10^9°K/sec, it will still not be to the QSS after a one percent temperature drop at a plasma time of 1.15×10^{-8} sec. This time is almost three times that indicated in Table 9 for the same temperature drop.

This case CJ reinforces the hypothesis just presented that in an environment in which T_e is continuously changing, the QSS will "chase" the T_e change. Although the conclusions must be based upon phenomenological observations, it is apparent that in the 10,000°K to 9,900°K temperature range, the maximum temperature gradient which will allow application of the QSS is less than -9×10^{10} °K/sec. Extension of these observations to the cases in which the plasma suffers a 500°K electron temperature decay indicates that the time for the plasma to return to the QSS would be considerably in excess of the 3.92×10^{-7} sec reported in Table 9.

6.5 PERTURBATION OF RATE COEFFICIENTS, CASE CK

The discussion of the rate coefficients in Section 3.0 indicated that they should be overestimated by no more than a factor of two. In order to investigate the effect of this possibility, the transient decay of case C was recomputed with all rate coefficients, K(p;q), reduced by a factor of two. The time development of the population density of quantum levels two and three ratioed to the Saha equilibrium value for this case CK is shown in Fig. 39.

Comparison of the plasma decay illustrated in Fig. 39 to case C illustrated in Fig. 9 shows that the population densities are spread out more for case CK than for case C. For example, the 2^3S level has a QSS ordinate of 4.9 for case CK and only 2.7 for case C. This would be expected since lower rate coefficients would physically mean poorer collisional efficiency, and thus radiation will have a greater effect. An interesting consequence of this is that the 2^1S density has a larger QSS value for case CK than for case C while the 2^1P level has the same QSS density for both cases. Thus the CRR coefficient will have approximately the same value for both case CK and case C. Quantum level 3 states

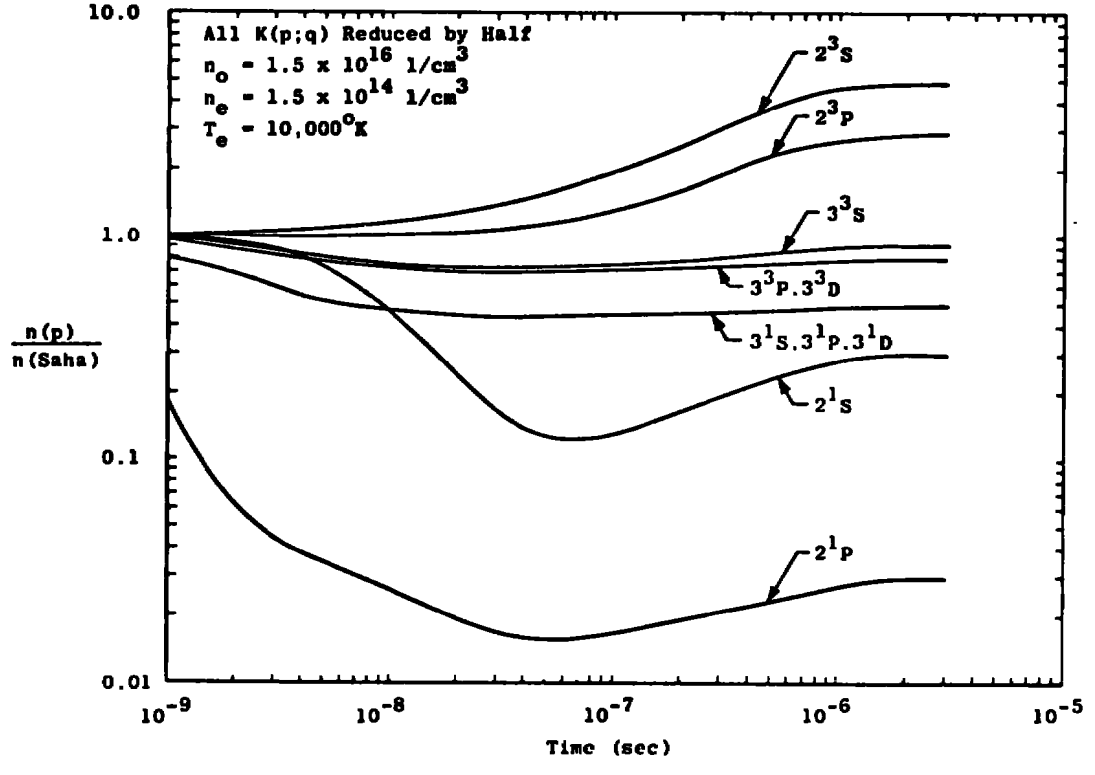

Figure 39. n(p)/n(Saha) versus time for quantum levels two and three, case CK.

generally show lower densities for case CK than for case C, as one would expect, with collisions being less important. The other quantum levels below the critical level will also show slightly lower densities for case CK than for case C. Those quantum levels above the critical level will show the same densities for both cases. The critical level for case CK with the 10 percent criterion was five; that for case C was four.

Figure 40 shows the $\dot{n}_e/\dot{n}(1)$ and $\alpha(t)/\alpha(QSS)$ curves for case CK and case C. This shows that case CK, with the collisional coefficients cut in half, requires approximately twice as long to acquire QSS as does case C. Further, the overshoot of case CK is larger than that of case C.

This is all because, with lower collisional coefficients, particularly the 2^3S level must achieve a higher density at QSS. This causes the larger overshoot because the 2^1P density is allowed to depopulate further before collisional processes balance radiative processes.

A consequence of these observations is that the results for the other cases studied will generally be conservative. If the Gryzinski cross sections used in this study are too large, as anticipated, the true times for the acquisition of the QSS will be larger.

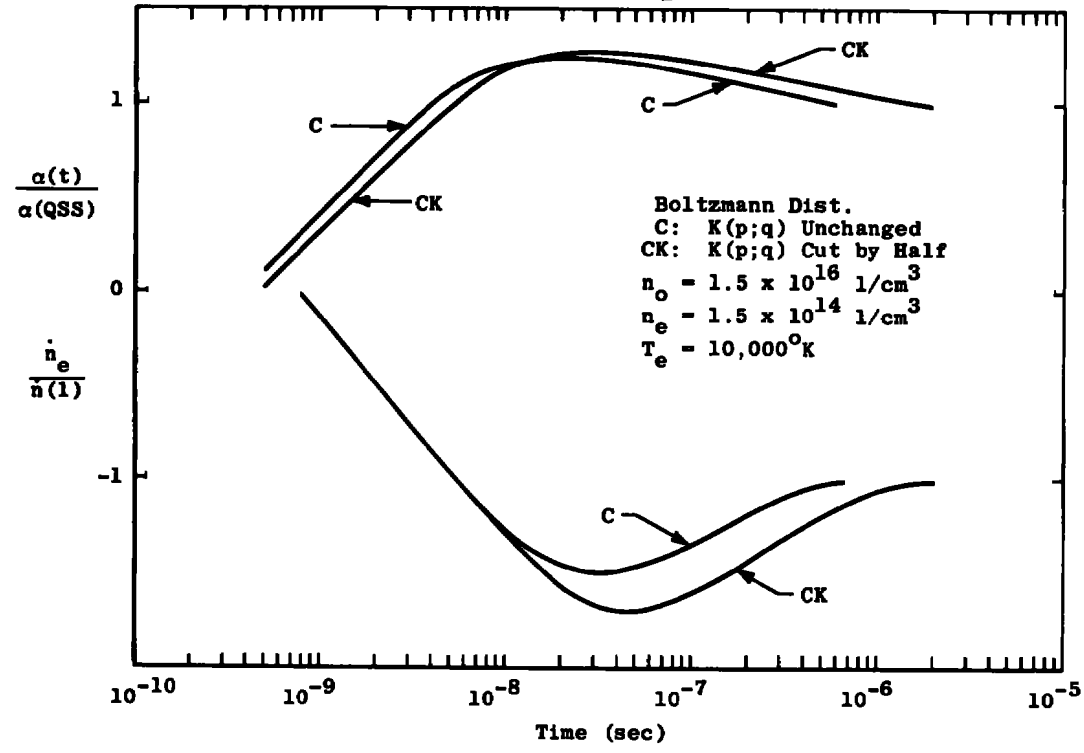

Figure 40. $\dot{n}_e/\dot{n}(1)$ and $\alpha(t)/\alpha(QSS)$ versus time, case CK.

6.6 ABSORPTION

Although absorption phenomena require precise knowledge of geometry for explicit study, the effects can be accounted for by simply reducing the appropriate Einstein transition probability. Thus, if the plasma absorbs half of the radiation of a specific wavelength, this is the same as if only half the radiation were emitted and this is described by simply reducing the transition probability for the emission by 50 percent.

The effects of absorption were studied in this way for a plasma at T_e = 10,000°K, $n_o = 1.5 \times 10^{16}$ 1/cm^3, one percent ionization, and an equilibrium distribution from the first excited state, the same initial conditions as case C. Four plasmas were studied in which all radiative transition probabilities from an elevated bound state to the ground state were reduced. The plasmas were assumed optically thin to continuum radiation, a minor constituent at these conditions. The identification and amount of reduction for each case is given below:

1. Case C25: 25 percent.
2. Case C50: 50 percent.
3. Case C75: 75 percent.
4. Case C100: 100 percent.

Figure 41 summarizes the decay characteristics of these plasmas. The ordinate is the ratio $\dot{n}_e/\dot{n}(1)$. With increasing reduction in transition probability the overshoot of QSS of both $\dot{n}_e$ and $\dot{n}(1)$ increases slightly through the 75 percent reduction. These plasmas all reach QSS in very near the same times, again progressively longer with increasing reduction. The transition from the 75 percent to the 100 percent reduction shows a dramatic increase in the overshoot of the $\dot{n}_e/\dot{n}(1)$ curve. The scale of Fig. 41 does not permit showing the point at which $\dot{n}_e/\dot{n}(1)$ reaches its minimum, which is -30 at $t = 1 \times 10^{-8}$ sec. Even with such an increase in the overshoot, however, the plasma achieves QSS within five percent at $t = 1.6 \times 10^{-6}$ sec, just slightly greater than the other conditions.

The sudden change in the $\dot{n}_e/\dot{n}(1)$ characteristic is easily explained by observing the change in the transition probabilities. The spontaneous transition probability for the $2^1P - 1^1S$ transition for example is 1.8×10^9 1/sec. In going from optically thin to the 75 percent reduction, the transition probability is reduced to 4.5×10^8 or approximately one order of magnitude. In going from the 75 percent to the 100 percent

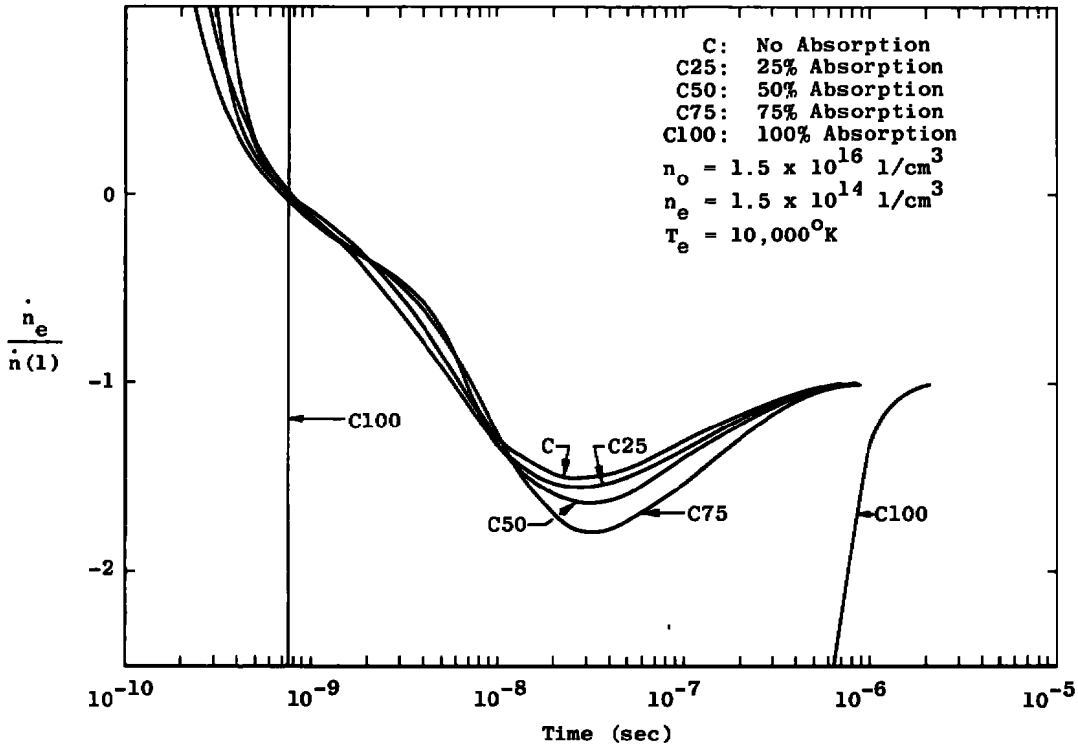

Figure 41. $a(t)/a(QSS)$ versus time, cases C, C25, C50, C75, and C100.

reduction, the probability is reduced to zero, or eight orders of magnitude, a much greater change. Hence, with absorption less that 100 percent, there will still be appreciable depopulation of the 2^1P level and then a subsequent increase in the 2^1P level as the metastable levels increase in density. For case C100, however, the 2^1P level does not have this mechanism to depopulate and hence there is no ground state rate overshoot.

Illustrated in Figs. 42, 43, 44, and 45 is the time development of substates of quantum levels 2 and 3 for cases C25, C50, C75, and C100, respectively, in the same manner that Fig. 9 illustrates case C. These show the lessening 2^1P depopulation with increasing absorption with the somewhat dramatic development of no 2^1P depopulation for case C100 in Fig. 45. The substates of quantum level 3 show an initial decrease in density in Fig. 45 because of radiative transitions to substates of quantum level 2. Another interesting observation is the gradual increase of the 2^3S QSS density. This is because the 2^1P level provides a progressively smaller sink to the various substates of quantum level 2. Hence, collisional depopulation of the 2^3S level is smaller and the state must reach a higher QSS density to balance radiative population with collision depopulation.

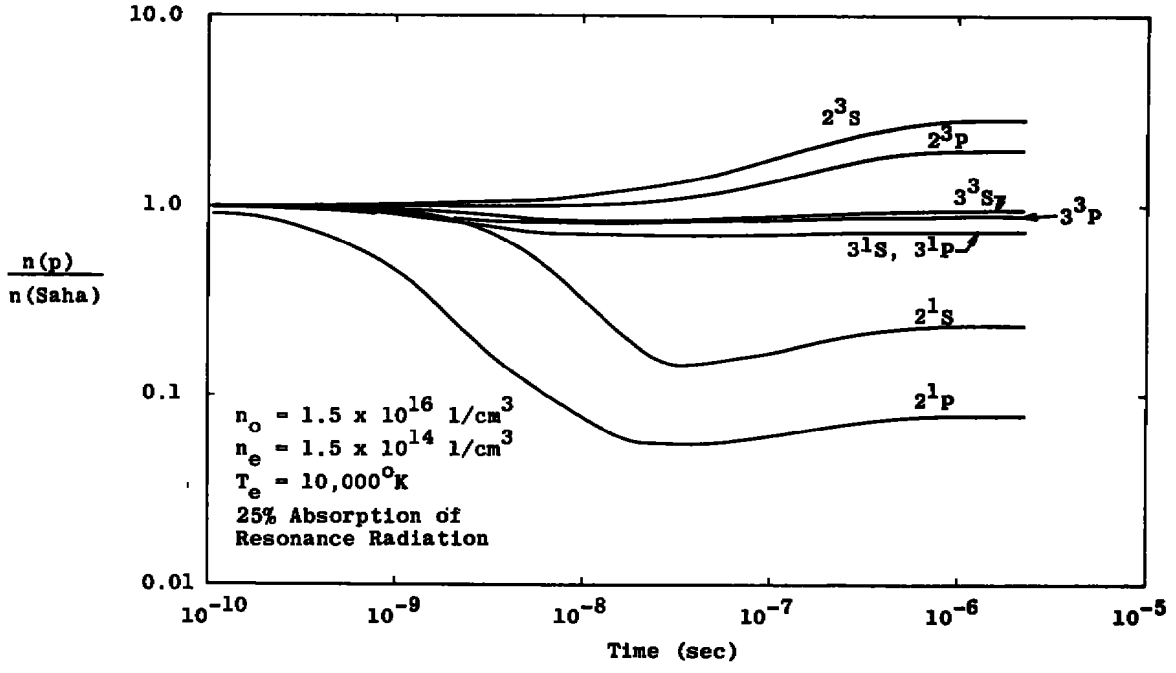

Figure 42. n(p)/n(Saha) versus time for quantum levels two and three, case C25.

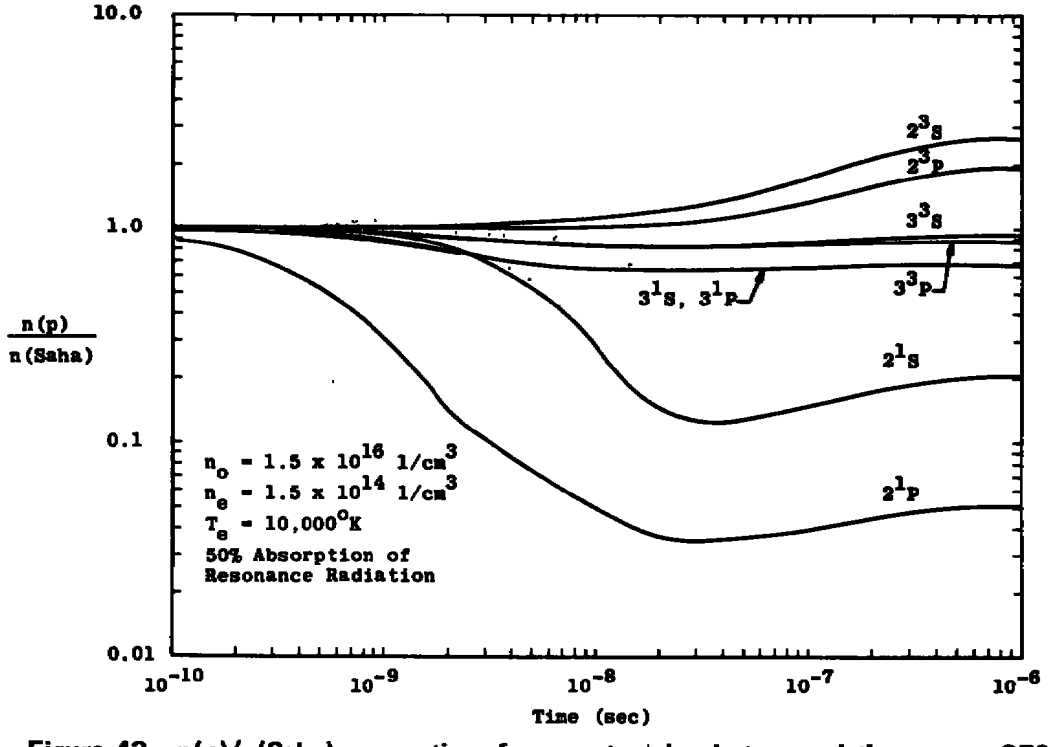

Figure 43. n(p)/n(Saha) versus time for quantum levels two and three, case C50.

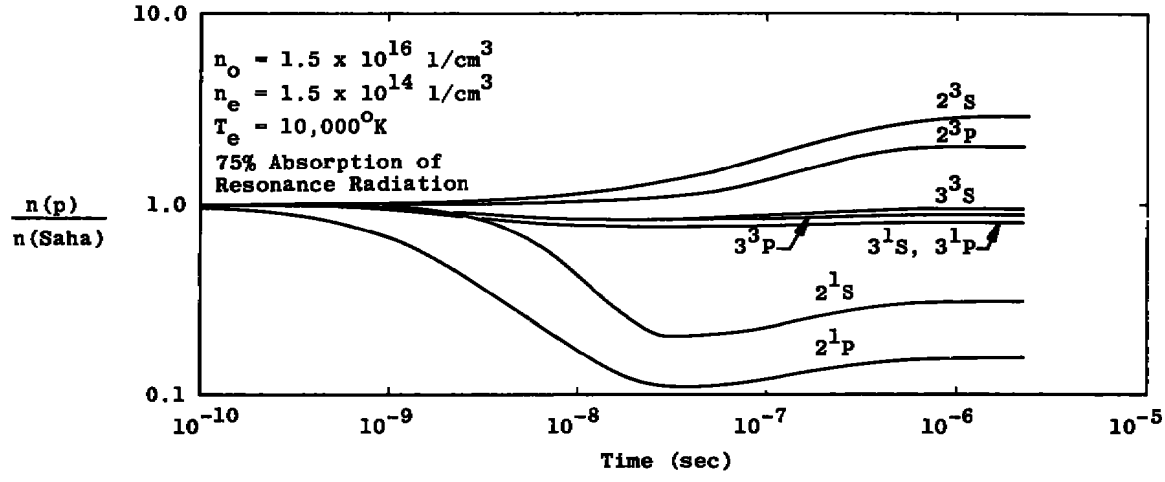

Figure 44. n(p)/n(Saha) versus time for quantum levels two and three, case C75.

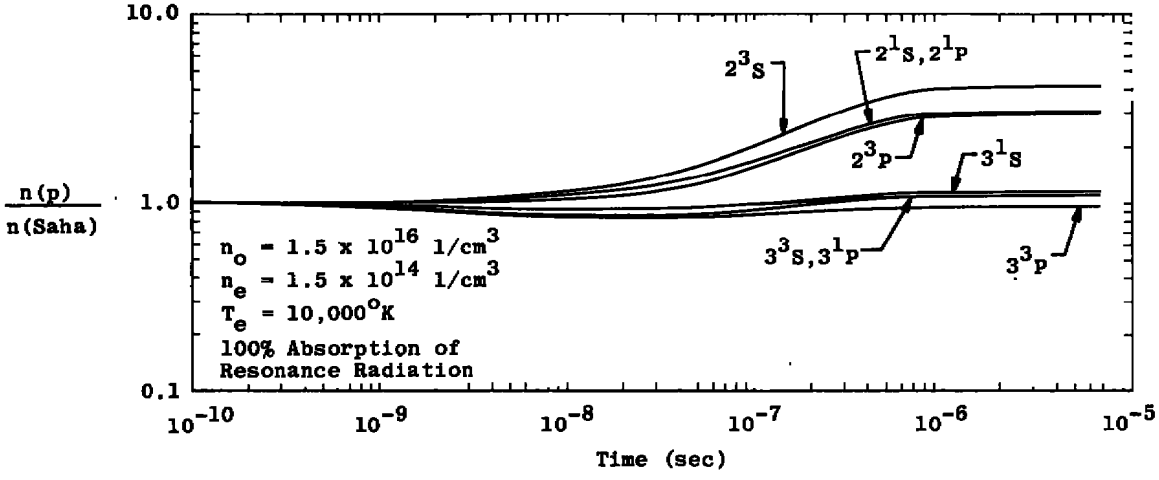

Figure 45. n(p)/n(Saha) versus time for quantum levels two and three, case C100.

The overshoots of $\dot{n}_e/\dot{n}(1)$ for case C, C25, C50, and C75 were all due to overshoot of both $\dot{n}_e$ and $\dot{n}(1)$. However, for case C100, the overshoot is due entirely to overshoot of the continuum density. This is because for case C100, the ground state rate is determined principally by super-elastic collisional populating from all the higher levels. There is no way for these levels below the critical level to depopulate rapidly to a density less than their QSS value and then to fill collisionally with the growth of the metastable level as in case C. Instead the ground state rate follows the collisional rate from the upper levels as they fill to their QSS value. The large value of the overshoot of case

C100 is in part due to the value of the ground state rate which is an order of magnitude less than the cases which allow some radiative transitions. For those cases which allow at least some radiation to the ground state, this radiative rate contributes to the ground state rate as well as eventually determining the electronic rate. For case C100, this radiation is not allowed, so that the QSS rate is determined by collisions and for these conditions is approximately one order of magnitude slower. Hence, through the development of the QSS, the electronic rate is principally determined by radiative transitions downward to the metastable levels. This proceeds at a rapid pace until QSS is approached yielding an inordinately high continuum rate. As the QSS is approached, the low-lying levels become sufficiently populated radiatively that they collisionally feed back to the continuum and slowly reduce its rate. The low levels continue to fill and reduce the continuum rate until approaches the rate with which the ground state is filling, which is significantly smaller than when ^1P transitions are allowed. Thus, the large overshoot of QSS for case C100 is due to the comparatively low QSS rate.

The effect of partial absorption has little effect upon $\alpha(t)/\alpha(QSS)$ characteristics of the plasma showing the same general character as the $\dot{n}_e/\dot{n}(1)$ curves. Case C25 showed a rather significant overshoot, as would be expected from the overshoot of the electronic rate. The QSS values of the CRR coefficient for each of the cases C, C25, C50, C75, and C100 is given below.

Case C:	$\alpha = 2.16 \times 10^{-12}$	cm^3/sec
Case C25:	$\alpha = 1.90 \times 10^{-12}$	cm^3/sec
Case C50:	$\alpha = 1.68 \times 10^{-12}$	cm^3/sec
Case C75:	$\alpha = 1.43 \times 10^{-12}$	cm^3/sec
Case C100:	$\alpha = 1.01 \times 10^{-13}$	cm^3/sec

The effect of absorption thus has noticeable effects upon the decay characteristics of an afterglow plasma. A consequence of these results is that a plasma which is 100 percent absorbing to these transitions will have an afterglow lasting more than 20 times as long as one which is completely optically thin.

7.0 EFFECTS ON MEASUREMENTS

As has been demonstrated in the previous chapters, the QSS can require physically significant times to be established. This was particularly illustrated by cases CA, CB, CH, CI, and CJ.

The cases CH, CI, and CJ are perhaps the most meaningful of the perturbation studies made since these examine changes in the electron temperature which affects the entire distribution. Experimental afterglow studies are invariably subjected to changes in the electron temperature. The present studies have shown that if the plasma conditions are such that the metastable levels are increasing in density, the recombination rates based upon the electron density will be higher than recombination rates based upon the excited state density distribution. Further, it was shown that, depending upon the temperature gradient and the amount of temperature change studied, the QSS might never be reached even from a pragmatic standpoint.

Although there has been considerable investigation of helium recombination, little of that reported contains sufficient detail to examine the results critically with the ERE. Also, much of the reported work is at high enough pressures that the molecular helium ion is present and must be accounted for. An exception is the work of Johnson and Hinnov (Ref. 22) in which the excited state densities and electron densities are studied as functions of time for low density (5×10^{-4} torr -1×10^{-3} torr) helium plasma produced in the C-Stellerator. During the early time periods of their studies the temperature gradient was quite steep, typically of the order of -1×10^{7}°K/sec, but flattened to only about -2×10^{4}°K/sec near the end of their studies.

The goal of their work was to determine a semi-empirical formula for collisional cross sections for helium that would reproduce experimental observations so as to allow comparison of experimental and theoretical predictions. Their technique was simply to use an assumed cross section functional form with certain adjustable parameters for the collisional transitions and then to use the QSS assumption to calculate excited state densities and compare them to measured densities. They include exchange collisional transitions between singlet and triplet states with the same principal quantum number and orbital angular momentum for $L > 2$ and also have introduced cross sections for optically forbidden ($\Delta L \neq 1$) transitions for "some" of their calculations. This is in contrast to the present work which simply assumed Gryzinski's form of the exchange calculation for all transitions which are optically forbidden. In either case these transitions are not particularly important except for those substates of quantum level 2.

Their work was successful in that they were able to obtain fairly good agreement between measured and calculated population densities at low electron temperatures ($T_e \leq \sim 3,500$°K). They make little

reference to the higher temperature data except to note that it was necessary to include the 2^3S - 2^1S collisional transition to obtain agreement for the low-lying levels. They do not report any population densities below quantum level 3.

Although the bulk of their reported analysis is carried out on data whose conditions lie below those which can be conveniently examined by the present ERE program, they do report one set of data which can be examined. The electron temperature versus time for that set of data is shown in Fig. 46.

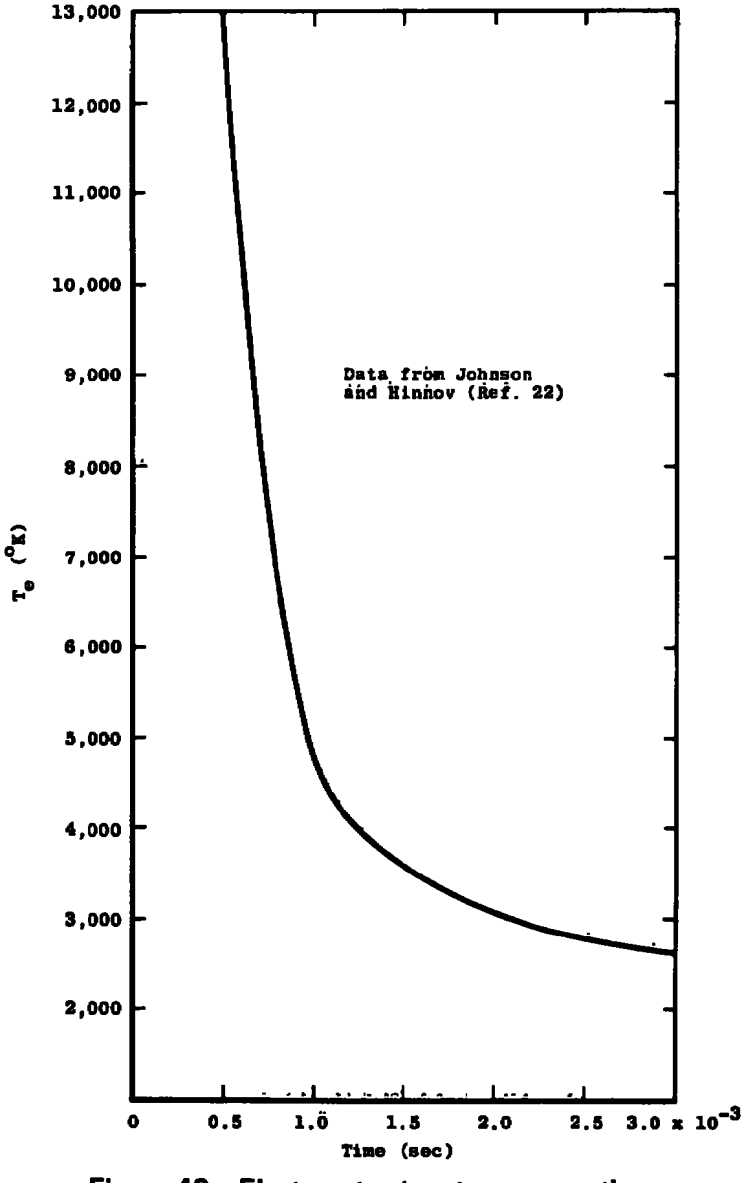

Figure 46. Electron temperature versus time.

In an effort to examine this work with the ERE solution, a QSS distribution was obtained at an electron temperature of 7,500°K. to compare to their measurements at 7,543°K. They do not report the accuracy of their population density measurements except through reference to some earlier work (Ref. 52) which reports an accuracy of within 20 percent for "reasonably strong signals" for the absolute intensity measurements. Electron density measurements were estimated accurate within 15 percent. Considering the uncertainty in their electron density measurements and since the states above the critical level can be described by the Saha relation, which has quadratic electron density dependence, there is an immediate uncertainty of 30 percent in. comparing their results to the ERE. Table 10 shows the ratio of the computed or measured population density to the corresponding density which would be in Saha equilibrium with that state at 7,500°K.

Table 10. Ratio of Excited State Population Densities to Saha Equilibriu.n Values for ERE Calculations and Measurements, n_e = 2.5 x 10^{13} $1/cm^3$, T_e = 7,500°K.

State	n(p)/n(Saha) ERE	n(p)/n(Saha) measurement[a]
3^1P	0.18	0.24
3^1D	0.18	0.26
3^3S	0.50	0.42
3^3P	0.40	0.63
3^3D	0.40	0.46
4^1S	0.72	1.00
4^1P	0.74	0.68
4^1D	0.74	0.92
4^3S	0.83	1.15
4^3P	0.87	1.00
4^3D	0.87	1.04
5^1S	0.92	1.19
5^1P	0.93	1.30
5^1D	0.93	0.96
5^3S	0.95	1.10
5^3P	0.96	1.10
5^3D	0.96	1.05
6^1S	0.97	0.87
6^1P	0.94	1.05
6^1D	0.98	0.74
6^3S	0.98	0.96
6^3P	0.99	0.92
6^3D	0.99	0.87
9^1D	1.0	1.22
9^3D	1.0	1.22

[a]Measurements from Johnson and Hinnov (Ref. 22)

Their data and the ERE calculations show good agreement for quantum levels 5 and 6 if allowance is made for the uncertainties in their data and one ignores the occasional flyers such as the 5^1P and 6^1D levels. For these calculations the critical level with the 10 percent criterion would be quantum level 5. Since their electron density was used for both the calculations and measurements and the ratios for the high levels show reasonable agreement, the electron density measurement is satisfactorily accurate for these comparisons.

Comparison of the levels below the critical level show that in general the measurements and calculations are still within experimental error with the exception of the 3^3P, 4^1S, 4^3S, 5^1S, and 5^1P states.

Some interesting observations can be made about the distribution. The ERE calculations show the results of very strong coupling between the ^1P and ^1D states as well as the ^3P and ^3D states as evidenced by their relationship to the free electron density. This is not necessarily evident in the measurements except for the singlet states of quantum level 3 and the triplet states of quantum levels, 4, 5, and 6. The coupling is, however, evident within the experimental error for all the levels. The calculations show a generally flatter distribution than do the measurements, which may be indicative of an overestimation of the cross sections by the Gryzinski technique. Although Johnson and Hinnov refer to entrapment of resonance radiation being present, they account for it in an approximate way and its presence is not well indicated by the measurements except for the 5^1P and 6^1P levels. If resonance radiation entrapment were present, the ^1P and ^1D measurements should show significantly higher relationships to the continuum than the calculations, which assumed no absorption, but the converse is true.

The above observations have been directed at the absolute densities themselves which, because of uncertainties in both rate coefficients and measurements, are quite difficult to use for reliable analysis of plasma conditions. Of a somewhat more sensitive nature is an examination of recombination rates. Johnson and Hinnov also investigated this, using the cross sectional forms they deduced from their measurements for calculations assuming QSS and comparing to direct measurement for the electron density rate. A characteristic of their results is a lower recombination rate from calculation than from measurement for the early periods of measurements.

One feature of early transitions already noted is that when the lower-lying levels are increasing in density, as with a decaying electron

temperature, the ground state rate will underestimate QSS conditions while the electron density rate will overestimate the QSS condition. As was shown earlier, the response of the system to changes in the electron temperature is quite nonlinear with respect to the time scale of the temperature gradient. The time to maintain QSS conditions for a series of small temperature changes was significantly longer than when the temperature change was made in one step.

To examine the possibility that the QSS had not been established during the early states of the measurements of Ref. 22, three calculations were performed. The first of them subjected the QSS distribution of case M reported above ($n_e = 2.69 \times 10^{13}$ $1/cm^3$) to a sudden electron temperature drop of 2,500°K to 7,500°K. The second calculation involved suddenly dropping the electron temperature from 7,500°K to 7,000°K in one step for the QSS distribution reported in Table 10. The third calculation dropped the electron temperature from 7,500°K to 7,000°K in 10°K increments with the plasma being allowed to come to the QSS before each succeeding drop. The time for QSS to be established at the terminal conditions for each of the above calculations was: 8×10^{-6} sec ($\Delta T = 2,500°K$, one step), 7×10^{-6} sec ($\Delta T = 500°K$, one step), and 1.4×10^{-5} sec ($\Delta T = 500°K$, 50 steps). From Fig. 46, page 173, the experimental temperature gradient for this period was about -2.1×10^{7} °K/sec. Thus, it required 2.4×10^{-5} sec for the electron temperature to decay from 7,500°K to 7,000°K in the experiment.

The obvious non-linearity of the response of the ERE to temperature changes, the close proximity of the time calculated with the 10°K increments compared to the experimental times, and the qualitative agreement of the predictions of this study with their results for the early afterglow makes it inescapable that the QSS had not been established during the early portions of their work. Further, their observed discrepancies between the measured and computed recombination rates are in direct qualitative agreement with the predictions of this study. To be more quantitative will require development of an ERE computer program with a continuously variable electron temperature.

Since the data (Ref. 22) used to obtain cross sections were taken at a later time in the afterglow when the electron temperature was lower and the gradient smaller, their work will probably give adequate predictions for most cross sections. The ERE should be used for at least the early portion of their studies. This will affect their reported

results for the $2^3S - 2^1S$ cross section which were obtained in the early portion of their studies with the QSS approximation.

8.0 SUMMARY

The system of rate equations describing the transient behavior of a singly ionized, optically thin, monatomic helium plasma has been solved numerically for various plasma conditions.

The objectives of this study, as outlined in Section 1.2, were achieved by studying the early decay characteristics of plasmas which were initially in a Boltzmann distribution for all excited states and also by examining the time to reacquire the QSS following an instantaneous perturbation of plasma parameters. To the author's knowledge, this is the first study of these early plasma decay characteristics or of the perturbational effects upon the plasma which includes the transient coupling between the various energy states.

8.1 NUMERICAL VALIDITY

Because these studies necessarily involve very short time periods which are generally beyond experimental technique, the validity of the solution was examined by comparing the collisional-radiative recombination coefficients determined after the transient solution had developed to the QSS with the calculations of Chen (Ref. 21), who determined recombination coefficients based upon assuming QSS conditions. These comparisons (Table 3) showed favorable agreement. Stability of the calculations, an important consideration in investigations of this type, were examined under two criteria on the time increment allowed for the calculation. The solution was found to adequately reproduce itself under the two criteria. Hence, it is concluded that the numerical results presented herein do represent physical processes to the limit of the accuracy of the parameters used in the calculation.

8.2 PURE AFTERGLOWS

The study of the pure afterglows, in which the plasma relaxes from an initial LTE distribution, given in detail in Section 5.0, provided a response to the specific objectives outlined in Section 1.2. These may be summarized as follows:

1. There is no single common mechanism by which the QSS is established. However, the establishment of the QSS is principally controlled by the time-dependent characteristic of the 2^3S density and its effects on the densities of the several adjacent quantum levels.

2. Generally, the results of CRR theory can be applied to helium plasmas before the QSS condition for excited atomic state densities is in fact reached. This is becaused the continuum rate is largely determined by recombination into the high-lying quantum levels and the QSS configuration is established rapidly for these. The ground state rate, however, is largely determined by the low-lying quantum levels and the QSS distribution for these requires a comparatively appreciable time to be established.

3. The time required for the QSS to be established varied with the plasma conditions, being shortest for those plasmas which were strongly collision dominated and surprisingly long for those which were least collision dominated. A summary of these times for each plasma to achieve the QSS as well as the time at which CRR could be applied to the electron density decay is listed in Table 11.

4. The processes by which plasmas decay are indeed complex and subtle. The study of the ERE solutions has illustrated this because of the ability to examine each individual process singly as well as its coupling effects with other mechanisms in the plasma decay. Very rarely in low density helium plasmas such as were studied here can one mechanism (e.g., 2^3S - 2^1P collisional transfers) be singled out as a dominant feature of the decay but rather, the total coupled features of the decay must be considered in the transient mode. Steady-state theories largely mask the interplay between the various states and cannot account for such phenomena as, say, the momentary radiative overdepopulation of the 2^1P density and then the subsequent rise in the 2^1P density via 2^3S - 2^1P, 2^3S - 2^3P - 2^1P, 2^3S - 2^1S - 2^1P, etc. collisional transfers.

Table 11. Summary of Plasma Conditions, Time to Acquire Quasi-Steady State, and Time at Which Collisional-Radiative Recombination Theory Applies to Free Electron Density

Case	T_e °K	n_o l/cm^3	n_e l/cm^3	Time (QSS) sec	Time (CRR) sec
A	1.0^4	1.63^{17}	1.63^{15}	2.0^{-8}	1.8^{-8}
B	1.0^4	4.40^{16}	4.40^{14}	7.0^{-8}	2.0^{-8}
C	1.0^4	1.50^{16}	1.50^{14}	8.0^{-7}	3.0^{-7}
D	1.0^4	6.59^{15}	6.59^{13}	1.3^{-6}	1.2^{-6}
E	1.0^4	5.00^{14}	5.00^{12}	3.1^{-5}	5.0^{-6}
F	1.0^4	1.50^{14}	1.50^{12}	1.2^{-4}	6.5^{-8}
G	1.0^4	5.00^{13}	5.00^{11}	3.5^{-4}	2.2^{-7}
H	1.4^4	1.63^{17}	1.63^{15}	2.7^{-9}	1.7^{-9}
I	1.4^4	1.50^{16}	1.50^{14}	2.0^{-7}	2.0^{-7}
J	1.4^4	5.00^{14}	5.00^{12}	1.8^{-5}	1.0^{-5}
K	1.4^4	5.00^{13}	5.00^{11}	2.1^{-4}	1.0^{-4}
L	1.0^4	2.69^{15}	5.38^{14}	3.0^{-8}	2.5^{-9}
M	1.0^4	2.69^{15}	2.69^{13}	4.3^{-6}	3.0^{-6}
N	1.0^4	2.69^{15}	2.69^{12}	6.0^{-5}	6.0^{-6}
O	1.0^4	2.69^{15}	2.69^{11}	6.6^{-4}	2.5^{-7}
P	8.0^3	1.50^{16}	1.50^{14}	6.6^{-7}	3.0^{-7}
Q	6.0^3	1.50^{16}	1.50^{14}	1.2^{-6}	3.0^{-8}

In addition to the listing above, the pure afterglow studies showed an additional unexpected phenomena. This was overshoot, in which the plasma decay would overshoot QSS conditions and then return to the QSS at a later time. It was found that this phenomena was physical rather than artificial. The study of overshoot can be summarized thus:

1. Plasmas which are strongly collision dominated at their initial conditions will not show overshoot of the QSS.

2. Plasmas whose initial conditions are such that there is no clearcut domination of radiation or collisions show the strongest continuum rate overshoot.

3. As excitation temperature increases in the range $8,000°K \leq T_e \leq 14,000°K$, overshoot of the continuum rate becomes progressively greater because of improved collisional efficiency.

4. For lower electron temperatures $T_e \leq 8,000°K$, overshoot becomes progressively less, and there is no overshoot of the continuum rate at $T_e = 6,000°K$ because of poor collisional efficiency.

5. The ground state rate shows generally greater overshoot as the collision dominance decreases although there are inconsistencies in this behavior for increasing electron temperature.

The plasma conditions and the magnitude of overshoot encountered in this study were summarized in Table 7.

8.3 PERTURBATIONS

The perturbational studies, Section 6.0, in which the plasma relaxes after a perturbation of some plasma parameter, reinforced the conclusions drawn from the pure afterglow studies. They additionally indicated that an environment supporting a transient electron temperature could have a significant effect upon the QSS. The findings of the perturbational studies may be summarized as follows:

1. Parametric changes affecting the entire distribution require significantly longer times to achieve the QSS than if the perturbation affects the density of just one quantum level.

2. Perturbations of the density of a single quantum level will induce a ripple effect through the rest of the distribution because of the transient coupling to the density of the selected level.

3. Errors in the rate coefficients will have noticeable effects upon the transient decay of the plasma. There can be an appreciable effect upon the QSS distribution of densities for those levels below the critical level but no discernible effect upon the densities of levels above the critical level. The location of the critical level can be affected. It was estimated that the rate coefficients used in this study were too large; hence, the times calculated in this study will be short when compared to the physical situation.

4. The mathematical and thus the physical system show a strong non-linear response to changes in the electron temperature. The effects of a continuously changing electron temperature were approximated by a series of step function changes. For a series of small changes of electron temperature the plasma required appreciably longer times to reacquire QSS than for a single step with the same total change. The studies led to the observation that in an environment with a continuously changing temperature the QSS may never be reached.

5. Absorption of resonance radiation has a calculable but not significant effect on the times to achieve the QSS. Absorption of resonance radiation can have effects on the QSS density distribution, causing the ^1P and the adjacent states to maintain higher population densities.

8.4 EFFECTS ON MEASUREMENTS

The studies of the various plasma conditions indicated that when the conditions were such that the metastable states are increasing in density, the recombination rates based upon the electron density will be significantly higher than recombination rates based upon population densities. This predicted effect was observed in data published by Johnson and Hinnov (Ref. 22). In calculations with the ERE at their conditions a QSS distribution was established which agreed with their measurements, within experimental error. Their work was subjected to severe temperature gradients and because of the qualitative agreement of their results with the findings of this work, it is believed that they did not have QSS conditions, at least in the early stages of the decay.

The findings of this study have shown that the concept of the plasma passing from one QSS to another QSS as the plasma decays is not as "almost instantaneous" as is usually assumed. However, the results of CRR theory can generally be applied to electron recombination rates without the QSS being physically necessary. In studies in which plasma parameters are changing rapidly, great care must be exercised in relating density measurements of quantum states below the critical level to the electronic recombination rate via the QSS assumption. This

will be particularly true in apparata in which severe electron temperature gradients are present or when there are short time scales present.

8.5 CONCLUDING REMARKS

The study has provided detailed information and insight into plasma decays and the mechanisms by which the nonequilibrium eigenstate population density distribution function is established. These mechanisms have important fundamental implications for future work in plasma decays and their effects cannot be fully assessed without a transient solution to the ERE.

Several implications for future applications beyond the original intent of the work may also be drawn. Under proper experimental conditions and with an analytic approach similiar to that used here, a very critical detailed examination of rate coefficients may be made. This work would not have to necessarily be restricted to plasmas but the approach is applicable to other chemical processes. The ripple effect, discovered in the calculations concerned with perturbations of a specific energy level, suggest mechanisms by which specific rate coefficients may be determined through a selective absorption experiment. Another application which suggests itself is the study of the processes involved in population inversions with a view toward prediction of possible lasting transitions.

Of a more immediate nature, the approach of this study should be put to a critical test for comparison of calculations and experiment. Because physical plasmas are generally characterized by a spatial density variation and invariably by electron temperature variations, the work reported here must be considered as a first approximation to actual physical processes, and correct modeling will need to account for the effects of these additional transient phenomena. The need to consider continuous variations in density and electron temperature assumes added importance in light of the observations of the effects of step function electron temperature changes and the physically significant times for the QSS to be established. The development of these capabilities and completion of the critical evaluation will provide a basis for extension to more complex species, such as diatomic molecules, so that the internal energy distribution function development in the nonequilibrium environment may be studied.

REFERENCES

1. D'Angelo, N. "Recombination of Ions and Electrons." The Physical Review, Second Series, Vol. 121, No. 2, 15 Jan. 1961, pp. 505-507.

2. Byron, S., Stabler, R. C., and Bortz, P. I. "Electron-Ion Recombination by Collisional and Radiative Processes." Physical Review Letters, Vol. 8, No. 9, May 1, 1962, pp. 376-379.

3. Bates, D. R., Kingston, A. E., and McWhirter, R. W. P. "Recombination Between Electrons and Atomic Ions." Proceedings of the Royal Society of London, Series A, Vol. 267, 1962, pp. 297-312.

4. Bates, D. R., Kingston, A. E., and McWhirter, R. W. P. "Recombination Between Electrons and Atomic Ions: II, Optically Thick Plasmas." Proceedings of the Royal Society of London, Series A, Vol. 270, 1962, pp. 155-167.

5. McWhirter, R. W. P. "Spectral Intensities." Plasma Diagnostic Techniques, edited by R. H. Huddlestone and S. L. Leonard. Academic Press, New York, 1965, pp. 201-264.

6. McWhirter, R. W. P. and Hearn, A. G. "A Calculation of the Instantaneous Population Densities of the Excited Levels of Hydrogen-like Ions in a Plasma." Proceedings of the Physical Society, Vol. 82, July-Dec., 1963, pp. 641-654.

7. Drawin, H. W. "Collisional-Radiative Ionization and Recombination Coefficients for Quasi-Stationary Homogeneous Hydrogen and Hydrogenic Ion Plasmas." Zeitschrift für Physik, Vol. 225, 1969, pp. 470-482.

8. Drawin, H. W. "Influence of Atom-Atom Collisions on the Collisional-Radiative Ionization and Recombination Coefficients of Hydrogen Plasmas." Zeitschrift für Physik, Vol. 225, 1969, pp. 483-493.

9. Drawin, H. W. "Relaxation Times for Establishing Steady-State Populations in Optically Thin and Thick Plasmas." Journal of Quantitative Spectroscopy & Radiative Transfer, Vol. 10, No. 1, Jan. 1970, pp. 33-48.

10. Hinnov, E. and Hirschberg, J. G. "Spectroscopic Measurements of Helium Afterglow." Proceedings of the Fifth International Conference on Ionization Phenomena in Gases (Munich, 1961), Vol. I, edited by H. Maecker. North-Holland Publishing Company, Amsterdam, 1962, pp. 638-650.

11. Hinnov, E. and Hirshberg, J. G. "Electron-Ion Recombination in Dense Plasmas." The Physical Review, Second Series, Vol. 125, No. 3, 1 Feb. 1962, pp. 795-801.

12. Robben, F. and Kunkel, W. B. "Spectroscopic Study of Electron Recombination with Monatomic Ions in a Helium Plasma." The Physical Review, Second Series, Vol. 132, No. 6, 15 Dec. 1963, pp. 2363-2371.

13. Collins, C. B. and Robertson, W. W. "Spectra Excited in a Helium Afterglow." The Journal of Chemical Physics, Vol. 40, No. 3, 1 Feb. 1964, pp. 701-712.

14. Collins, C. B. and Robertson, W. W. "Helium Afterglow. I. Atomic Spectrum." The Journal of Chemical Physics, Vol. 40, No. 8, 15 Apr. 1964, pp. 2202-2208.

15. Collins, C. B. and Robertson, W. W. "Helium Afterglow. II. Molecular Spectrum." The Journal of Chemical Physics, Vol. 40, No. 8, 15 Apr. 1964, pp. 2208-2211.

16. Niles, F. E. and Robertson, W. W. "Spectral Emission of the Helium Afterglow." The Journal of Chemical Physics, Vol. 40, No. 10, 15 may 1964, pp. 2909-2914.

17. Niles, F. E. and Robertson, W. W. "Atomic Emission of the Helium Afterglow." The Journal of Chemical Physics, Vol. 40, No. 12, 15 June 1964, pp. 3568-3571.

18. Rogers, W. A. and Biondi, M. A. "Studies of the Mechanism of Electron-Ion Recombination. II." The Physical Review, Second Series, Vol. 134, No. 5A, 1 June 1964, pp. A1215-A1225.

19. Collins, C. B. and Hurt, W. B. "Time-Dependent Study of the Emitted Light and Electron Density in a Low-Pressure Helium Afterglow." The Physical Review, Second Series, Vol. 167, No. 1, 5 Mar. 1968, pp. 166-170.

20. Collins, C. B. "Calculation of the Dependence of Emitted Light on Charge Density for Two-Electron Collisional-Radiative Recombination in the Hydrogenic Approximation." The Physical Review, Second Series, Vol. 175, No. 1, 5 Nov. 1968, pp. 160-163.

21. Chen, C. J. "Collisional-Radiative Electron-Ion Recombination Rate in Rare-Gas Plasmas." The Journal of Chemical Physics, Vol. 50, No. 4, 15 Feb. 1969, pp. 1560-1566.

22. Johnson, L. C. and Hinnov, E. "Rates of Electron-Impact Transitions Between Excited States of Helium." The Physical Review, Second Series, Vol. 187, No. 1, 5 Nov. 1969, pp. 143-152.

23. Bates, D. R. and Kingston, A. E. "Collisional-Radiative Recombination at Low Temperatures and Densities." Proceedings of the Physical Society, Vol. 83, 1964, pp. 43-47.

24. Limbaugh, C. C., Carstens, J. C., McGregor, W. K., and Mason, A. A. "A Numerical Solution to the Collisional Radiative Model." Paper FA-7 presented at the Southeastern Section of the American Physical Society, Clemson University, Clemson, South Carolina, November 1967.

25. Gordiets, B. F., Gudzenko, L. I., and Shelepin, L. A. Relaxation of Hydrogen Population Levels in a Highly Ionized Plasma, Taking Radiation Reabsorption into Account." Journal of Quantitative Spectroscopy & Radiative Transfer, Vol. 8, No. 2, Feb. 1968, pp. 791-804.

26. Limbaugh, C. C. "A Numerical Study of the Early Population Density Relaxation of Thermal Atomic Hydrogen Plasmas." Master's Thesis, University of Tennessee, June 1969.

27. Limbaugh, C. C. and McGregor, W. K. "A Numerical Study of the Transient Hydrogen Afterglow." Paper K7 presented at the 22nd Gaseous Electronics Conference, Gatlinburg, Tennessee, June 1969.

28. Niles, F. E. "Compilation of Helium Transition Probabilities." Ballistic Research Laboratories Report No. BRL-R-1354, Aberdeen Proving Ground, Maryland, February 1967.

29. Wiese, W. L., Smith, M. W., and Glennon, B. M. Atomic Transition Probabilities: A Critical Data Compilation. U.S. National Bureau of Standards Bulletin NSRDS- NBS 4, Washington, D.C., May 1966.

30. Geen, L. C., Rush, P. P., and Chandler, C. D. Oscillator Strength and Matrix Elements for the Electric Dipole Moment for Hydrogen." Astrophysical Journal. Vol. 3, 1957, p. 37.

31. Moiseiwitsch, B. L. and Smith, S. J. Electron Impact Excitation by Atoms. U.S. National Bureau of Standards Bulletin NSRDS-NBS 25.

32. Ochkur, V. I. and Brattsev, V. F. "Exchange Excitation of Helium by Electron Impact." Optics and Spectroscopy, Vol. 19, No. 4, pp. 274-276.

33. Gryzinski, M. Classical Theory of Atomic Collisions. I. Theory of Inelastic Conditions." The Physical Review, Second Series, Vol. 138, No. 2A, 19 April 1965, pp. A336-A358.

34. Gryzinski, M. "Classical Theory of Electronic and Ionic Inelastic Collisions." The Physical Review, Second Series, Vol. 115, No. 2, 15 July 1959, pp. 374-383.

35. Gryzinski, M. "Two-Particle Collisions. I. General Relations for Collisions in the Laboratory System." The Physical Review, Second Series, Vol. 138, No. 2A, 19 April 1965, pp. A305-A321.

36. Gryzinski, M. "Two-Particle Collisions. II. Coulomb Collisions in the Laboratory System of Coordinates." The Physical Review, Second Series, Vol. 138, No. 2A, 19 April 1965, pp. A322-A335.

37. Dugan, J. V. and Sovie, R. J. "Volume Ion Production Costs in Tenuous Plasmas: A General Atom Theory and Detailed Results for Helium, Argon, and Cesium." NASA TND-4150, September 1967.

38. St. John, R. M., Miller, F. L., and Lin, C. C. "Absolute Electron Excitation Cross Sections of Helium." The Physical Review, Second Series, Vol. 134, No. 4A, 18 May 1964, pp. A888-A897.

39. Moustafa Moussa, H. R., De Heer, F. J., and Schutten, J. "Excitation of Helium by 0.05 - 6 keV Electrons and Polarization of the Resulting Radiation." Physica, Vol. 40, 1969, pp. 517-549.

40. Rapp, D. and Englander-Golden, P. "Total Cross Sections for Ionization and Attachment in Gases by Electron Impact. I. Positive Ionization." The Journal of Chemical Physics, Vol. 43, No. 5, 1 Sept. 1965, pp. 1464-1479.

41. Asundi, R. K. and Kurepa, M. V. "Ionization Cross Sections in He, Ne, A, Kr, and Xe by Electron Impact." Journal of Electronics and Control, First Series, Vol. 15, No. 1, July 1963, pp. 41-50.

42. Long, D. R. and Geballe, R. "Electron-Impact Ionization of He ($2s^3S$)." Physical Review A, Third Series, Vol. 1, No. 2, February 1970, pp. 260-265.

43. Fite, W. L. and Brackmann, R. T. "Electron Collisions with Atomic and Molecular Oxygen." Proceedings of the Sixth International Conference on Ionization Phenomena in Gases, Vol. I, edited by P. Hubert and E. Crémieu-Alcan. Paris, 1963, pp. 21-26.

44. Drawin, H. W. "Collision and Transport Cross Sections." Plasma Diagnostics, edited by W. Lochte-Holtgreven. North-Holland Publishing Company, Amsterdam, 1968, pp. 842-873.

45. Seaton, M. J. "Radiative Recombination of Hydrogenic Ions." Monthly Notices of the Royal Astronomical Society, Vol 119, No. 2, 1959, pp. 81-89.

46. Lowry, J. F., Tomboulian, D. H., and Ederer, D. L, "Photoionization Cross Section of Helium in the 100- to 250-Å Region." The Physical Review, Second Series, Vol. 137, No. 4A, 15 Feb. 1965, pp. A1054-A1057.

47. Moore, C. E. Atomic Energy Levels, Vol. I. National Bureau of Standards, Washington, D. C., 1949.

48. Richter, J. "Radiation of Hot Gases." Plasma Diagnostics, edited by W. Lochte-Holtgreven. North Holland Publishing Company, Amsterdam, 1968, pp. 1-63.

49. Drawin, H. W., Emard, F., and Tittle, H. O. "Collisional-Radiative Ionization and Recombination Coefficients for Helium Plasmas." Ninth International Conference on Phenomena in Ionized Gases, edited by Geavit Musa, et al. Bucharest, 1969, p. 2.

50. Gusinow, M. A., Gerardo, J. B., and Verdeyen, J. T. "Investigation of Electronic Recombination in Helium and Argon Afterglow Plasmas by Means of Laser Interferometric Measurements." The Physical Review, Second Series, Vol. 149, No. 1, 9 Sept. 1966, pp. 91-96.

51. Born, G. K. and Buser, R. G. "Temperature Decay and Recombination in Helium Afterglow Plasmas." The Physical Review, Second Series, Vol. 181, No. 1, pp. 423-429.

52. Johnson, L. C. "Excitation of Neutral Helium in Non-LTE Discharges." Plasma Physics Laboratory Report MATT-436, Princeton University, Princeton, New Jersey, August 1966.

53. Hildebrand, F. B. Introduction to Numerical Analysis. McGraw-Hill Book Company, New York, 1956.

APPENDIX A
NUMERICAL TECHNIQUES

1. RATE COEFFICIENTS

The rate coefficient integrations indicated in Section 3.0 were performed using 32-point Laguerre-Gauss quadrature. Quadrature techniques are described in most numerical analysis books (Ref. 53, for example) and derivation will not be given here. The basis of the technique is to use a weighting function so that

$$\int_a^b w(x) f(x) dx = \sum_{i=1}^{n} w(x_i) f(x_i) \tag{A-1}$$

where $w(x)$ is the weighting function and $w(x_i)$ is the value of the weighting coefficient at the point x_i.

It turns out that if a weighting function

$$w(x) = e^{-x} \tag{A-2}$$

is used, the weighting coefficients are a function of the Laguerre polynomials (Ref. 53)

$$w(x_i) = \frac{(n!)^2 \, x_i}{[L_{n+1}(x_i)]^2} \tag{A-3}$$

where the x_i are the roots of the n^{th} Laguere polynomial.

Further, use of Laguerre-Gauss quadrature is valid on the interval $(0, \infty)$. The integrations in Section 3.0 do not extend to ∞, but the lower limit is one. Compatability with the interval $(0, \infty)$ is accomplished by a simple transformation of coordinate.

Various quadrature techniques are generally part of the library in numerical analysis laboratories. The particular one used here was generated by K. R. Kneile, Analyst, Central Data Processing, Arnold Engineering Development Center (AEDC), and is in subroutine form for ease of use. The 32 abcissas and the values of the weighting coefficients are given in Table A-1.

Table A-1. Abscissa and Weighting Coefficients for 32-Point Laguerre-Gauss Quadrature

i	x_i	$w(x_i)$	i	x_i	$w(x_i)$
1	0.04448936583326702	0.1141871057681048	17	22.63088901319677	2.884392092922042
2	0.2345261095196185	0.2660652168976152	18	25.62863602245925	3.113261327039586
3	0.5768846293018864	0.4187931373248530	19	28.86210181632347	3.356217692595803
4	1.072448753817818	0.5725328464998047	20	32.34662915396474	3.615869856484269
5	1.722408776444645	0.7276487883809713	21	36.10049480575197	3.895513044948550
6	2.528336706425795	0.8845367193402497	22	40.14571977153944	4.199394104711585
7	3.492213273021994	1.043618875892077	23	44.50920799575494	4.533114978534362
8	4.616456769749767	1.205349274152353	24	49.22439498730864	4.904270287611245
9	5.903958504174244	1.370221338521781	25	54.33372133339691	5.323500972023666
10	7.358126733186241	1.538777256468645	26	59.89250916213402	5.806333214233621
11	8.982940924212596	1.711619352686457	27	65.97537728793505	6.376614674159653
12	10.78301863253997	1.889424063449484	28	72.6876280906627	7.073526580707242
13	12.76369798674273	2.072959340246534	29	80.18744697791352	7.967693509295901
14	14.93113975552256	2.263106633996964	30	88.73534041789240	9.205040331278190
15	17.29245433671531	2.460889072488236	31	98.82954286828397	11.16301309076787
16	19.85586094033605	2.667508126397117	32	111.7513980979377	15.39018041526064

2. TRANSIENT ERE

The numerical technique used to effect the solution to the ERE was the modified Euler's method. This technique has enjoyed some success in solution of reacting flow problems at AEDC and, because of the similarity in the mathematical systems, the use of the technique was suggested.

To describe the application of the method to the problem at hand, it is convenient to attack the problem in more general form. Thus, the various quantities will be described in functional form and as independent or dependent variables rather than closely tied to physical interpretation. The system of Eqs. (7) and (8) can thus be written

$$\frac{d\bar{y}}{dx} = f(\bar{y}) \tag{A-4}$$

where the single bar denotes a vectoral quantity, $\bar{y}$ is the dependent variable, x is the independent variable, and $f(\bar{y})$ is the functional form of the ERE.

The modified Euler's method proceeds straightforwardly from difference formula considerations and is written

$$\bar{y}_{i+1} = \bar{y}_i + \frac{\Delta x}{2} [f(\bar{y}_i) + f(\bar{y}_{i+1})] \tag{A-5}$$

where the subscript i denotes some point, x_i, at which the solution is known, i + 1 the next point, x_{i+1}, at which the solution is desired, and Δx is the difference in the points, $x_{i+1} - x_i$. This is obviously an implicit method since a function of the unknown solution, $\bar{y}_{i+1}$, resides on the right-hand side of Eq. (A-5).

The $f(\bar{y}_{i+1})$ in Eq. (A-5) can be approximated by expanding $f(\bar{y})$ in Taylor's Series in terms of the solution and keeping the first two terms,

$$f(y) = f(\bar{y}_o) + f'(\bar{y}_o)(\bar{y} - \bar{y}_o) \tag{A-6}$$

where $f'(\bar{y}_o)$ is the Jacobian

$$f'(\bar{y}_o) = \left(\frac{\partial f(\bar{y})}{\partial y_i} \right)_{\bar{y} = \bar{y}_o} \tag{A-7}$$

Thus, $f(\bar{y}_{i+1})$ can be written

$$f(\bar{y}_{i+1}) = f(\bar{y}_i) + f'(y_i)(\bar{y}_{i+1} - \bar{y}_i) \tag{A-8}$$

Defining the constant matrices

$$A = f(\bar{y}_i) - f'(\bar{y}_i)\ \bar{y}_i \tag{A-9}$$

and

$$B = f'(\bar{y}_i) \tag{A-10}$$

$f(\bar{y}_{i+1})$ is written

$$f(\bar{y}_{i+1}) = A + B\ \bar{y}_{i+1} \tag{A-11}$$

Note that with the definitions of A and B, $f(\bar{y}_i)$ can be written in the same manner:

$$f(\bar{y}_i) = A + B\ \bar{y}_i \tag{A-12}$$

Substituting Eqs. (A-12) and (A-11) into Eq. (A-5) and solving for $\bar{y}_{i+1}$, one has

$$\bar{Y}_{i+1} = \left(I - \frac{\Delta x}{2} B\right)^{-1} \left[\bar{y}_i + \frac{\Delta x}{2} (2A + B \bar{y}_i)\right] \qquad \text{(A-13)}$$

where I is the unit matrix. Thus, the unknown solution, $\bar{y}_{i+1}$, is known as a function of the solution of the previous point, $\bar{y}_i$, and the independent variable increment, Δx. The B matrix is readily evaluated analytically if the function $f(\bar{y})$ is known, as it is in this case.

Relatively simple considerations of the approximations involved in establishing Eq. (A-13) yield a relationship between the approximate error and Δx and has been worked out by Mr. F. C. Loper, of AEDC. The error associated with expressing $\bar{y}_{i+1}$ in the manner of Eq. (A-5) is of order Δx^3. The error associated with expressing $f(\bar{y})$ in the manner of Eq. (A-8) is of order $(\bar{y}_{i+1} - \bar{y}_i)^2$ which is of order Δx^2. This error in $f(\bar{y}_{i+1})$ substituted into Eq. (A-5) shows the subsequent error in $\bar{y}_{i+1}$ because of the local linearization of $f(\bar{y}_{i+1})$ is thus also of order Δx^3. Hence, the error in $\bar{y}_{i+1}$ is of order Δx^3 and the error can be written

$$E_{i+1} = g_{i+1} \Delta x^3_{i+1} \qquad \text{(A-14)}$$

where g_{i+1} is some unknown function. Relating this to the error in $\bar{y}_i$ and solving for Δx_{i+1} yields

$$\Delta x_{i+1} = \Delta x_i \left[\frac{g_i \, E_{i+1}}{g_{i+1} \, E_i}\right]^{1/3} \qquad \text{(A-15)}$$

Assuming the g function does not vary rapidly, $g_{i+1} \approx g_i$; then

$$\Delta x_{i+1} \approx \Delta x_i \left[\frac{E_{i+1}}{E_i}\right]^{1/3} \qquad \text{(A-16)}$$

So, with a desired accuracy in $\bar{y}_{i+1}$ and a known accuracy in $\bar{y}_i$, which can be evaluated from

$$\bar{E}_i \approx \frac{1}{2} \bar{y}_i - \left[\bar{y}_{i-1} + \frac{\Delta x}{2} (f(\bar{y}_{i-1}) + f(\bar{y}_i))\right] \qquad \text{(A-17)}$$

where $f(\overline{y}_i)$ is evaluated exactly, a Δx_{i+1} yielding the approximate accuracy can be obtained. It should be noted that $\overline{E}_i$ in Eq. (A-17) is in fact a vector. In practice, one uses the largest element of $\overline{E}_i$ from Eq. (A-17) for the estimation of Δx_{i+1} in Eq. (A-16).

The identification of the elements of the $\overline{y}$ with the population densities n(p), x with time, and $f(\overline{y})$ with the right-hand side of Eqs. (7) and (8) in Section 2.0 complete the description of the technique in terms of the physical parameters.